GOETHE UNIVERSITY FRANKFURT AM MAIN

Characterization of a putative LptC homologue involved in the transport of lipopolysaccharide in *Anabaena* sp. PCC 7120

Dissertation zur Erlangung des Doktorgrades der Naturwissenschaften

vorgelegt beim Fachbereich Biowissenschaften der
Johann Wolfgang Goethe-Universität Frankfurt am Main

Giang Ngo

aus Hanoi (Vietnam)

Frankfurt am Main 2022

D30

vom Fachbereich Biowissenschaften der Johann Wolfgang Goethe-Universität Frankfurt am Main als Dissertation angenommen

Dekan:	Prof. Dr. Sven Klimpel
Ester Gutachter:	Prof. Dr. Enrico Schleiff
Zweiter Gutachter:	Prof. Dr. Claudia Büchel

Datum der Disputation:

Table of Contents

Table of Contents

Table of Contents

Abbreviations

aa	amino acid
ana	*Anabaena* sp. PCC 7120
BLAST	basic local alignment search tool
bp	base pair
ec	*Escherichia coli*
EDTA	ethylenediaminetetraacetic acid
gDNA	genomic DNA
GST	Glutathione S Transferase
IM	inner membrane
Imp	increased membrane permeability
IPTG	isopropyl-β-D-thiogalactopyranoside
kDa	kilo Dalton
Kdo	3-deoxy-D-manno-oct-2-ulosonic acid
LB	lysogeny broth
LPS	lipopolysaccharide
Lpt	lipopolysaccharide transport
MBP	maltose binding protein
Ni-NTA	nickel nitrilotriacetic acid
OD	optical density
OM	outer membrane
OMP	outer membrane protein
OstA	organic solvent tolerance protein A
PBS	phosphate buffered saline
PCR	polymerase chain reaction
PDB	Protein database
Pfam	Protein family
PGL	peptidoglycan layer
PM	plasma membrane
RT	room temperature
SDS-PAGE	sodium dodecyl sulfate-polyacrylamide gel electrophoresis
TEM	transmission electron microscopy
Tris	Tris (hydroxymethyl) amino methane
v/v	volume per volume
w/v	weight per volume

Abstract

Lipopolysaccharide (LPS) is a major glycolipid component in the outer leaflet of the outer membrane of Gram-negative bacteria and known as endotoxin exhibited by the lipid A moiety, which serves as a membrane anchor. The effective permeability barrier properties of the outer membrane contributed by the presence of LPS in the extracellular layer of the outer membrane confer Gram-negative bacteria a high resistance against hydrophobic compounds such as antibiotics, bile salts and detergents to survive in harsh environments. The biogenesis of LPS is well studied in *Escherichia coli* (herewith *E. coli)* and the LPS transport (Lpt) is carried out by a transenvelope complex composed of seven essential proteins (LptABCDEFG), which are located in the three compartments of the cell such as the outer membrane, the inner membrane and the periplasm. The Lpt system also exists in *Anabaena* sp. PCC 7120 (herewith *Anabaena* sp.), however, homologues of LptC and LptE are still missing.

BLAST search failed to identify a homologue of LptC, in contrast, the secondary structure analysis using the Pfam database based on the existing *ec*LptC secondary structure identified one open reading frame All0231 as the putative *Anabaena* sp. homologue of LptC, which is designated *ana*LptC. Despite the low sequence similarity, the secondary structure alignment between *ana*LptC and *ec*LptC using the HHpred server showed that both proteins share high secondary structural similarities. The genotypic analysis of the insertion mutant *ana*LptC did not identify a fully segregated genome and its phenotypic analysis revealed that it was sensitive against chemicals, suggesting that the *analptC* gene is essential for the growth of *Anabaena* sp. and involved in the outer membrane biogenesis. This is further supported by the observation of the small cell phenotype in the *ana*LptC mutant via transmission electron microscopy. Moreover, physical interactions between the *ana*LptC periplasmic domain with *ana*LptA as well as with *ana*LptF were established, indicating that the *ana*LptC periplasmic domain is correctly folded and alone functional and that the transmembrane helix is not required for the interaction with *ana*LptA and *ana*LptF. Furthermore, the reduction of the O-antigen containing LPS was observed in the insertion mutant *ana*LptC and the dissociation constant Kd of the *ana*LptC periplasmic domain for *ec*LPS was determined.

Abstract

The three-dimensional structure of the periplasmic domain of *ana*LptC was solved by X-ray crystallography with a resolution of 2.8 Å. The structural superposition between the *ec*LptC crystal structure (PDB number 3my2) and the crystal structure of *ana*LptC periplasmic domain obtained by this study showed the similarity in the folding of the two proteins with a Cα r.m.s.d value of about 1 Å and confirmed that the length of *ana*LptC is more than two times longer than that of *ec*LptC. The structural comparison also revealed that both structures share the typical β-jellyroll fold and conserved amino acids, which were shown in *ec*LptC to bind to LPS *in vivo* and found in *ana*LptC. Overall, these data strongly suggest that *ana*LptC is involved in the transport of LPS and support the model whereby the bridge spanning the inner membrane and the outer membrane would be assembled via interactions of the structurally conserved β-jellyroll domains shared by five (LptACDFG) out of seven Lpt proteins.

Zusammenfassung

Die äußere Membran, der periplasmatische Raum, der das dünne Peptidoglykan enthält, und die innere Membran sind drei Zellkompartimente der Gram-negativen Bakterienzellhülle. Die äußere Membran ist eine einzigartige asymmetrische Doppelschicht mit der inneren Schicht aus Phospholipiden und der extrazellulären Schicht aus Lipopolysacchariden (LPS). Dagegen ist die innere Membrane symmetrisch und besteht aus Phospholipiden. LPS ist als Endotoxin bekannt, welches als hitzestabiles Gift von verschiedenen pathogenen Gram-negativen Bakterien produziert wird und erstmals Ende des 19. Jahrhunderts vom deutschen Arzt Richard Pfeiffer beschrieben wurde. Das Vorhandensein von LPS in der extrazellulären Schicht der äußeren Membrane trägt weitgehend zu den Permeabilitätsbarriereeigenschaften bei und ermöglicht es Gram-negativen Bakterien, in toxischen und extremen Umgebungen zu überleben und mehrere Antibiotika auszuschließen, die gegen Gram-positive Bakterien wirksam sind.

LPS ist ein Glucosamin Disaccharid mit einen konservierten Lipid A als hydrophober Membrananker, einem inneren und äußeren Kern aus Oligosacchariden und einem langkettigen O-Antigen aus Polysacchariden. Negativ geladene LPS-Moleküle wechseltwirken *in vivo* mit zweiwertigen Kationen. Dadurch wird eine undurchlässige Schicht hergestellt, um den Zufluss von hydrophoben Molekülen wie Antibiotika, Gallensalzen und Detergenzien in den Zellen zu verhindern. Die LPS-Biogenese ist ein komplexer Prozess. Sie umfasst die Synthese der verschiedenen Einheiten von LPS an der inneren Membran, die Translokation durch die innere Membran, den Transport durch den wässrigen periplasmatischen Raum und die Insertion in der extrazellulären Schicht der äußeren Membrane.

Die Biogenese von LPS ist am besten in *E. coli* beschrieben und findet mit der Produktion von Lipid A zwischen der inneren Membran und Zytosol statt. Das Kern-Oligosaccharid wird anschließend durch das Waa Protein an das Lipid A angehängt. MsbA, ein ABC transporter (ATP-binding cassette transporter) dreht den Komplex aus Lipid A und Kern-Oligosaccharid auf die periplasmatische Seite der inneren Membran um, wo er mit O-Antigen zu Bildung des reifen LPS durch WaaL-Protein ligiert wird. Der Weitertransport des LPS wird von einem transmembranen LPS Transporter Komplex (LptABCDEFG) durchgeführt, welches es über das Periplasma transportiert und in die äußere Membran einfügt. Dabei bilden LptB, LptF und LptG ein Komplex

in der inneren Membran verantwortlich für die Extraktion von LPS aus der Membran und die Lieferung auf LptC. Der LptBFG Komplex assoziiert mit LptC, ein bitopisches Protein in der Plasmamembran, welches das LPS an das periplasmatische Protein LptA transferiert. LptA trägt eine OstA Domäne (organic solvent tolerance), welche ebenfalls in LptC und im N-Terminus von LptD vorhanden ist. Das äußere Membranprotein LptD enthält eine C-terminale transmembrane β-Barrel Domäne, die das Lipoprotein LptE bindet. LptE wird nicht nur für den Assemblierung von LptD benötigt, sondern bildet auch eine Plug-Domäne für die β-Barrel-Domäne von LptD. Darüber hinaus dient LptE als Erkennungsstelle für LPS und hilft bei der Assemblierung von LPS in die extrazelluläre Schicht der äußeren Membran.

Anabaena sp. PCC 7120 (hier als *Anabaena* sp. bezeichnet) ist ein filamentöses und multizelluläres Cyanobakterium, welches im Süßwasser lebt und zu den Gram-negativen Bakterien gehört. Deswegen besitzt es ebenfalls die typische Zellhülle Gram-negativer Bakterien, welche aus der LPS enthaltenden äußeren Membran, der Peptidoglykanschicht, die sich im periplasmatischen Raum befindet, und der inneren (zytoplasmatischen) Membran besteht. Die Peptidoglykanschicht von *Anabaena* sp. sowie anderer Arten der Phyllum Cyanobakterien ist jedoch dicker als die der Phyllum Proteobakterien wie bspw. *E. coli*.

In der Zusammensetzung des LPS gibt es entscheidende Unterschiede zwischen den LPS-Molekülen von *E. coli* und Cyanobakterien. Das cyanobakterielle O-Antigen ist ebenfalls sehr variabel aber wird durch seltene O-Methylzucker terminiert. In der Kern-Oligosacchariden von Cyanobakterien ist Heptose nicht vorhanden und KDO-Einheiten werden durch Glucose ersetzt. Das proteobakterielles Lipid A wird an Position 1’ und 4’ phosphoryliert, während das von Cyanobakterien nur an Position 1’ phosphoryliert wird. Durch das Fehlen der Phosphorylierung zeigt das cyanobakterielle LPS geringe Toxizität im Vergleich zu dem von Proteobakterien.

Während viele Komponenten des Lpt-Komplexes Gram-negativer Bakterien konserviert sind, fehlen LptC und LptE in manchen Organismen. In *Anabaena* sp. wurden fünf Homologe der Lpt Proteine identifiziert, allerdings fehlen die Homologe von LptC und LptE. Die anderen fünf Homologe von Lpt Proteinen wurden in *Anabaena* sp. gefunden, wobei Homologe von LptA, LptB, LptF und LptG durch die BLAST Analyse unter Verwendung von *E. coli* Lpt Proteinsequenzen identifiziert wurden, während die Identifizierung des LptD Homologs über die konservierte OstA-

Domäne erfolgte. Tatsächlich zeigt das Sequenz Alignment mittels Needle Algorithmus, dass der *ana*LptF zugewiesene offene Leserahmen Alr4069 eine hohe Ähnlichkeit sowohl mit *ec*LptF als auch mit *ec*LptG aufweist und zu einem einzigen Operon mit *ana*LptA und *ana*LptB gehört. Dagegen befinden sich in *E. coli* LptA, LptB und LptC alle im selben Operon. Somit kann vermutet werden, dass die unterschiedliche Organisation im Operon für jeden Organismus artspezifisch ist. Darüber hinaus legt die proteomische Analyse der Zellwandfraktion vegetativer Zellen nahe, dass *ana*LptA auch im periplasmatischen Raum lokalisiert ist, wie zuvor für *ec*LptA gezeigt wurde.

LptD in *E. coli* ist ein essentielles Protein, welches vier Cystein Aminosäurereste enthält, zwei in der N-terminalen Domäne, zwei nahe dem C-Terminus. Die aktive Form von LptD erfordert die Bildung von zwei Disulfidbrücken in der richtigen Reihenfolge, was von der korrekten Bildung des äußeren Membrantranslokons abhängt, welcher durch das Lipoprotein LptE und das Außenmembranprotein LptD gebildet wird. Die Bildung der Disulfidbrücken in der korrekten Reihenfolge wird durch die Bindung an LptE ausgelöst. Allerdings hat *Anabaena* sp. keine Cystein Reste in LptD und kein LptE. Trotz dieses signifikanten Unterschieds zwischen den beiden LptD Proteine von *E. coli* und *Anabaena* sp. enthalten sie die charakteristische N-terminale OstA Domäne. Es wurde gezeigt, dass der N-terminus von *ana*LptD mit *ana*LptA über die OstA Domäne interagiert, wie es auch für LptA and LptD von *E. coli* beobachtet wurde. Obwohl die konservierte OstA-C Domäne, die als eine β-Barrel Domäne am C-terminus *ec*LptD gefunden wurde, nicht in *Anabaena* sp. LptD identifiziert wurde, zeigen sowohl *ec*LptD als auch *ana*LptD Proteine ein empfindliches Verhalten gegenüber Lipid A in elektrophysiologischen Experimenten. Darüber hinaus zeigen *ec*LptD und *ana*LptD in voller Länge eine experimentell vergleichare Konduktanz, was drauf hindeutet, dass die beiden Proteine kationenselektive Poren mit ähnlichen Innendurchmessern bilden.

Die Sekundärstrukturanalyse mit Hilfe der Pfam Datenbank konnte einen offene Leserahmen All0231 als ein mögliches LptC Homologe anhand der vorhandenen *ec*LptC Sekundärstruktur identifizieren. Dabei wurde LptC strukturelle Family mit der Pfam Domäne PF06835 über die gesamte Länge des All0231 Proteins vorhergesagt. Diese Vorhersage wurde weiter bestätigt durch die Sekundärstrukturanalyse zwischen All0231 und *ec*LptC Protein unter Verwendung des HHpred Servers, so zeigte sich, dass beide Proteine hohe sekundäre strukturelle Ähnlichkeiten

haben. Trotz der geringen Sequenzähnlichkeit sagte der HHpred Server voraus, dass das All0231 Protein aus vielen β-Strängen besteht, die in *ec*LptC vorhanden sind. Insgesamt deuten diese Daten stark darauf hin, dass All0231 das Homologe von *ec*LptC sein könnte und hier weiter als *ana*LptC bezeichnet wird.

Um in der vorliegenden Studie zu evaluieren, ob *ana*LptC *in vivo* an dem Transport von LPS beteiligt ist, wurde die Insertionsmutante AFS-I-*analptC* generiert. Die genotypische Analyse der AFS-I-*analptC* Mutante zeigte keine vollständig segregierten Genome, was darauf hindeutet, dass das *analptC* Gen für das Wachstum von *Anabaena* sp. essentiell ist. Die AFS-I-*analptC* Mutante zeigte ein reduziertes Wachstum im Vergleich zum Wildtyp mittels der Wachstumsanalyse in der Anwesenheit der verschiedenen Chemikalien wie Salz und Ethanol. Die Untersuchung mittels Transmission-Elektronenmikroskopie zeigte eine Verringerung der Zellgröße der AFS-I-*analptC* Mutante, während eine Veränderung der Ultrastruktur der äußeren Membran nicht bestätigt werden konnte. In der vorliegenden Arbeit konnte sowohl die Abnahme der mit O-Antigen versehenen LPS Population im AFS-I-*analptC*-Stamm als auch die Affinität von *ana*LptC für *ec*LPS festgestellt werden, was auf eine Beteiligung von *ana*LptC in Transport von LPS hindeutet.

Ein weiteres Ziel der vorliegenden Arbeit ist es, die Interaktionen zwischen *ana*LptC und *ana*LptF sowie *ana*LptA *in vitro* zu untersuchen, die durch die β-Jellyroll Struktur erfolgen könnten, wie es für *E. coli* bereits gezeigt wurde. Zu diesem Zweck wurde die periplasmatische Domäne von *ana*LptC ohne die Transmembran-Helix exprimiert. Interaktionen zwischen periplasmatischer Domäne *ana*LptC mit *ana*LptA sowie *ana*LptC mit *ana*LptF konnten gezeigt werden, was impliziert, dass die *ana*LptC periplasmatische Domäne korrekt gefaltet und allein funktionsfähig ist und dass die Transmembran-Helix nicht erforderlich für die Interaktion mit *ana*LptA und *ana*LptF ist.

Die Sequenzanalyse zwischen LptC von Cyanobakterien und Proteobakterien zeigt einen signifikanten Unterschied zwischen den beiden Stämmen. Das LptC Protein vom cyanobakteriellen *Anabaena* sp. ist doppelt so lang wie das vom proteobakteriellen *E. coli* Stamm. Deswegen ist es für die vorliegende Arbeit von besonderem Interesse aufzuklären, ob diese Beobachtung auch für die periplasmatische Domäne von *ana*LptC gilt und ob sie ebenfalls die charakteristische β-Jellyroll Struktur aufweist, wie es in *E. coli* bekannt ist. Mittels

Röntgenkristallographie konnte die dreidimensionale Struktur der periplasmatischen Domäne von *ana*LptC mit einer Auflösung von 2.8 Å gelöst werden. Der strukturelle Vergleich zwischen der vorhandenen *ec*LptC Kristallstruktur (PDB Nummer 3my2) und der durch die vorliegende Arbeit gewonnenen Kristallstruktur von *ana*LptC periplasmischen Domäne zeigt die Ähnlichkeit in der Faltung der beiden Proteine mit einem Cα rmsd-Wert von etwa 1 Å, und bestätigt, dass *ana*LptC länger als *ec*LptC ist. Darüber hinaus wurde gezeigt, dass die β-Jellyroll Struktur von *ec*LptC sich in der gesamten Struktur von *ana*LptC wiederfindet. Außerdem konnten durch den strukturellen Vergleich der beiden Kristallstrukturen konservierte Aminosäuren in *ana*LptC identifiziert werden, für die eine Interaktion zwischen LptC und LPS in *E. coli* nachgewiesen wurde. Weitere Ähnlichkeiten sowie Unterschiede in den Eigenschaften von *ana*LptC im Vergleich zur *ec*LptC Struktur werden in der vorliegenden Arbeit beschrieben und diskutiert. Trotz geringer Ähnlichkeit der Proteinsequenz geht die vorliegende Studie aufgrund der erhaltenen Daten davon aus, dass *ana*LptC vergleichbare Funktion in LPS Transport besitzen könnte, und unterstützt das Brücken-Modell, welches sich über die innere und äußere Membran über die durch eine konservierte strukturhomologe Jellyroll-Domäne vermittelte Interaktionen spannt.

1 Introduction

1.1 Cyanobacteria

Formerly known as blue-green algae, cyanobacteria represent a large and diverse group of Gram-negative bacteria (Gademann & Portmann, 2008). Their impressive abilities support their proliferation in aquatic and terrestrial ecosystems (Whitton & Potts, 2000). They flourish in salty as well as freshwater, as a number of cyanobacterial species is able to grow in regions containing high concentrations of sodium chloride (Reed et al., 1984). Another impressive ability of cyanobacteria is that they colonize in infertile substances such as volcanic ash, desert sand and rocks (Dor & Danin, 1996; Horath & Bachofen, 2009). Further remarkable feature is their ability to tolerate extremely high as well as low temperatures, as they are found in hot springs, Arctic and Antarctic (Ward et al., 1998; Comte et al., 2007).

Cyanobacteria is one of the oldest organisms on earth, appearing around 2 billion years ago (Demoulin et al., 2019). They are responsible for bringing oxygen in the early atmosphere on the earth and the only prokaryotes that are capable to perform oxygenic photosynthesis (Schopf, 2000). The endosymbiotic theory holds that the plastids in the photosynthetic eukaryotes likely evolved from cyanobacteria being engulfed and codeveloped in a phagotrophic host (Keeling, 2010; McFadden, 2014). According to the traditional taxonomic classification, cyanobacteria are divided into five subsections based on morphology, reproduction and differentiation (Rippka et al., 1979). The basic morphology of the cyanobacteria consists of unicellular, colonial, multicellular, filamentous to branched filamentous forms. Unicellular cyanobacteria are categorized into section I and II, whereas species appear in filamentous forms classified to sections III to V. Species in section I duplicate by binary fission or budding, while those in section II reproduce by multiple and binary fission. Species in sections III and IV form unbranched filaments and divide in one plane. Section IV and V species share the differentiation ability, whereby they are able to develop vegetative cells into nitrogen fixing heterocysts. However, section V species are able to form branched filaments by dividing in multiple planes (Rippka et al., 1979). Besides being oxygen and biomass producer, diazotrophic cyanobacteria provide an important source of nitrogen as biofertilizers for sustainable agriculture (Chittora et al., 2020). Nowadays, cyanobacteria have gained research attention because of the possible positive use

such as a food supplement, natural chemicals to substitute synthetic cosmetics and pharmaceutical compounds (Vanthoor-Koopmans et al., 2014; Singh et al., 2017).

The model organism *Anabaena* sp. PCC 7120 (herewith *Anabaena* sp.) in this study is a filamentous, freshwater and heterocyst forming cyanobacterium, which belongs to section IV. Its genome is completely sequenced and consists of one chromosome and six plasmids (alpha to zeta), which are composed of 7,211,789 nucleotides and encode for 6,135 putative genes (Kaneko et al., 2001). *Anabaena* sp. is a polyploid species, because it contains about 8 copies of chromosomes per cell (Hu et al., 2007). Since genetic tools and cultivation methods are well-established, *Anabaena* sp. is a good model organism for studies of differentiation of the cell, nitrogen fixation and photosynthesis.

Like all species of section IV, *Anabaena* sp. has the ability to perform nitrogen fixation. Under condition of nitrogen depletion, vegetative cells irreversibly differentiate to heterocysts, that are morphologically and physiologically adapted cells and devoted to fix elemental nitrogen (Golden & Yoon, 1998). Vegetative cells supply herterocysts with carbon source such as sucrose (Wolk, 1968), in turn, heterocysts provide vegetative cells with the fixed nitrogen incorporated into amino acids including glutamine (Wolk et al., 1976). Metabolites can be then exchanged between the two cell types during diazotrophic growth (Flores & Herrero, 2010). Another difference between the two cells type is that heterocysts bear the heterocyst-specific envelope composed of heterocyst-specific glycolidpid (HGL) and heterocyst envelope polysaccharide (HEP) (Kumar et al., 2010; Herrero et al., 2016). By utilizing these two essential HGL and HEP layers, heterocysts create a micro-oxic environment to protect nitrogenase complex, which is otherwise sensitive to oxygen generated by the photosynthetic process (Flores & Herrero, 2010). Therefore, the compartmentalization of the oxygenic photosynthesis and the nitrogen fixation in two different cell types is the solution to the incompatibility problem between the two processes and the distinction in the cell envelope of the nitrogen fixing cyanobacteria from that of proteobacteria provides evidence for the diversity in the architecture of Gram-negative bacterial membranes (Flores & Herrero, 2010).

1.2 The properties of the cell envelope of Gram-negative bacteria

Bacteria evolved a cell envelope organized in a complex multilayered structure, which serves as a barrier responsible for the uptake of nutrients and to protect themselves from changing and often hostile environments (Silhavy et al., 2010). Cell envelopes of Gram-negative bacteria are composed of the lipopolysaccharide (LPS) containing outer membrane, the thin peptidoglycan layer located in the periplasmic space and the inner (cytoplasmic) membrane (Wu et al., 2006). In contrast, cell envelopes in Gram-positive bacteria lack an outer membrane but consist of multiple peptidoglycan layers which are much thicker than those of the Gram-negative bacteria including proteobacteria such as *E. coli* (Silhavy et al., 2010). Based on this fundamental difference in the membrane architecture, Gram-negative bacteria can be distinguished from Gram-positives by the well-known Gram´s staining method (Shah et al., 1997).

The inner membrane is a symmetric lipid bilayer containing phospholipids and proteins (Koebnik et al., 2000; Ruiz et al., 2006). It is the innermost layer of the bacterial cell envelope with essential functions such as protein translocation, nutrient transport, lipid biosynthesis and oxidative phosphorylation (Duong et al., 1997). The membrane-spanning domains of the inner membrane proteins are α-helical, whereas the membrane-spanning domains of the outer membrane proteins are β-barrel shaped (Koebnik et al., 2000; Schulz, 2002). Like other phyla of Gram-negative bacteria, the inner membrane of cyanobacteria also surrounds each cell regardless of unicellular or filamentous forms (Wilk et al., 2011). However, most cyanobacteria contain an additional membrane derived from the thylakoids (Nickelsen et al., 2011). The previous electron tomography analysis proposed that the thylakoid center is connected to the inner membrane (Van De Meene et al., 2006). Evidence supporting this proposal was provided by the observation of the specialized regions of the inner membrane, in which the thylakoid membrane and the inner membrane converge in some regions of the cyanobacterial filamentous *Anabaena* sp. cells as well as unicellular *Synechocystis* sp. PCC 6803 (Van De Meene et al., 2006; Wilk et al., 2011). Another specialized region of the inner membrane found in filamentous cyanobacteria such as *Anabaena* sp. is the septum containing up to 500 septosomes, which allows transport of metabolites between adjacent cells (Hahn & Schleiff, 2014).

Peptidoglycan layer is located in an aqueous periplasmic space between the inner membrane and the outer membrane and composed of repeating units of the disaccharide N-acetyl glucosamine N-acetyl muramic acid, which are cross-linked by pentapeptide side chains (Vollmer et al. 2008). It contains membrane-derived oligosaccharides, soluble binding protein, components of transport systems and chaperones (Duong et al., 1997). Because of the rigidity of its mesh network, the peptidoglycan layer provides cell shape and prevents cell lysis through the turgor pressure of the cytoplasm (Joseleau-Petit et al., 2007; Gan et al., 2008).

Although the overall structure of the peptidoglycan layer is similar among Gram-negative bacteria, the dimension of this layer in cyanobacteria reveals significant difference from that of *E. coli* (Figure 1 A). The peptidoglycan thickness previously determined for cyanobacterial species such as *Anacystis nidulans*, *Phormidium uncinatum* and *Oscillatoria princeps* is 10 nm, 15-35 nm and 300-700 nm, respectively (Golecki, 1977; Hoiczyk & Baumeister, 1995). Similarly in the range, the peptidoglycan layer of *Anabaena* sp. is 14 ± 2 nm thickness, which is more than two times thicker than that of *E. coli* with a thickness of approximately 6.35 ± 0.53 nm (Matias et al., 2003; Wilk et al., 2011). In line with this, the periplasmic space in *Anabaena* sp. is 46 ± 3 nm significantly larger compared to that in *E. coli* with a distance of 18-21 nm. (Silhavy et al., 2010; Wilk et al., 2011). Furthermore, the degree of the pentapeptide crosslinks in cyanobacterial peptidoglycan layer in the range of 56-63% is similar to that of Gram-positive bacteria but much higher than that with 20-33% in proteobacteria (Jürgens et al., 1983; Glauner et al., 1988). Moreover, the L-lysine component typical for Gram-positive bacteria is found in cyanobacteria (Kodani et al., 1999; Hoiczyk & Hansel, 2000). Therefore, these evidences suggest that cyanobacterial peptidoglycan layer might be the combination between the typical features of Gram-negative and the typical Gram-positive layers.

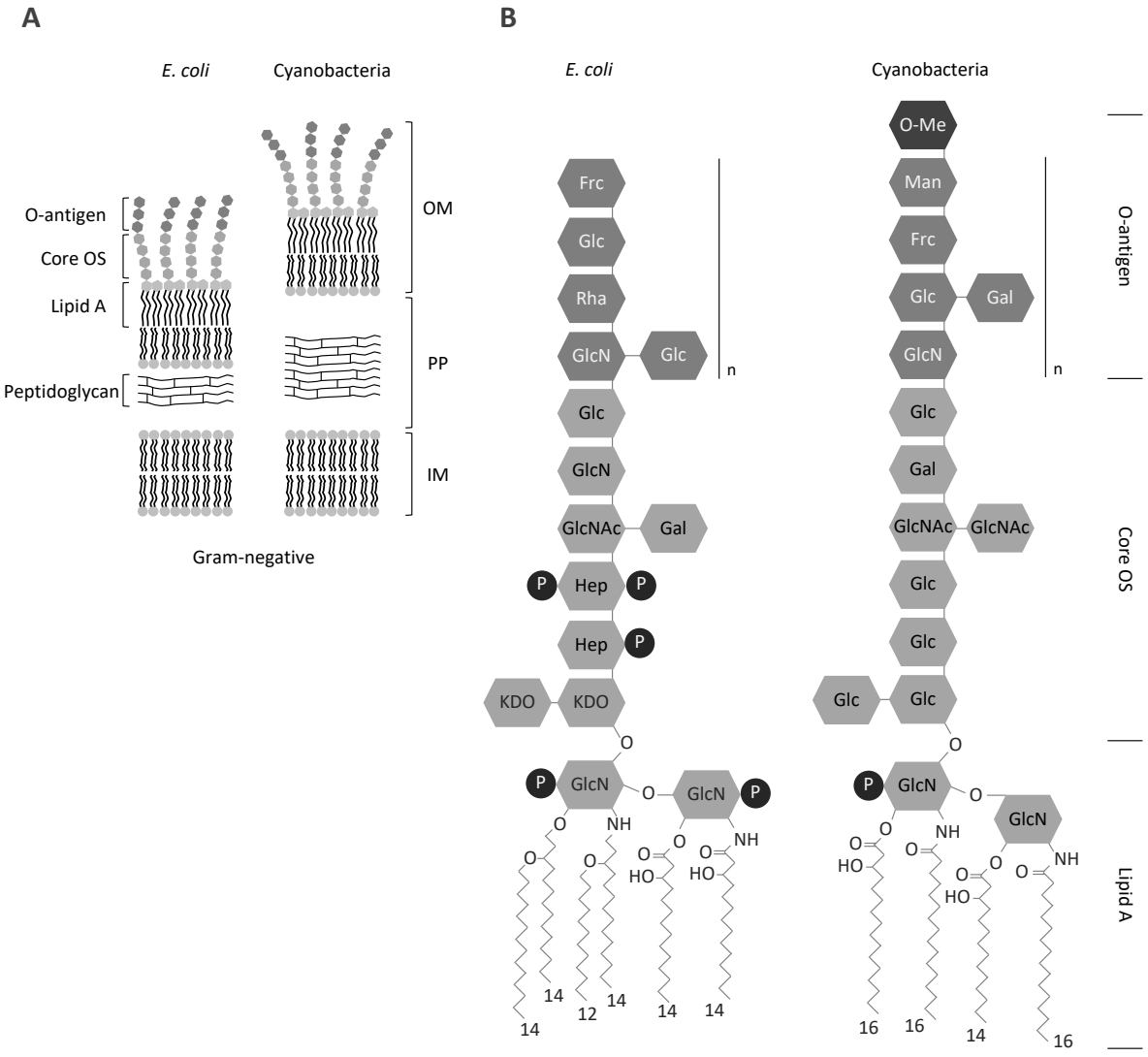

Figure 1: Comparison of bacterial cell envelopes and lipopolysaccharide (LPS).
A) Cell envelopes of Gram-negative bacteria are composed of the inner membrane (IM), the peptidoglycan layer residing in the periplasm (PP) and the outer membrane (OM). However, the peptidoglycan layer of cyanobacteria is thicker than that of *E. coli*. B) The structure of LPS from *E. coli* and cyanobacteria consists of the lipid A, the core oligosaccharide (core OS) and the O-antigen. The figure adopted from Hahn & Schleiff, 2014.

The outer membrane is the outermost layer of the cell envelope and the distinguishing feature of Gram-negative bacteria, which is absent in Gram-positive bacteria (Silhavy et al., 2010). It is an essential organelle of the cell and serves as a permeability barrier against unregulated diffusion of hydrophilic molecules and hydrophobic molecules (Raetz & Whitfield, 2002; Nikaido, 2003; Ebbensgaard et al., 2018). Moreover, the outer membrane acts as a selective permeable barrier that allows the passive diffusion of small molecules such as mono- and disaccharides as well as amino acids and the regulated diffusion of specific molecules through the most abundant outer

membrane proteins such as porins (Cowan et al., 1992; Silhavy et al., 2010). Components of the outer membrane such as proteins and lipids synthesized in the cytoplasm or at the inner leaflet of the inner membrane need to be transported to and assembled at the outer membrane in the correct orientation in order to maintain the barrier function during the cell growth and the cell division (Wu et al., 2006). β-barrel proteins are inserted into the OM, while lipoproteins are attached to the inner leaflet of the OM via their lipid moieties (Wu et al., 2006). Proteins participated in transporting the outer membrane components across the inner membrane have been identified and characterized, however, how they are transported across the aqueous periplasmic space and inserted into the outer membrane needs further investigation (Wu et al., 2006).

The composition and structural organization of the outer membrane are different from those of the plasma membrane. In fact, the plasma membrane is a symmetric bilayer formed by phospholipids, in contrast, the outer membrane is an highly asymmetric bilayer with phospholipids in the inner leaflet and LPS in the outer leaflet (Koebnik et al., 2000; Ruiz et al., 2006; Konovalova et al., 2017; Figure 1 A). LPS is an essential component of the outer membrane in most Gram-negative bacteria, because the protective function of the outer membrane relies on the proper assembly of LPS molecules (Bertani & Ruiz, 2018). LPS is composed of the lipid A bearing hydrophobic fatty acid chains, the core region and the O-antigen (Delcour, 2009; Figure 1 B). The O-antigen made of repeating units of polysaccharide is the highly diverse part of LPS (Lerouge & Vanderleyden, 2002). In cyanobacteria, the composition of sugar units in the O-antigen is also highly variable and terminated by rare O-methyl sugars (Hahn & Schleiff, 2014; Figure 1 B, right). The core region consists of inner and outer core oligosaccharides attached to the lipid A and is found to be conserved in proteobacteria and highly phosphorylated because of the presence of heptose and 2-keto-3-deoxyoctonate (KDO) units (Heinrichs et al., 1998; Figure 1 B, left). In contrast, heptose is not found in cyanobacteria and KDO units are replaced by glucose (Figure 1 B, right), indicating that the phosphorylation level in cyanobacteria is much lower than that of proteobacteria (Keleti & Sykora, 1982; Snyder et al., 2009; Durai et al., 2015). Consistently, β (1–6)-linked D-glucosamine disaccharide of proteobacterial lipid A is phosphorylated at position 1’ and 4’, while that of cyanobacterial is only phosphorylated at position 1’ (Delcour, 2009; Hahn & Schleiff, 2014). Nevertheless, the lipid A is considered as the most conserved part of LPS and

serves as a membrane anchor of LPS (Bertani & Ruiz, 2018). The lipid A is known to be the most inflammatory part of the endotoxin that is capable to trigger a strong immune response (Raetz & Whitfield, 2002). The fact that the *E. coli* lipid A differs from a typical phospholipid by having six saturated fatty acid chains instead of two saturated or unsaturated chains reveals that the asymmetric outer membrane bilayer possesses the low fluidity and high hydrophobicity than the typical phospholipid bilayer due to the strong lateral interaction between LPS molecules (Delcour, 2009). In addition, interactions of negatively charged phosphate groups from LPS molecules with strongly divalent cations such as Ca^{2+} or Mg^{2+} allow LPS molecules to pack tightly (Nikaido, 2003). Thus, LPS molecules assemble into a highly ordered network of sugar chains on the cell surface that prevents hydrophobic compounds from entering into the cells (Okuda et al., 2016).

The filamentous multicellular cyanobacteria have an additional feature showing that the outer membrane does not enter the septum between two adjacent cells. This feature is observed by previous studies on the section III cyanobacterium *Phormidium uncinatum* (Hoiczyk & Baumeister, 1995). In agreement with this observation are studies on *Anabaena* sp. ultra-structure which revealed that the outer membrane appears to be continuous along the filament of cells and does not penetrate the septum between two consecutive cells via electron tomography, however, the peptidoglycan layer surrounds each cell (Flores et al., 2006). This implies that the periplasmic space between the inner and outer membranes might also be continuous (Flores et al., 2006). Furthermore, the peptidoglycan layers are thought to be connected to plasma membranes via septosomes, through which the transport of nutrients and metabolites as well as signal transduction can occur between cells (Wilk et al., 2011).

1.3 The biogenesis of LPS in *E. coli*

LPS biogenesis takes place at the cytoplasmic side of the inner membrane with the production of Lipid A moiety, which is synthesized by Lpx (lipoxygenase) proteins (Anderson & Raetz, 1987; Wyckoff et al., 1998; Raetz et al., 2009). Subsequently, the core oligosaccharide is attached to the lipid A by Waa protein to form the lipid A-core oligosaccharide complex, which is flipped to the periplasmic side of the inner membrane by MsbA with the function of an ATP-binding cassette transporter (ABC transporter) located at the inner membrane (Karow & Georgopoulos,

1993; Zhou et al., 1998; Raetz & Whitfield, 2002; Doerrler et al., 2004; Polissi & Sperandeo, 2014). Afterwards, O-antigenic polysaccharide is ligated onto the lipid A-core oligosaccharide complex to form the mature LPS by WaaL protein (Hug et al., 2010; Figure 2).

There are more than 100 genes involved in the biogenesis of LPS and the components responsible for the transport of LPS from the inner membrane to the outer membrane have been identified, however, the molecular mechanism for the transport and the assembly of LPS onto the cell surface still remains elucidative (Raetz et al., 2007; Laguri et al., 2017). This complex is composed of seven essential proteins (LptABCDEFG) spanning three cellular compartments such as the inner membrane, periplasmic space and the outer membrane (Chng et al., 2010). They are all required for the export of LPS from the inner membrane across the periplasmic space to the outer membrane (Okuda et al., 2016). Depletion of any Lpt proteins results in the accumulation of LPS in the periplasmic leaflet of the inner membrane (Ruiz et al., 2008; Sperandeo et al., 2008). The LPS accumulating on the periplasmic side of the inner membrane is modified with colanic acid residues (Sperandeo et al., 2011). Therefore, this modification is indicative of transport defects occurring downstream of the MsbA-mediated translocation of LPS to the outer leaflet of the inner membrane (Sperandeo et al., 2008).

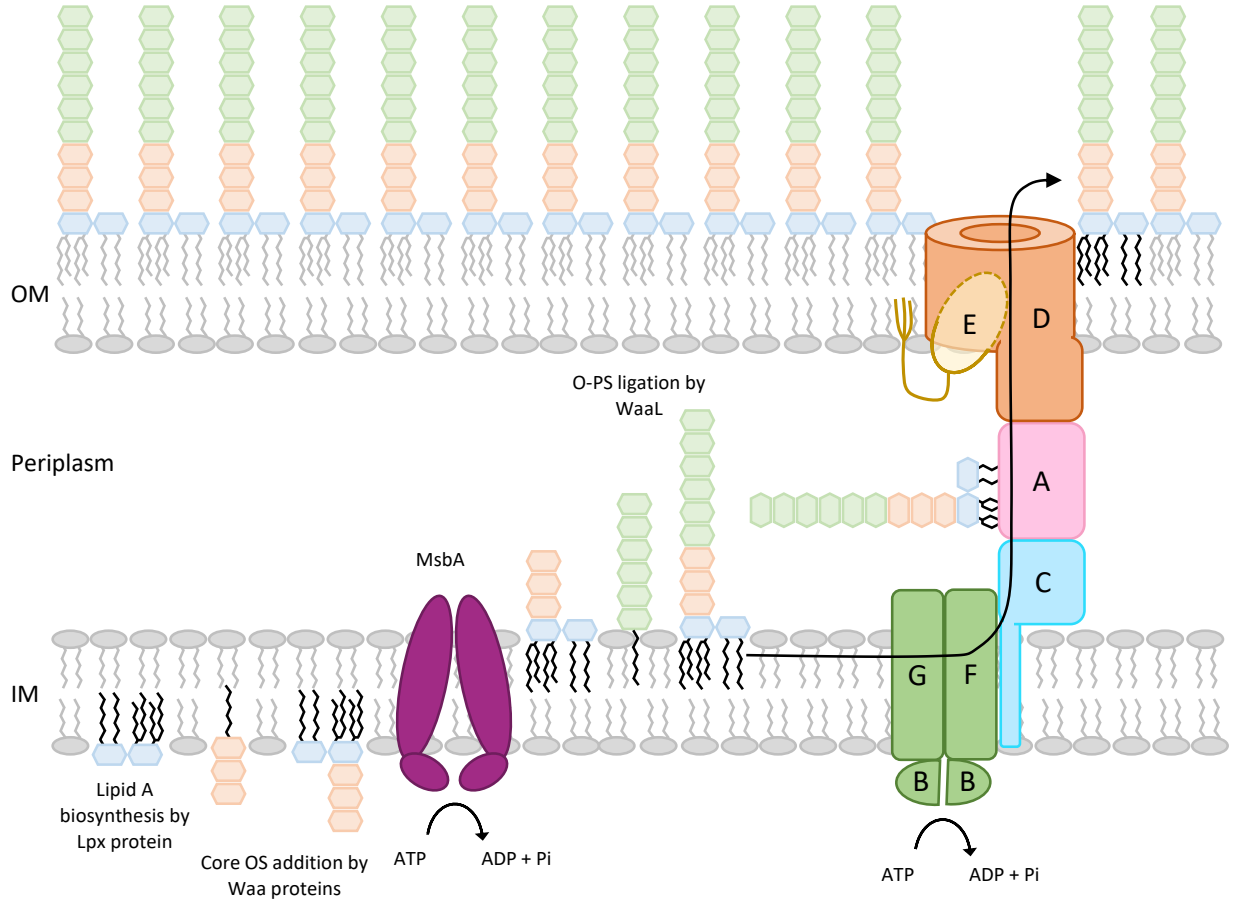

Figure 2: Representation of the biosynthesis of lipopolysaccharide (LPS) in *E. coli*.
The lipid A-core oligosaccharide (core OS) complex is synthesized on the cytosolic side of the inner membrane by Lpx and Waa proteins, then flipped to the periplasmic side by MsbA. The complete LPS is formed by ligation of the O-antigenic polysaccharide (O-PS) with the nascent lipid A-core oligosaccharide complex. The inner membrane (IM) located LptBFG complex acting as an ABC transporter extracts LPS upon hydrolyzation of ATP and transfers it to the periplasmic bridge composed of LptA, LptC and N-terminus of LptD. Finally, LPS is translocated in outer leaflet of the outer membrane (OM) by the translocon LptD/E. Figure is reproduced from Whitfield & Trent, 2014.

The three proteins LptB, LptF and LptG form a subcomplex LptBFG located at the inner membrane, which acts as an ABC transporter and provides the energy for the transport of LPS across the periplasm via ATP hydrolysis (Qiao et al., 2014). LptF and LptG are the transmembrane components, while LptB is the inner membrane-associated ATP binding protein (Ruiz et al., 2008; Narita & Tokuda, 2009; Villa et al., 2013). Physical interaction between the subcomplex LptBFG and LptC has been demonstrated (Narita & Tokuda, 2009). LptC is an inner membrane-anchored protein containing a single transmembrane helix and a large periplasmic domain that is required for the interaction with the IM LptBFG complex (Tran et al., 2010; Villa et al., 2013). However, its

association does not affect the ATPase activity of the LptBFG complex (Ruiz et al., 2008; Narita & Tokuda, 2009; Villa et al., 2013; Owens et al., 2019).

At the outer membrane, the β-barrel LptD protein and the LptE lipoprotein form the translocon that is in charge of the assembly of LPS at the cell surface (Laguri et al., 2017). LptD known as Imp (**i**ncreased **m**embrane **p**ermeability) and OstA (**o**rganic **s**olvent **t**olerance) protein consists of a N-terminal OstA domain and a C-terminal membrane embedded β-barrel OstA_C domain (Sampson et al., 1989; Aono et al., 1994; Bos et al., 2007; Suits et al., 2008). LptD is the largest bacterial outer membrane β-barrel and its biogenesis requires the β-barrel assembly machinery (BAM) (Ricci & Silhavy, 2012; Dong et al., 2014). The mature form of LptD contains two non-consecutive disulfide bonds, one of which is efficient for LptD to function and depends on the proper assembly of LptDE complex (Chng et al., 2010; Ruiz et al., 2010; Chimalakonda et al., 2011; Freinkman et al., 2011; Freinkman et al., 2012). LptE is proposed not only to act as a plug protein that blocks the channel of the LptD β-barrel domain, but also to bind LPS as well as stabilize LptD by interacting with its C-terminal domain, indicating that LptE serves as a substrate recognition site at the outer membrane (Chng et al., 2010; Freinkman et al., 2011).

The crystal structure of the LptC periplasmic domain of *E. coli* was solved and LptC was shown to bind LPS *in vitro* (Tran et al., 2010). Like LptC, LptA located in the periplasm physically interacts with LPS *in vitro*, and the results of pulldown experiments suggest that the translocation of LPS from LptC to LptA occurs in a unidirectional manner (Tran et al., 2010). Despite a lack of sequence similarity, LptA, the periplasmic domain of LptC and the periplasmic N-terminal domain of LptD belong to the OstA structural superfamily (Bos et al., 2007; *Finn* et al., 2008; Freinkman et al., 2012) and share a very similar β-jellyroll fold also predicted for the periplasmic domains of LptF and LptG (Sperandeo et al., 2011; Villa et al., 2013; Martorana et al., 2016). In fact, structural and photo-crosslinking studies have already shown that the periplasmic loops of LptF and LptG, the periplasmic domain of LptC, LptA and the N-terminal domain of LptD interact with each other via their homologous β-jellyroll fold to form the trans-periplasmic bridge connecting the inner membrane with the outer membrane for the transport of LPS (Freinkman et al., 2012; Okuda et al., 2016; Laguri et al., 2017; Owens et al., 2019).

1.4 The Lpt complex in cyanobacterial *Anabaena* sp. PCC 7120

LPS is present in almost all Gram-negative bacteria including cyanobacteria such as *Anabaena* sp. (Schmidt et al., 1980). Bioinformatic analyses of the COGs (Clusters of Orthologous Groups of proteins) database indicate that not all components of the Lpt pathway are conserved across Gram-negative bacteria (Tran et al., 2010). Several bacterial species including *Helicobacter pylori, Campylobacter jejuni, Mesorhizobium loti, Caulobacter crescentus, Aquifex aeolicus, Thermotoga maritima, Deinococcus radiodurans, Rickettsia prowazekii, Chlamydia trachomatis, Treponema pallidum, and Borrelia burgdorferi* do not have the structural gene for LptC and LptE (Tran et al., 2010). In *Anabaena* sp., the periplasmic component LptC and the lipoprotein LptE are not identified. However, the other five homologues of Lpt proteins were found in *Anabaena* sp., whereby homologues of LptA, LptB, LptF and LptG were identified by the BLAST analysis using *E. coli* Lpt protein sequences as baits (Figure 3), while the identification of the LptD homologue via the conserved OstA domain search (Haarmann et al., 2010). In fact, the sequence alignment calculated with the Needle algorithm identified one open reading frame Alr4069 assigned as *ana*LptF showing high similarity with both LptF and LptG of *E. coli* (Haarmann et al., 2010). While *ana*LptF belongs to a single operon with *ana*LptA and *ana*LptB, LptA and LptB are in the same operon with LptC in *E. coli* (Haarmann et al., 2010). Nevertheless, the proteomic analysis of the cell wall fraction of vegetative cells suggests that *ana*LptA also localizes in periplasmic space as previously observed for *ec*LptA (Moslavac et al., 2005). A further Lpt component identified in *Anabaena* sp. is the homologue of LptD. Similar to *ec*LptD, *ana*LptD possesses the characteristic OstA domain which is located at N-terminal region of the protein (Haarmann et al., 2010; Hsueh et al., 2015). According to earlier results from electrophysiological experiments, both *ec*LptD and *ana*LptD proteins exhibit sensitive behaviors to lipid A and the conductance values reveal that their pore diameters are comparable (Hsueh et al., 2015). Although, the four cysteine amino acid residues shown to be important for the maturation of active LptD protein in *E. coli* (Chng et al., 2010; Ruiz et al., 2010; Freinkman et al., 2012) are not present in *ana*LptD. The fact that not all components of Lpt complex are conserved in *Anabaena* sp. compared to that of *E. coli* indicates that there might be subtle variations in the Lpt pathway across Gram-negative bacteria (Haarmann et al., 2010).

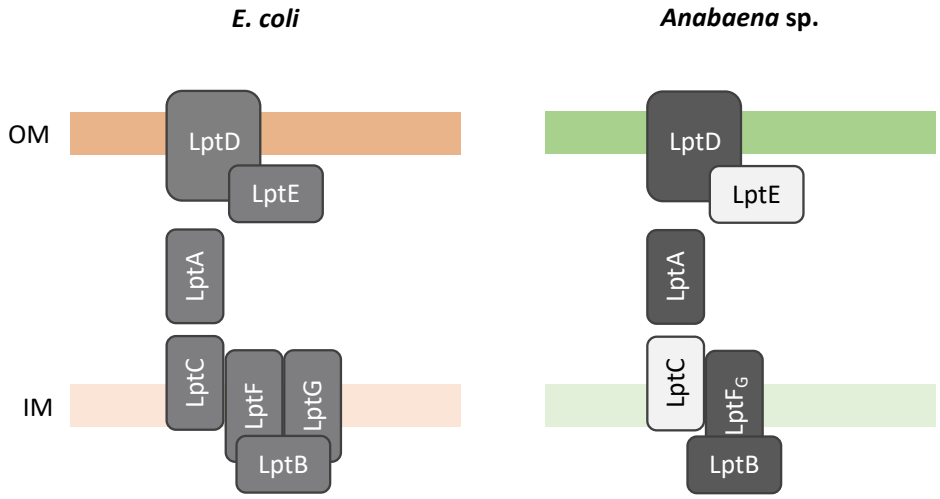

Figure 3: The composition of components required for Lpt transport complex in *Anabaena* sp. and *E. coli*.
Lpt complex in *E. coli* is composed of seven proteins (LptABCDEFG), whereas *Anabaena* sp. homologues of the five proteins (LptABDFG) are identified. The missing components LptC and LptE in *Anabaena* sp. are indicated in light gray boxes. Figure is adapted from Haarmann et al., 2010.

1.5 Objectives

BLAST search using the amino acid sequence of LptC from *E. coli* K 12 (Uniprot accession no. P0ADV9) as a query did not find a homologue of the periplasmic component LptC in the *Anabaena* sp. Lpt complex. In contrast, the secondary structural analysis using HHpred server identified one open reading frame encoded by *all0231* gene with structural similarities in comparison to *E. coli* LptC (herewith *ec*LptC). Interestingly, the periplasmic domain of All0231, designated *ana*LptC, is predicted to consist of many β-strands found in *ec*LptC, despite the low identity of their protein sequences.

The first aim of this study is to elucidate whether the putative *ana*LptC protein identified via the structural prediction with the HHpred server is involved in LPS transport *in vivo*. To address this, an insertion mutant of *ana*LptC will be generated by homologous recombination via insertion of the pCSV3 plasmid in the target gene. Subsequently, the outer membrane permeability of this mutant will be examined whether it is affected due to the inactivation of *ana*LptC via phenotyping tests using different chemicals. In addition, the ultra-membrane structure of the *ana*LptC mutant will be investigated by transmission electron microscopy. Moreover, the LPS isolation of the *ana*LptC mutant will be performed to define whether any alteration in LPS profile occurs.

To gain more insights about the functionality of *ana*LptC in LPS transport pathway, *in vitro* interaction of *ana*LptC with other *Anabaena* sp. Lpt components such as *ana*LptA and *ana*LptF will be analyzed. For this purpose, the periplasmic domain of the truncated *ana*LptC protein with His-tag and without the transmembrane segment, *ana*LptA with MBP-tag and the periplasmic loop of *ana*LptF containing GST-tag will be generated and heterologous expressed in *E. coli*. Afterwards, interaction studies of *ana*LptC with *ana*LptF and *ana*LptA will be performed via affinity chromatography methods. Furthermore, LptC and LptA from *E. coli* have been shown to bind LPS *in vitro* (Tran et al., 2010). To test whether the *ana*LptC periplasmic domain interacts with LPS of *E. coli* and to determine the dissociation constant (Kd) of *ana*LptC for *ec*LPS, interaction studies via fluorescence spectroscopy will be conducted.

Cyanobacterial LptC proteins appear to be different from those of proteobacteria, indeed, they are two times longer than proteobacterial proteins based on the sequence analysis. To answer the questions whether this observation holds true for the periplasmic domain of *ana*LptC, when compared to *ec*LptC, and whether *ana*LptC also has the characteristic β-jellyroll structure previously shown to be present in the five Lpt components such as LptF, LptG, LptA, LptC and LptD, the determination of the crystal structure of the *Anabaena* sp. LptC periplasmic domain will be performed by means of X-ray crystallography. To achieve this, the *ana*LptC periplasmic domain with a cleavable His-tag will be generated and expressed in *E. coli* cells. Then, the *ana*LptC periplasmic domain will be purified via His-tag by using Ni-NTA affinity chromatography, followed by the removal of His-tag prior size exclusion chromatography. The purified protein will be crystallized by sitting drop vapor diffusion technique. Properties of *ana*LptC will be investigated by the structural analysis using crystallographic data obtained from crystal structure of *ana*LptC in order to determine the structural and functional relationship in LPS transport.

2 Material and Methods

2.1 Material

2.1.1 Chemicals

Metal ingredients in form of salts were purchased from Merck (Darmstadt, Germany); Sigma-Aldrich (St Louis, USA); Roth (Karlsruhe, Germany) and VWR (Radnor, USA) to prepare media for cultivation of *Anabaena* sp PCC 7120. For preparation of plates, 1.5% bacto agar was used from Becton Dickinson GmbH (Heidelberg, Germany). *Anabaena* mutants grew in the presence of 5 µg/µl Streptinomycin purchased from Roth (Karlsruhe, Germany) and Spectinomycin purchased from Sigma (St Louis, USA). For cloning and conjugation with *E. coli*, ampicillin was ordered from Roth (Karlsruhe, Germany), kanamycin and chloramphenicol were purchased from Roth (Karlsruhe, Germany). Potassium sulfate BioXtra, ≥99.0% from Sigma-Aldrich (St Louis, USA) was used for protein crystallization.

2.1.2 Affinity chromatography

Glutathione Sepharose TM 4B for GST-tagged protein from GE Healthcare (München, Germany) Ni-NTA for His-tag protein from Qiagen (Hilden, Germany) and amylose resin for MBP-tagged protein from New England Biolab (Ipswich, USA) were purchased. In addition, Ni-NTA magnetic beads for pulldown assay via His-tag from Cube Biotech (Monheim, Germany) was used.

2.1.3 Enzymes and Kits

Pfu-polymerase was prepared by the working group Schleiff (Frankfurt, Germany) for cloning. T4-DNA ligase from Eppendorf (Hamburg, Germany), restriction enzymes from Fermentas (St. Leon-Rot, Germany) were used. Taq-polymerase prepared by the working group Schleiff (Frankfurt, Germany) was used for genotypic analysis. DNA extraction kits were ordered from Omega (VWR).For initial crystallization trials, commercial screening kits from Molecular Dimensions (Newmarket, UK) as well as NeXtal Classics II Suite crystallization kit from Qiagen (Hilden, Germany) were used.

2.1.4 Oligonucleotides

All oligonucleotides used in this study were purchased from Sigma Aldrich (Munich, Germany) and stored in 100 µM stock solution.

Table 1. Oligonucleotides used for cloning and screening in this study

Primer	Sequence	Purpose
all0231_fwd all0231_rev	CTGTGAGATCTCCGCAGAGTTACCCC CTGTGAGATCTGGTGAAGCGGAAAGTCCC	generation of single recombinant mutant
all0231_Scr_F all0231_Scr_R	CGGTATTCTCATTTCTCCCTGATTAGC GTAGCTTGTGGGGTTAAAGCTCC	screening for single recombinant mutant
alr4067_fwd alr4067_rev	CTGTGAGATCTGCCTTGCCTAACCAATTATCG CTGTGAGATCTCTAATTGGAACGTCG	generation of single recombinant mutant
alr4067_Scr_F alr4067_Scr_R	CGTAGCGTCAAGATTTCAGC CCTGTAGCAATGTAGAACGTCG	screening for single recombinant mutant
pCSV3-R	CTGATGCCGCATAGTTAAGCC	screening for single recombinant mutant
all0231_FX_fwd all0231_FX_rev	atatatGCTCTTCtAGTaaagctcccaataatactcaatcaaat tatataGCTCTTCaTGCattcctcgtgcttggttcttgtggaa	protein expression of *ana*LptC$_{\Delta TM}$-HRV 3C-His$_{10}$
T7, forward primer T7 term, reverse primer	TAATACGACTCACTATAGGG GCTAGTTATTGCTCAGCGG	sequencing of p7XC3H-all0231
alr4069_fwd alr4069_rev	GATCGGATCCGACAAACCCACGTTTAAGC GATCCTCGAGTTATTCTGCCAAGCTTAAGGG	protein expression of GST-*ana*LptF

2.1.5 Plasmids

The expression vector pGEX-6P-1 purchased from Cytiva (Amersham, UK) and p7XC3H from Addgene (Teddington, UK), which was derived from the vector backbone of pET26b, have been used for the generation of recombinant proteins *ana*LptF and *ana*LptC, respectively.

Table 2. Plasmids used in this study

Plasmid	Antibiotic resistance	Purpose	Reference
pCSV3	Sp^R Sm^R	insertion mutant	Elhai & Wolk, 1988
pCSV3-all0231	Sp^R Sm^R	insertion mutant	This study
pCSV3-alr4067	Sp^R Sm^R	insertion mutant	This study
pGEX-6P-1-alr4069	Amp^R	GST-*ana*LptF	This study
p7XC3H-all0231	Kan^R	*ana*LptC$_{\Delta TM}$-HRV 3C-His$_{10}$	This study
pMAL-c4x_anaLptA-MBP	Amp^R	*ana*LptA-MBP	Hsueh et al., 2015

2.1.6 *Anabaena* sp. PCC 7120 strains

Table 3. *Anabaena* sp. PCC 7120 strains

Strain	Resistance	Genotype	Reference
Anabaena sp. PCC 7120	-	wild-type	
AFS-I-*anaomp85*	Sp^R Sm^R	*alr2269*::pCSV3	Nicolaisen et al., 2009
AFS-I-*analptA*	Sp^R Sm^R	*alr4067*::pCSV3	This study
AFS-I-*analptC*	Sp^R Sm^R	*all0231*::pCSV3	This study
AFS-I-*analptD*	Sp^R Sm^R	*alr1278*::pCSV3	Hsueh et al., 2015

2.1.7 *E. coli* strains

DH5α and BL21 from Life Technologies (Darmstadt, Germany) were used for cloning and overexpression of proteins, respectively.

HB101 and RP-4 strains were used for conjugation with *Anabaena* (Wolk et al., 1984; Elhai & Wolk, 1988)

2.1.8 Media

BG11 medium was prepared according to Rippka et al., 1979 using stock solution 100x BG11 ($MgSO_4$ x 7 H_2O: 7.5 g; $CaCl_2$ x 2 H_2O: 3.6 g; citric acid: 0.6 g; ferric-ammonium citrate: 0.6 g; Na_2EDTA: 93 mg; Na_2CO_3: 2 g; H_3BO_3: 286 mg; $MnCl_2$ x 4 H_2O: 181 mg; $ZnSO_4$ x 7 H_2O: 22.2 mg; $NaMoO_4$ x 2 H_2O: 39 mg; $CuSO_4$ x 5 H_2O: 7.9 mg; $CoCl_2$ x 6 H_2O: 4.94 mg; fill up to 1 l with H_2O).

LB medium was prepared according to standard protocols for the growth of *E. coli* (Sambrook et al., 2001).

2.2 Methods

2.2.1 *Anabaena* sp. growth conditions

For the growth analysis, precultures was prepared by taking cell material from *Anabaena* sp. strains growing on BG11 plates not older than two weeks and incubated into 50 ml liquid BG11 media supplied with 17.6 mM of $NaNO_3$ as a source of nitrogen according to Rippka et al., 1979. The main cultures were incubated photo-autotrophically at 30° under constant shaking at 94 rpm and light intensity at 70 µmol photons*m-2*s-1 (Nicolaisen et al., 2009). The mutant strains were grown in presence of 5 µg*µl-1 Spectinomycin (Sp) and 5 µg*µl-1 Streptinomycin (Sm) as selection markers.

For the growth investigation in $BG11_0$ liquid media, the strains grown in BG11 were harvested and washed three times with $BG11_0$ before inoculation.

For the phenotyping analysis on plates, *Anabaena* sp. strains were grown in BG11 to an OD_{750nm} = 0.5. After being washed, samples were prepared with OD_{750nm} = 0.5 and OD_{750nm} = 1 for each strain. Then, 5 µl of these samples were spotted on onto the plates. Incubation was performed under constant white light and incubated at 30°C for 7 days.

For phenotyping in liquid media, *Anabaena* sp. cultures were inoculated with a start OD_{750nm} of 0.02. The OD_{750nm} was measured at indicated times using Jasco V-630 spectrophotometer. The experiment was performed four times with two biological samples and two technical measurements for each strain. Statistical significance of growth difference after indicated times was determined by t-test.

2.2.2 Generation of *Anabaena* sp. PCC 7120 insertion mutants

All strains used in this study are listed in the table 3. The mutants AFS-I-*analptD* and AFS-I-*anaomp85* were generated and characterized in previous publications (Nicolaisen et al., 2009; Hsueh et al., 2015). The mutants constructed in this study were generated by homologous recombination of PCSV3 carrying homologous fragment of the target genes according to described methods (Wolk et al., 1984; Elhai & Wolk, 1988; Elhai et al., 1997; Moslavac et al., 2007). In brief, a 450 bp internal homologous fragment of *analptC* (*all0231*) and 400 bp internal

homologous fragment of *analptA* (*alr4067*) were amplified by PCR on genomic DNA of *Anabaena* sp. wild-type, introducing BglII restriction sites with oligonucleotides listed in table 1. BglII digested PCR product was cloned into pCSV3 plasmid predigested with BamHI. The plasmid pCSV3 with the homologous gene fragment was used for conjugation in *Anabaena* sp. PCC 7120 wild-type to generate insertion mutants (Elhai et al., 1997). Homologous fragment cloned with blunt ends into the pCSV3 can be ligated into the vector in both direction, which can insert in the genome in both directions. Thus, colony PCR was performed to identify successfully inserted mutants and to check the directional insertion into the genome using oligosnucleotides binding to the antibiotic resistance cassette of pCSV3 plasmid as well as to regions located about 150-200 bp upstream or downstream from the homologous fragment cloned into pCSV3 plasmid.

2.2.3 Cloning, expression and isolation of *ana*LptC$_{\Delta TM}$-HRV 3C-His$_{10}$

Transmembrane helix truncated protein *ana*LptC$_{\Delta TM}$ encoded by *all0231* gene was constructed with a removable C-terminal His$_{10}$ tag by using FX Cloning kit (fragment exchanged cloning) of Addgene according to strategy described previously (Geertsma & Dutzler, 2011). DNA fragment encoding residues 27-385 of All0231 (*ana*LptC) protein was generated by PCR using genomic DNA of *Anabaena* sp. PCC 7120 with primer pairs listed in table 1 and cloned first into SapI restriction site of pINIT_cat cloning vector (Addgene) according to the protocol described in Sambrook et al., 1989. p7XC3H expression vector (Addgene) carrying the removable His$_{10}$ and HRV 3C protease recognition site was mixed with pINIT_cat containing *ana*LptC$_{\Delta TM}$ fragment in presence of SapI restriction enzyme. The mixture was incubated at 37°C for 1 h and followed by heat inactivation of enzyme at 65°C for 20 minutes. Ligation of fragments was performed by adding T4 ligase (Thermo scientific, Waltham, USA) and incubated further for 16 hours at 22°C (Sambrook et al., 1989). Subsequently, chemically competent E. coli MC1061 cells were transformed with the ligation mixture. MC1061 cells containing p7XC3H derivative encoding *ana*LptC$_{\Delta TM}$-HRV 3C-His$_{10}$ were selected on LB-agar supplemented with 7% (w/v) sucrose.

For protein expression of *ana*LptC$_{\Delta TM}$-HRV 3C-His$_{10}$, plasmids were transformed into *E. coli* strain BL21, which was grown in LB media supplemented with kanamycin (50 µg/ml) overnight at 37°C on shaker as described in Hsueh et al., 2015. The preculture was then diluted into 1 l fresh LB

media, inoculated at 37°C and induced by adding isopropyl-β-D-thiogalactopyranoside (IPTG) to a final concentration of 1mM at OD_{600nm} = 0.8 for 4 hours. The isolation of the heterologously produced protein was adopted from Hsueh et al., 2015 as described in the following section. Cells were harvested by centrifugation at 4°C and 6000 x g for 10 min, resuspended in lysis buffer (20 mM Tris-HCl pH 7.0, 150 mM NaCl) and lysed by using a French press (Thermo Scientific, Waltham, USA) at 1200 psi. Cell lysate is centrifuged (30 000 x g at 4°C for 30 min). Supernatant was collected and loaded onto Ni-NTA affinity resin (Qiagen, Hilden, Germany). After collecting the flow through for subsequent purification analysis, the resin was washed with wash buffer (20 mM Tris-HCl pH 7.0, 150 mM NaCl, 40 mM Imidazol). On-column cleavage of histidine tag via PreScission protease is performed in reaction buffer (50 mM Tris-HCl pH 7.0, 150 mM NaCl, 1 mM EDTA, 1 mM DTT). Here, an enzyme: protein ratio of 1:50 is used. After that, protein is collected in the flow-through. Subsequently, protein was further purified via size exclusion chromatography with Superdex 200 (GE Healthcare, München, Germany) with buffer consisting of 20 mM Tris-HCl pH 7.0 and 150 mM NaCl. For crystallization, the purified protein was concentrated to 10 mg/ml.

For expression of Selenomethionine-labeled protein, *E. coli* strain BL21 containing *ana*$LptC_{\Delta TM}$-HRV 3C-His_{10} vector was grown in 50 ml LB media supplemented with kanamycin (50 µg/ml) at 37°C (Hsueh et al., 2015). Cells were harvested after 17 hours and washed three times with 50 ml of autoclaved water. Cells were inoculated at 30 °C in 1 liter of freshly prepared SelenoMet base media and nutrients (Molecular Dimensions, Newmarket, UK) supplemented with 4 ml SelenoMethionine solution (Molecular Dimensions, Newmarket, UK) and antibiotics. Cells were induced by adding Isopropyl-β-D-thiogalactopyranoside (IPTG) with final concentration of 1 mM at OD_{600nm} = 0.5 and grown at 30 °C for 6 hours.

2.2.4 Production and isolation of GST-*ana*LptF protein

For the production of N- terminally GST-tagged *ana*LptF, gDNA of *Anabaena* sp. was used to amplify a 339 bp gene fragment of *alr4069* (*analptF*) coding for the soluble domain by PCR using primers with the BamHI and XhoI restriction sites (Table 1). The PCR fragment was cloned into BamHI and XhoI restriction sites of the pGEX-6P-1 vector (GE Health care, München, Germany).

For protein expression, *E. coli* BL21 cells were transformed with this plasmid and grown in LB media supplemented with ampicillin (50 µg/ml) overnight at 37°C (Hsueh et al., 2015). 1 l LB-media inoculated with the preculture, was incubated at 37°C and protein expression induced at OD_{600nm} = 0.8 by addition of 1mM isopropyl-β-D-thiogalactopyranoside (IPTG). After four hours, cells were harvested by centrifugation (4°C; 6000 x g; 10 min). N-terminal GST-*ana*LptF protein was purified using Glutathione Sepharose beads (GE Healthcare, München, Germany). Cells were resuspended in 30 ml binding buffer (140 mM NaCl; 2.7 mM KCl; 10 mM Na_2HPO_4 and 1.8 mM KH_2PO_4; pH 7.3) and passed three times through French press (1200 psi). Subsequently, lysate was cleared by centrifugation at 30000 x g for 30 minutes at 4 °C. Supernatant was collected and loaded onto Glutathione Sepharose beads. After collecting the flow through for subsequent purification analysis, the resin was washed four times with 5 ml binding buffer. Protein was collected three times 1 ml each with elution buffer (50 mM Tris pH 8.0; 10 mM reduced Glutathione (Sigma Aldrich, St Louis, USA) and 10 mM NaOH)

2.2.5 Production and isolation of *ana*LptA-MBP protein

Expression and isolation of *ana*LptA-MBP were performed following previously described protocol (Hsueh et al., 2015) with some modifications. *E. coli* strain BL21 containing construct of C-terminally MBP-tagged *ana*LptA was grown in LB medium added with ampicillin (50 µg/ml). This culture was transferred in to 1 l fresh LB medium with a dilution of 1: 50 and inoculated at 37°C until it reached an OD_{600nm} = 0.8. Protein overexpression was induced by addition of 1mM isopropyl-β-D-thiogalactopyranoside (IPTG) for four hours. Then cells were harvested by centrifugation (4°C; 6000 x g; 10 min) and resuspended in binding buffer (20 mM Tris pH 7.5; 150 mM NaCl). Lysate obtained after passing through French press (Thermo scientific, Waltham, USA) at 1200 psi three times was cleared by centrifugation at 30000 x g for 30 minutes at 4 °C. The supernatant was loaded onto with binding buffer pre-equilibrated amylose resin (New England Biolab, Ipswich, USA). After the bound resin was washed five times with binding buffer, the bound proteins were eluted with elution buffer (20 mM Tris pH 7.5; 150 mM NaCl and 100 mM maltose).

2.2.6 Analysis of protein-protein interaction

The *in vitro* protein-protein interaction analysis was carried out as described previously (Hsueh et al., 2015). Briefly, 5 µg of purified *ana*LptC$_{\Delta TM}$-HRV 3C-His$_{10}$ and 5 µg *ana*LptA-MBP were added to 200 µl reaction buffer (20 mM Tris-HCl pH 7.0 and 75 mM NaCl). The reaction was incubated at 4°C for 15 min on a rotary shaker to allow formation of protein complexes. Next, 5 µl Ni-NTA magnetic bead from Cube Biotech (Monheim, Germany) was added to the reaction mixture. After the supernatant was collected, the resin was then washed four times 100 µl each with wash buffer (20 mM Tris-HCl pH 7.0, 75 mM NaCl and 20 mM Imidazol) to ensure complete removal of any unbound proteins. The protein complex was eluted with 50 µl of elution buffer (20 mM Tris-HCl pH 7.0, 75 mM NaCl and 400 mM Imidazol). The formation of protein complex was separated by 12% SDS-PAGE, examined and visualized by western blotting, Silver staining and Coomassie colloidal.

5 µg GST-*ana*LptF, 5 µg *ana*LptC$_{\Delta TM}$-HRV 3C-His$_{10}$ and 7 µg *ana*LptA-MBP were used to determine complex formation between proteins with the same procedure performed as described above.

2.2.7 *In vitro* crosslinking of *ana*LptC$_{\Delta TM}$-His$_{10}$ protein

A series of different crosslinkers were used for *in vitro* crosslinking experiments of *ana*LptC$_{\Delta TM}$-His$_{10}$ protein performed with the help from Dr. Roman Ladig according to the protocol from Iacobucci et al., 2018. Briefly, purified recombinant proteins were incubated with one of crosslinkers in buffer composed of 20 mM HEPES, pH 7.5, 150 mM NaCl at 4°C for 60 minutes. Final concentrations of crosslinkers used are 50 mM for dihydrazide sulfoxide (DHSO); 0.5 mM for zero length protein crosslinker N,N'-carbonyldiimidazole (CDI); 10 mM for disuccinimidyl dibutyric urea (DSBU) and 10 mM disuccinimidyl sulfoxide (DSSO). The crosslinking reaction was inactivated by adding quenching solution of 25 mM Tris or NH_4HCO_3.

The crosslinked peptides were analyzed by LC-MS/MS using an ultra-HPLC Proxeon EASY-nLC 1000 system coupled online to Q Exactive Plus mass spectrometer (Thermo Fisher Scientific, Waltham, USA). Reversed-phase separation was performed using a 30 cm analytical column (100 µm diameter) DNU-MS (Novak) packed in-house with Reprosil-Pur 120 C18-AQ (2.4 µm

diameter). Mobile-phase solvent A consisted of 0.1% formic acid and 4% acetonitrile in water, and mobile-phase solvent B consisted of 0.1% formic acid in 80 % acetonitrile. The flow of the gradient rate was set to 200 nl/min. A 90-min gradient was used (0–40% solvent B within 60 min, 40–100% solvent B within 10 min, 100% solvent B for 10 min, 100–0% solvent B within 5 min and 0% solvent B for 5 min).

Data acquisition was performed with the ddMS2 method (Brouwer et al., 2019). For the MS scans, the scan range was set to 250–2,000 m/z at a resolution of 70,000, and the automatic gain control (AGC) target was set to 1×106. For the MS/MS scans, top 15 ions were chosen, the resolution was set to 35,000, the AGC target was set to 1×105, the precursor isolation width was 2 Da and the maximum injection time was set to 80 ms.

MaxQuant was used to analyze the LC-MS/MS data (Cox & Mann, 2008), which allows identification analysis. The Uniprot reference *Nostoc* database (proteomes – *Nostoc* (*Anabaena* sp. PCC 7120 / SAG 25.82 / UTEX 2576) and the Uniprot reference *E. coli* strain K12 database (proteomes – *E. coli* (strain K12 / MG1655 / ATCC 47076) were used for the identification of target and contaminating proteins, respectively. Default settings for fixed modifications were used. Dynamic modifications were set: Oxidation for M and Acetylation for K. Contaminants were included for peptide detection of a minimum length of 6 amino acids.

2.2.8 Transmission electron microscopy (TEM)

Phenotypic analysis of *Anabaena* sp. strains was performed via TEM according to Tripp et al., 2012. *Anabaena* sp. strains were grown in 50 ml BG11 medium to a OD_{750nm} = 2. Cells were harvested and washed twice with buffer (80 mM Na-Cacodylat pH 7.3 and 10% (w/v) saccharose). Then, the sample was treated with fixation buffer (80 mM Na-Cacodylat pH 7.3 and 2% (v/v) Glutaraldehyd) for 4 hours. Subsequently, cells were embedded in araldite and incubated at 60°C for 48 hours. The specimen was prepared with a thickness of 50 nm, investigated with Zeiss EM 900 and documented with CCD camera.

2.2.9 Crystallization of proteins

Crystallization experiments for *ana*LptC$_{\Delta TM}$-HRV 3C-His$_{10}$ and *ana*LptC$_{\Delta TM}$ without His-tag proteins using sitting drop vapor diffusion technique were performed in 96-well plates at 290.15 K with a 1:1 ratio of protein and precipitant solutions (0.5 µl of each) according to standard protocols as described in Ducruix & Giege´, 1999. The initial crystals of protein grew after 3-7 days in condition composed of 16% PEG 8000; 20% Glycerol and 0.06 M K_2SO_4 as well as in conditions of commercial screens such as Clear Strategy™ Screen I HT-96, HELIXTM HT-96 and PACT premierTM HT-96 (Molecular dimensions, Newmarket, UK).

Optimizations were performed by varying concentration of salt, precipitant and screening additives from Morpheus crystallization screen (Molecular dimensions, Newmarket, UK).

2.2.10 Data collection and data processing

Crystals were cryoprotected by treatment with reservoir buffer containing 18% sucrose before flash-cooling in liquid nitrogen (Köster et al., 2009). Data collection was performed at the synchrotron radiation facilities such as P13 beamline of the German Electron Synchrotron (DESY); ID30A-3, ID29 and ID23-1 beamlines of the European Synchrotron Radiation Facility (ESRF) and X10SA (PXII) beamline at the Swiss Light Source (SLS) under the stream of nitrogen gas at 100 K. Data indexing, integration, and scaling were performed using the XDS program package (Kabsch, 1993; Kabsch, 2010).

2.2.11 Isolation of LPS from *Anabaena* sp.

LPS was isolated from *Anabaena* sp. strains according to described methods (Apicella et al., 1994). In brief, 1 ml of cells at OD_{750nm} = 0.6 from BG11 cultures were harvested and washed three times by centrifugation at 14000 rpm for 2 minutes with 1 ml cold 1x PBS. Cells were resuspended in 50 µl lysis buffer of 60 mM Tris/HCl pH 6.8; 1 mM EDTA; 2% SDS; 4% 2-mercaptoethanol; 10% glycerol and bromphenol blue. The sample was boiled at 95°C for 10 min and 5 min of incubation at room temperature. 10 µg/µl proteinase K were added to the sample

incubated at 60°C for 1h. LPS was separated by 14% polyacrylamide gels by SDS-PAGE and visualized by silver staining.

2.2.12 Determination of tryptophan fluorescence

The tryptophan fluorescence was determined by following the previously described protocol (Brouwer et al., 2019) with some modifications. In brief, 2 µM of the purified *ana*LptC$_{\Delta TM}$-His$_{10}$ were added in buffer (20 mM Tris pH 7.5 and 75 mM NaCl) in addition of 8 M urea, 2 % (v/v) acrylamide or 1 mg LPS. The samples were incubated for 15 min at room temperature before excitation at 250 nm. The fluorescence spectra were recorded from 300 nm to 440 nm.

To determine the dissociation constant K_D of *ana*LptC$_{\Delta TM}$-His$_{10}$ protein for LPS, concentrations of 1.25; 2.5; 3.75; 5; 9.5; 15.5; 25; 50; 62.5 µM LPS were used. These indicated concentrations of LPS of *E. coli* strain O111:B4 purchased from Sigma Aldrich (St Louis, USA) were mixed with 0.2 µM protein. After the indicated sample was excited at 250 nm, fluorescence spectra were monitored and recorded from 300 nm to 440 nm. The values were analyzed with sigma plot using the equation least square fit analysis (f = a*x/(b+x) + y0).

3 Results

3.1 The putative LptC protein in *Anabaena* sp. PCC 7120 encoded by *all0231* is involved in outer membrane biogenesis

3.1.1 The putative LptC protein in *Anabaena* sp. PCC 7120

The *all0231* encoded protein assigned as *ana*LptC was identified as a potential homologue of LptC in *Anabaena* sp. using the protein family database Pfam (http://pfam.xfam.org) based on the secondary structure of *E. coli* LptC (*ec*LptC). The result from Pfam algorithm (El-Gebali et al., 2019) showed three significant hits related to the LptC structural protein family PF06835 found in three regions of the *ana*LptC protein with E-values of 1.0e-12; 3.1e-09 and 2.0e-07 for the corresponding regions of residues 15-124; 152-244 and 254-365, respectively (Figure 4).

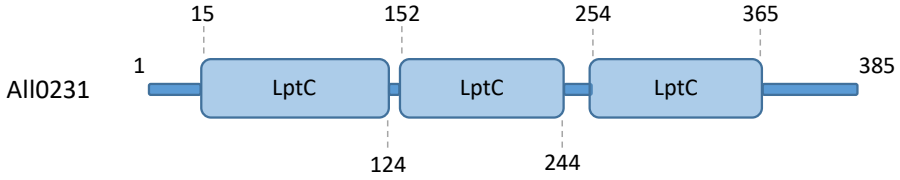

Figure 4: All0231 protein predicted as the *Anabaena* sp. homologue of LptC via Pfam algorithm.
Pfam analysis identified three regions of the All0231 protein related to LptC structural protein family involved in lipopolysaccharide assembly. The first and the last amino acid of the three regions with the corresponding significant E-values are depicted on the All0231 protein sequence. LptC stands for the Lipopolysaccharide-assembly, LptC related domain identified with E-value of 1.0 e-12, 3.1 e-09 and 2.0 e-07, respectively.

Although the *ana*LptC protein of 385 amino acids is significantly longer in comparison to *ec*LptC of 191 amino acids, they share a series of similarities in their amino acid sequence in an alignment performed with T-Coffee (Figure 5). Furthermore, the secondary structure prediction analysis via the HHpred server (Söding et al., 2005) indicated that the two proteins have high structural similarities, whereby both *ana*LptC and *ec*LptC contain the transmembrane helix located near the N-terminus predicted by TMHMM (Krogh et al., 2001) with residues Asn^{7}- Val^{26} and Trp^{7}- Ala^{25}, respectively. Additionally, the *ana*LptC protein was predicted to contain many β-strands found in *ec*LptC (Figure 5). Therefore, the data presented here strongly suggest that *ana*LptC is the homologue of *ec*LptC.

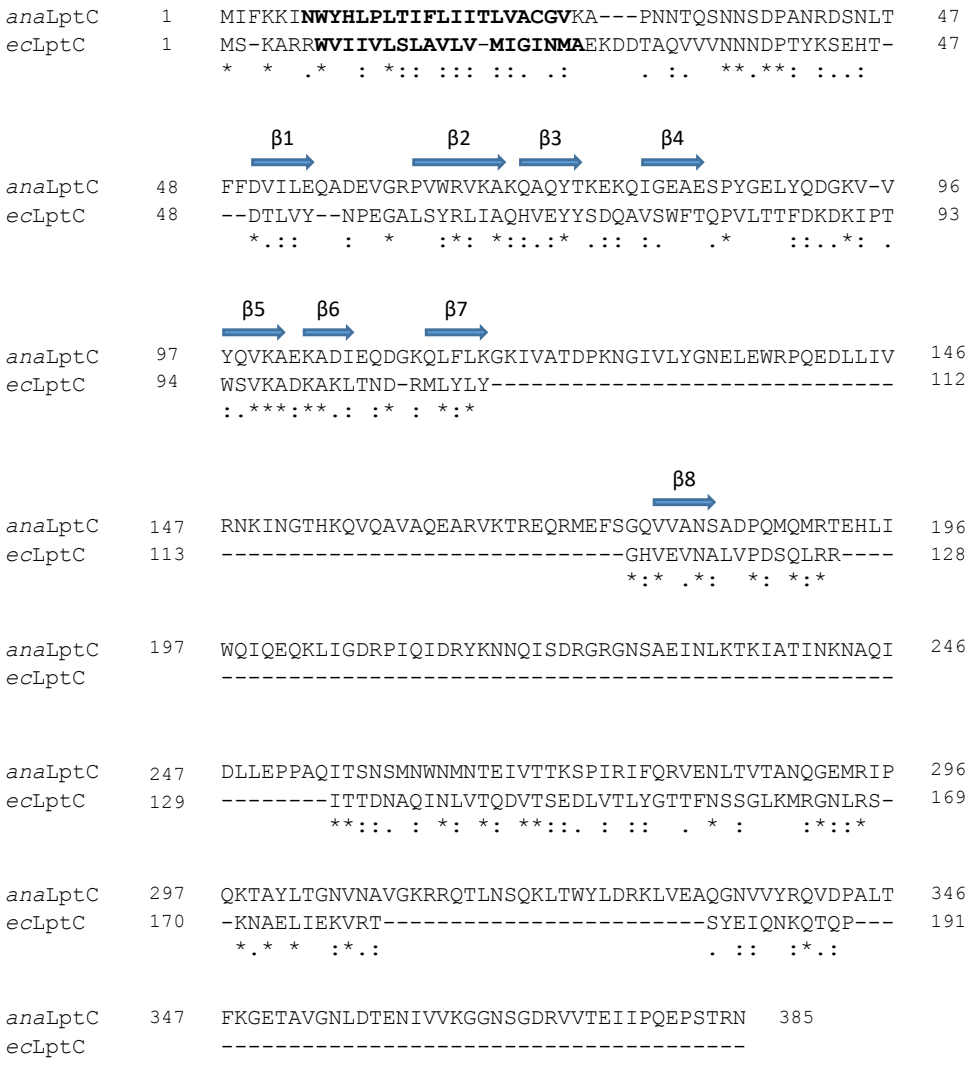

Figure 5: Alignment between *ana*LptC and *ec*LptC proteins.
Amino acid sequence of *ana*LptC encoded by the gene *all0231* from *Anabaena* sp. was aligned with that of LptC from *E. coli* (*ec*LptC). The protein sequence alignment was performed with T-coffee showing conserved residues with high sequence identity or similarity (https://www.ebi.ac.uk/Tools/msa/tcoffee/). Secondary structure alignment between *ana*LptC and *ec*LptC (PDB 3MY2) created with HHpred server (Söding et al., 2005) predicted regions containing β-strands in the two proteins. Both proteins were predicted to contain a short transmembrane helix shown in bold letter.

3.1.2 Genotypic analysis of the *analptC* insertion mutant

To clarify whether *ana*LptC is involved in outer membrane biogenesis in general and in LPS biogenesis in particular *in vivo*, an *Anabaena* sp. LptC insertion strain, AFS-I-*analptC*, was generated via interruption of the *analptC* gene with the pCSV3 plasmid by homologous recombination. In addition, an *analptA* insertion mutant was generated to compare its phenotype with that of *analptC* mutant as well as mutant of the other *lpt* gene like *analptD*, since

mutants of the same transport pathway might show a similar phenotype. The interruption of *analptC* and *analptA* genes via the pCSV3 plasmid insertion was verified by PCR with two independent conjugates for each strain using isolated genomic DNA as templates. The directional insertion of the plasmid into the genome was analyzed using one oligonucleotide binding to the antibiotic resistance cassette of the plasmid and one of the two gene specific oligonucleotides located about 150-200 bp either upstream or downstream from the homologous fragment (Figure 6 A).

The result showed all conjugates of both strains AFS-I-*analptC* and AFS-I-*analptA* contained the pCSV3 plasmid inserted in their genomic DNA. However, both AFS-I-*analptC* conjugates were not segregated as the wild-type copy of the *analptC* gene amplified with gene specific oligonucleotides was observed (Figure 6 B, left, upper lane). While both AFS-I-*analptA* conjugates were segregated as the wild-type copy of the *analptA* gene was not available (Figure 6 B, right, upper lane). The presence of non-segregated AFS-I-*analptC* mutants indicated that *ana*LptC might be essential for the cell viability.

This hint is in agreement with the result obtained from the preliminary growth analysis of AFS-I-*analptC* and AFS-I-*analptA* mutants (Figure 6 C). To judge their growth behaviors, the growth of AFS-I-*analptC* and AFS-I-*analptA* mutants was performed in BG11 as well as $BG11_0$ liquid cultures and compared with wild-type, AFS-I-*analptD* and AFS-I-*anaomp85*. The standard medium BG11 was supplemented with nitrogen source, which was omitted in the $BG11_0$ medium. In previous studies *Anabaena* sp. LptD and Omp85 have been shown to be essential for cell viability, as fully segregated mutants of AFS-I-*analptD* and AFS-I-*anaomp85*, respectively, were not generated (Nicolaisen et al., 2009; Hsueh et al., 2015). As expected, two strains AFS-I-*analptD* and AFS-I-*anaomp85* were not able to grow in the $BG11_0$ medium. Similarly, AFS-I-*analptC* did not survive in this medium either. However, all three strains AFS-I-*analptC*, AFS-I-*analptD* and AFS-I-*anaomp85* grew but slowly in standard medium BG11 when compared to wild-type. AFS-I-*analptA* showed the same growth behavior in BG11 but slower growth in $BG11_0$ in comparison to wild-type (Figure 6 C). Taken together, this result demonstrated the essential role of the *ana*LptC protein in cell viability under both normal and no nitrogen source conditions.

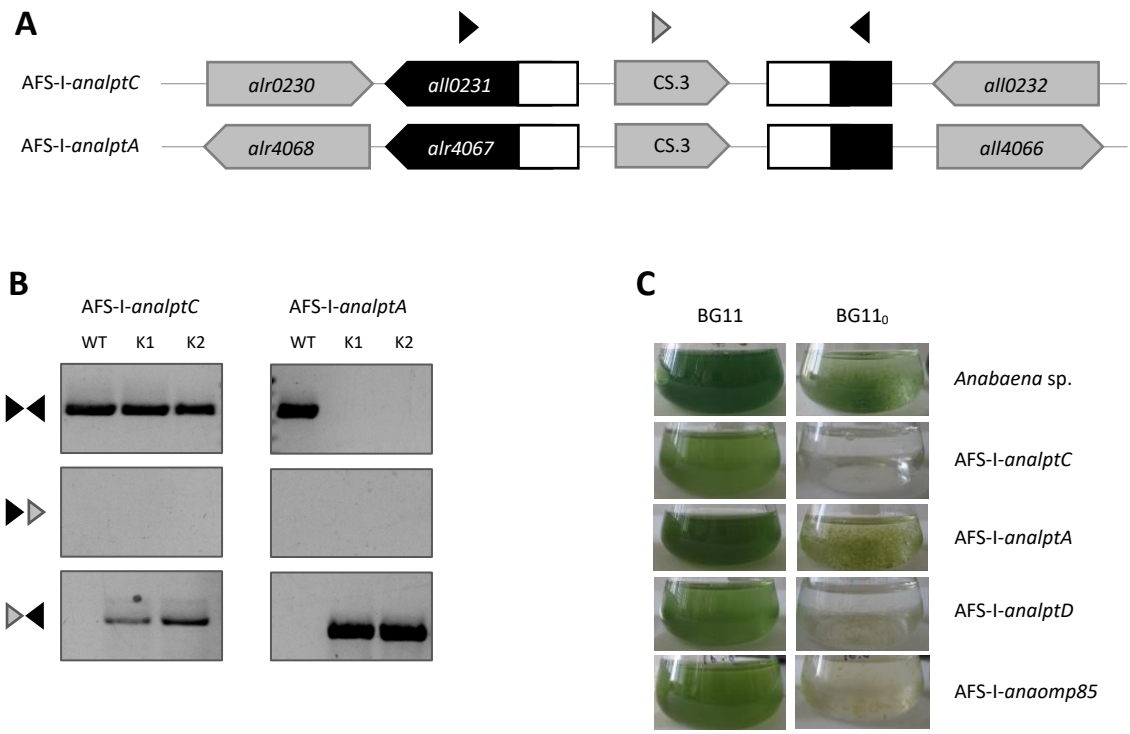

Figure 6: Generation of AFS-I-*analptC* and AFS-I-*analptA* insertion mutants.
A) Schematic representation of the genomic organization in the AFS-I-*analptC* and AFS-I-*analptA* mutants. The *all0231* gene encoding putative LptC and *alr4067* encoding LptA in *Anabaena* sp. are interrupted and colored in black. Homologous fragments are colored in white. Resistance cassette CS.3 is colored in grey. The black triangles show gene specific oligonucleotides, while oligonucleotide binding on resistance cassette is presented in grey triangle. B) Insertion mutants and segregation analyses were investigated by PCR using genomic DNA as templates isolated from two independent conjugates (K1, K2) of AFS-I-*analptC* (left) and AFS-I-*analptA* (right). Genomic DNA from wild-type *Anabaena* sp. strain (WT) was used as control. C) Growth behaviors of AFS-I-*analptC* in BG11 and $BG11_0$ liquid cultures in comparison to wild-type *Anabaena* sp. strain and AFS-I-*analptA*, AFS-I-*analptD*, AFS-I-*anaomp85* mutants.

3.1.3 Phenotypic characterization of mutants of factors involved in LPS transport

The outer membrane acts as an important barrier of the cell maintained by the extracellular lipopolysaccharide layer as well as outer membrane proteins, which provide the structural integrity of the outer membrane against toxic substances (Nikaido, 2003; Delcour, 2009; Wang et al., 2015). The altered outer membrane integrity of AFS-I-*anaomp85* and AFS-I-*analptD* mutants documented in previous publications demonstrated that the defect in Omp85, that is involved in the insertion of outer membrane proteins, and LptD protein of the LPS transport in *Anabaena* sp. leads to sensitivity of these mutants to chemical treatments due to increased permeability of the outer membrane (Nicolaisen et al., 2009; Hsueh et al., 2015). Therefore, the insertion strain AFS-I-*analptC* generated by homologous recombination was also treated with

different chemicals in growth experiments in order to elucidate the role of *ana*LptC in outer membrane biogenesis *in vivo* and compare the growth effect among mutants of other Lpt factors involved in the transport of LPS.

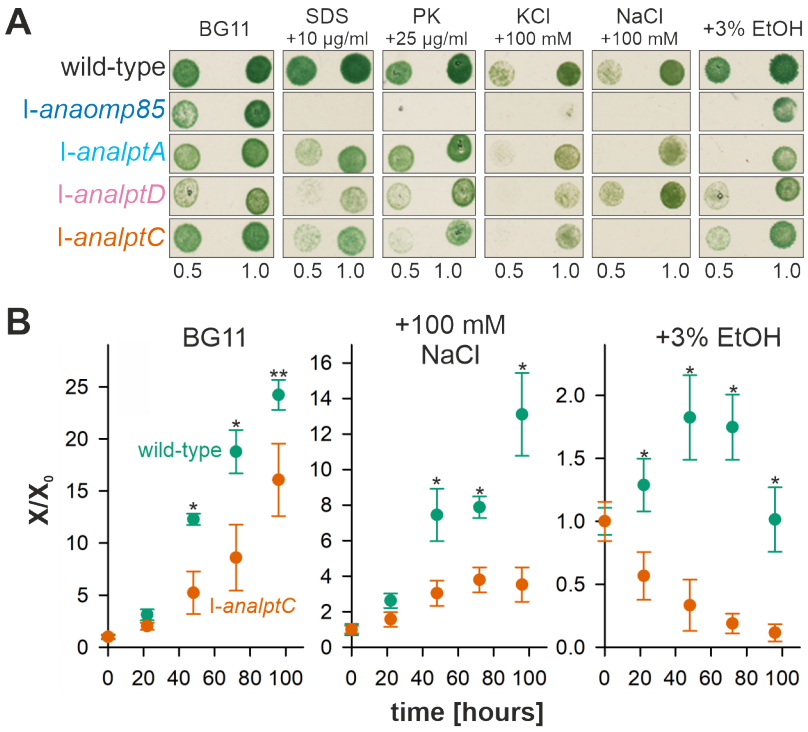

Figure 7: Phenotypic analysis of *analptC* mutant in comparison with other *Anabaena* sp. strains.
A) Growth analysis on solid BG11 media. The *Anabaena* sp. wild-type strain and mutants AFS-I-*analptC*, AFS-I-*analptA*, AFS-I-*analptD*, AFS-I-*anaomp85* were grown in BG11 liquid culture for 5 days. After the cells were washed three times with BG11 liquid media, 5 µl of cells with $OD_{750\,nm}$ of 0.5 and 1 were spotted on the solid BG11 media supplemented with sodium dodecyl sulfate (SDS), proteinase K (PK), KCl, NaCl and ethanol with the indicated concentration. The plates were incubated for further 7 days before imaging. B) Growth of *Anabaena* sp. wild-type strain (green) and *analptC* mutant (orange) in BG11 liquid media supplemented with 100 mM NaCl or 3% ethanol and growth monitored at OD_{750nm}. The average of eight replicas is shown. The statistical significance of growth difference was determined by t-test and $p<0.01$ (**) or $p<0.001$ (*) is indicated.

For the growth analysis, all five strains, *Anabaena* sp. wild-type, AFS-I-*analptC*, AFS-I-*analptA*, AFS-I-*analptD* and AFS-I-*anaomp85*, were grown on solid BG11 medium supplemented with different substances such as ethanol, sodium chloride, potassium chloride, SDS and proteinase K to investigate the permeability of the outer membrane in these strains. The growth of four strains AFS-I-*analptC*, AFS-I-*analptA*, AFS-I-*analptD* and AFS-I-*anaomp85* on BG11 plates was reduced in comparison to wild-type, while AFS-I-*analptD* mutant showed most affected with cells looked very pale even on the standard medium containing nitrogen source (Figure 7 A, first column). On BG11 plates supplemented with SDS, proteinase K and potassium chloride the growth of AFS-I-*analptC*, AFS-I-*analptA* and AFS-I-*analptD* was reduced in comparison to wild-type, while the

growth of AFS-I-*anaomp85* was diminished (Figure 7 A, second to fourth column). On BG11 plates containing sodium chloride the growth of AFS-I-*anaomp85* and AFS-I-*analptC* was completely diminished, while AFS-I-*analptA* and AFS-I-*analptD* reduced their growth when compared to wild-type (Figure 7 A, fifth column). The growth of all mutants compared to wild-type was inhibited in the presence of 3% ethanol. AFS-I-*analptC* and AFS-I-*analptD* exhibited the same reduction of growth, while AFS-I-*analptA* and AFS-I-*anaomp85* showed similarly reduced growth (Figure 7 A, sixth column).

To gain more details about the osmotic stress behavior of the *analptC* mutant, AFS-I-*analptC* and *Anabaena* sp. wild-type strains were grown in the BG11 liquid media added with 100 mM NaCl or 3% ethanol. The result is consistent with the previous result on the solid media and showed that AFS-I-*analptC* mutant grew slower in BG11 in comparison to wild-type (Figure 7 B, left). AFS-I-*analptC* immediately reduced the growth after being transferred to liquid media containing 3% ethanol, while wild-type grew steadily and reduced the growth after 60 hours (Figure 7 B, right). In the presence of NaCl, both strains grew much slower when compared to the standard condition. The growth of AFS-I-*analptC* declined after 80 hours in condition containing 100 mM NaCl (Figure 7 B, middle).

The observed increased permeability phenotype of AFS-I-*analptC* with reduced growth in conditions containing ethanol, salt, SDS and proteinase K is a hint that the structure of the outer membrane might be destabilized, or the content of lipopolysaccharides (LPS) might be altered. Hence, the LPS content of AFS-I-*analptC* was isolated, analyzed and compared with *Anabaena* sp. wild-type and AFS-I-*anaomp85*. For that, one milliliter of cells from culture of each strain grown to exponential phase with an optical density of 0.6 at 750 nm was used. After washing one time in cold phosphate-buffered saline (PBS), the bacterial pellets were solubilized in buffer containing sodium dodecyl sulfate (SDS) and boiled at 95°C for 10 minutes in order to obtain the whole cell lysate. For preparations of LPS samples, the whole cell lysate was added with proteinase K and incubated at 60°C for one hour. The digested products were subjected to SDS-polyacrylamide gel electrophoresis (PAGE) followed by silver staining for visualization of LPS profiles. The whole cell lysate samples without proteinase K treatment were used for the determination of protein

profiles, which were investigated by SDS-PAGE and visualized by Coomassie staining for the loading control.

The results revealed that protein profiles were comparable among the three strains *Anabaena* sp. wild-type, AFS-I-*analptC* and AFS-I-*anaomp85* (Figure 8, right). The silver-stained SDS-PAGE of LPS samples from the three strains showed the typical LPS migration pattern of Gram-negative bacteria including the variable-sized O-antigen containing LPS, the core region and the lipid A moieties (Figure 8, left). The content of the core region and the lipid A was comparable in all strains. Whereby the AFS-I-*anaomp85* strain showed the content of O-antigen containing LPS was slightly decreased in comparison to wild-type. In contrast, the amounts of the LPS with O-antigen detected in the AFS-I-*analptC* strain were very low.

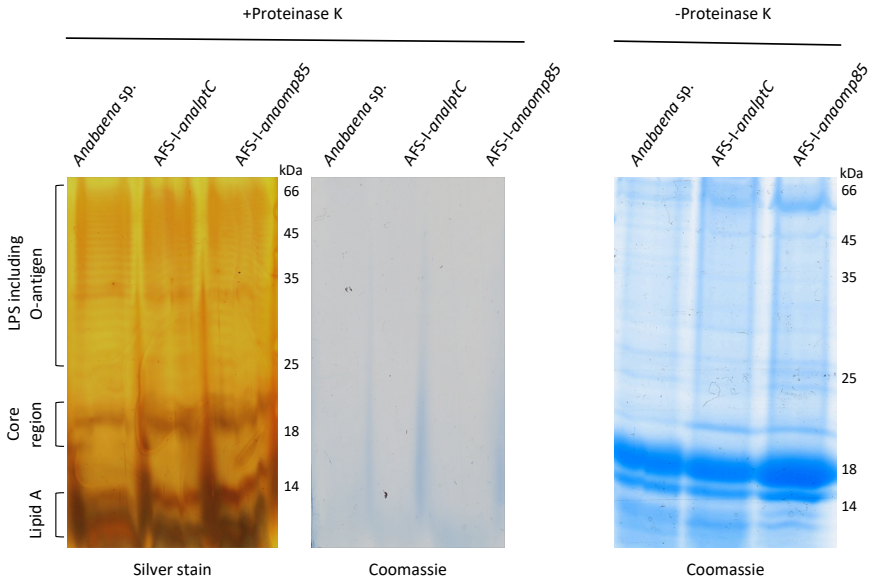

Figure 8: Analysis of LPS content in *analptC* mutant in comparison with other *Anabaena* sp. strains.
Cell envelopes were isolated from *Anabaena* sp. wild-type, AFS-I-*analptC* and AFS-I-*anaomp85* grown to exponential phase with an optical density of 0.6 at 750 nm in BG11 media. The sample before (right) and after (middle) proteinase K treatment was subjected on SDS-PAGE and then stained with Colloidal Blue to visualize proteins. The sample after proteinase K treatment was loaded on SDS-PAGE followed by silver staining for visualization of LPS (left). The migration pattern of the O-antigen including LPS, the core region and the lipid A was indicated.

Motivated by these findings, ultra-structure of the outer membrane in AFS-I-*analptC* was investigated and compared to AFS-I-*analptA*, AFS-I-*analptD* and *Anabaena* sp. wild-type by transmission electron microscope (TEM). All mutants grown in BG11 liquid media showed a reduction in cell size and cell length when compared to *Anabaena* sp. wild-type (Figure 9, left and middle columns). Cell width was reduced in AFS-I-*analptA*, while it was increased in AFS-I-*analptC*. Remarkably, the distance of septum between the two neighbor cells was enhanced in

AFS-I-*analptC* mutant (Figure 9, second row, right column). Nevertheless, the typical cell envelope composed of the plasma membrane, the peptidoglycan layer and the outer membrane was observed in all strains (Figure 9, right column).

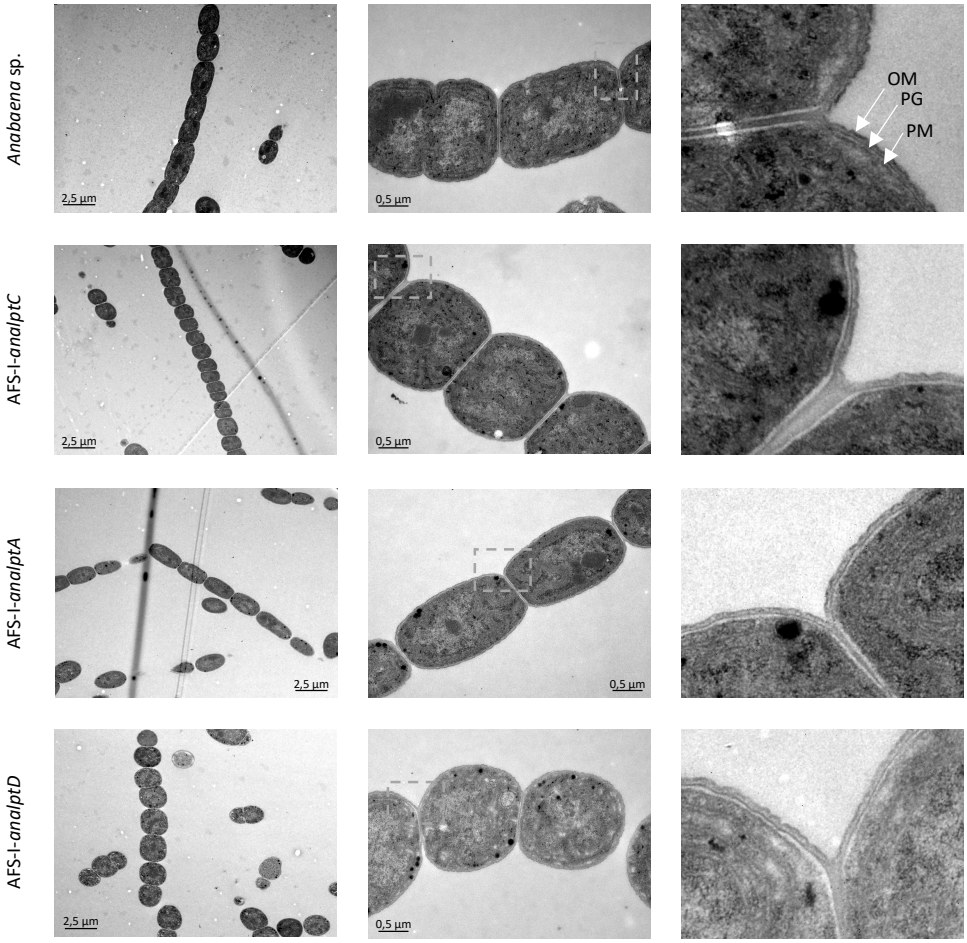

Figure 9: Ultra-membrane structure in *Anabaena* sp. strains.
The cells of *Anabaena* sp. wild-type, AFS-I-*analptC*, AFS-I-*analptA* and AFS-I-*analptD* cultured in BG11 media were investigated by transmission electron microscopy (TEM). The plasma membrane (PM), the peptidoglycan layer (PG) and outer membrane (OM) were indicated by the white arrows. The left images show up to 25-fold magnification of regions indicated by the dashed squares on the middle images.

For comparison of the three mutants of factors involved in LPS transport with wild-type cellular parameters were quantified. This analysis shows that reduction of cell length is a significant phenotype of AFS-I-*analptD* and AFS-I-*analptC* (Figure 10, left). The cell width is reduced in AFS-I-*analptA,* while it is enhanced in AFS-I-*analptC.* Calculating the volume of a cell assuming an ellipsoid like structure and using the median values for length and width revealed a volume of about 5.6 µm^3 for wild-type cells, of 4.4 µm^3 for AFS-I-*analptD*, of 3.3 µm^3 for AFS-I-*analptC* and of 2.6 µm^3 for AFS-I-*analptA.* Hence, the mutants of the LPS transfer system consistently show a

smaller cell size, and the reduction is not as pronounced in the partial segregated strains when compared to the fully segregated AFS-I-*analptA.*

The distance between the two plasma membranes in the septal junction as well as between plasma membrane (center) and the outward facing rim of the outer membrane was quantified as well (Figure 10, right). For AFS-I-*analptC* an enhanced spetal dimension was observed, while all mutants showed a reduced distance between plasma and outer membrane. Again, the fully segregated strain AFS-I-*analptA* was most drastically affected. This reduction is in line with a reduced deposition of LPS to the outward facing monolayer of the outer membrane.

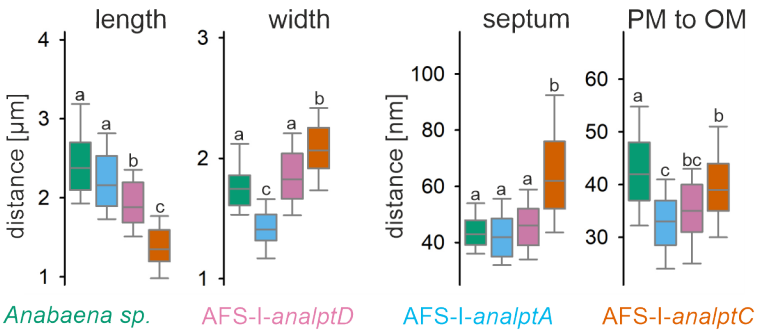

Figure 10: Quantification of ultra-membrane structure properties in *Anabaena* sp. strains.

The length and width of cells based on electron microscopic images (cells>70; more than 3 filaments) as well as the size of the septum (from plasma membrane to plasma membrane; cells>30; three randomly selected positions per septum) and the distance between middle of the plasma membrane and the outer side of the cell envelope (cells>50; five randomly selected positions per cell). The significance of the difference ($p<0.05$) was determined by ANOVA one way. The color code is indicated on the bottom.

3.2 The *in vitro* interactions of the *ana*LptC periplasmic domain

3.2.1 The *ana*LptC periplasmic domain interacts with *Anabaena* sp. LptF homologue

The periplasmic component *E. coli* LptC (*ec*LptC), which has a β-jellyroll structure, forms a complex with the inner membrane ABC transporter $LptB_2FG$ (Narita & Tokuda, 2009). Any single-residue substitution at the amino terminal region of the β-jellyroll structure of LptC disrupts the complex formation with $LptB_2FG$ indicating that the N terminus of the β-jellyroll of LptC is essential for the interaction with LptF and/or LptG (Villa et al., 2013; Okuda et al., 2016). In fact, crystallographic and crosslinking data demonstrated that *ec*LptC anchored in the inner membrane by a single transmembrane helix interacts with *ec*LptF via an edge to edge interaction

between their N- and C-terminal β-stranded regions in the β-jellyrolls, respectively (Owens et al., 2019).

In *Anabaena* sp. one reading frame identified with high similarity to both LptF and LptG from *E. coli* was Alr4069 designated *ana*LptF. To probe whether *ana*LptC interacts with *ana*LptF as shown in *E. coli*, constructs of the periplasmic domain of *ana*LptC and the periplasmic loop of *ana*LptF were generated. The periplasmic loop of *ana*LptF predicted to contain β-strands based on the secondary structural analysis was fused to N-terminal GST tag, while the periplasmic domain of *ana*LptC without the transmembrane helix was cloned with C-terminal His_{10} tag to generate a derivative p7XC3H encoding *ana*$LptC_{\Delta TM}$-HRV 3C-His_{10} protein (herewith *ana*$LptC_{\Delta TM}$-His_{10}). Recombinant proteins GST-*ana*LptF (40 kDa) and *ana*$LptC_{\Delta TM}$-His_{10} (43 kDa) were overexpressed in *E. coli* and purified via affinity chromatography. Via Ni-NTA affinity chromatography, *ana*$LptC_{\Delta TM}$-His_{10} was produced with high purity. However, the purification of GST-*ana*LptF using Glutathione Sepharose showed low purity, because fragment with the expected molecular weight but also additional fragments were purified (Figure 11 A).

To test whether *ana*LptC interacts with *ana*LptF, both purified proteins GST-*ana*LptF and *ana*$LptC_{\Delta TM}$-His_{10} were mixed together and incubated for 30 minutes. After *ana*$LptC_{\Delta TM}$-His_{10} was immobilized on magnetic Ni-NTA coated beads via His-tag, the protein complex bound resin was washed. The protein complex was then eluted and subjected on SDS gel. The interaction was examined by Coomassie staining. In addition, a control sample was prepared, in which only *ana*LptF was incubated with the magnetic Ni-NTA. The purification of the control sample was performed with the procedure described for Ni-NTA affinity chromatography. GST-*ana*LptF protein in each of purification fractions of the control sample was proved via Coomassie staining. The absence of GST-*ana*LptF in elution fraction derived from the control sample showed that the protein did not bind to Ni-NTA affinity resin (Figure 11 C). Despite the signal of the detected *ana*LptF was weak, both *ana*$LptC_{\Delta TM}$-His_{10} and GST-*ana*LptF proteins were observed in elution fraction (Figure 11 B). This result revealed that the periplasmic domain of *ana*LptC physically interacts with the predicted β-stranded periplasmic loop of *ana*LptF *in vitro*.

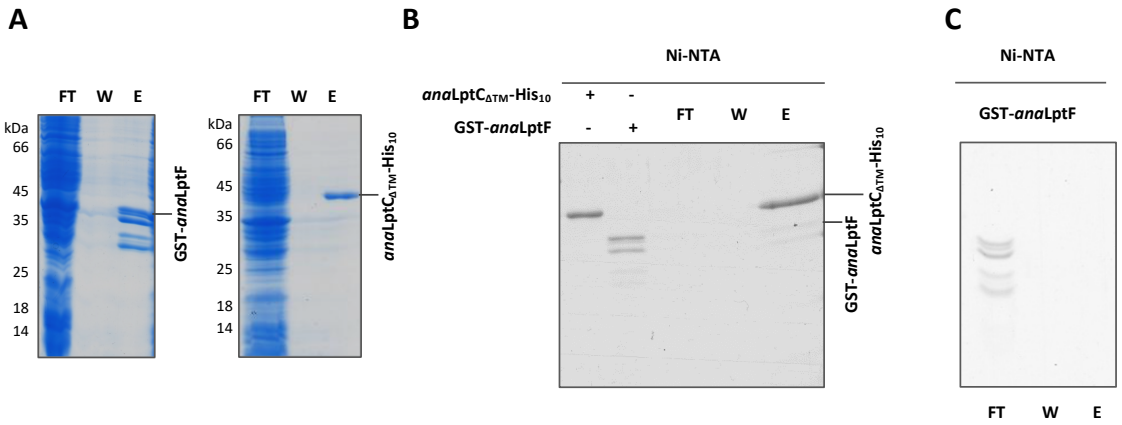

Figure 11: *In vitro* interaction between *ana*LptC and *ana*LptF.
A) *ana*LptC$_{\Delta TM}$-His$_{10}$ and GST-*ana*LptF were expressed in *E. coli* BL21 strain. The purification of *ana*LptC$_{\Delta TM}$-His$_{10}$ and GST-*ana*LptF was performed with Ni-NTA resin and Glutathione Sepharose, respectively. Flowthrough (FT), wash (W) and elution (E) fractions were separated by SDS gel and examined by Coomassie staining. B) The binding of *ana*LptC$_{\Delta TM}$-His$_{10}$ to GST-*ana*LptF was assessed by Ni-NTA affinity chromatography. Input proteins *ana*LptC$_{\Delta TM}$-His$_{10}$ and GST-*ana*LptF were shown. After the mixture of the two proteins was incubated for 15 min at 4°C, it was added to magnetic Ni-NTA beads. *ana*LptC$_{\Delta TM}$-His$_{10}$ with GST-*ana*LptF in flowthrough (FT), wash (W) and elution (E) fractions were also examined by Coomassie staining. C) Negative control. GST-*ana*LptF was incubated with magnetic Ni-NTA beads. The purification procedure was performed as described for Ni-NTA affinity chromatography. The presence of protein was confirmed in each flowthrough (FT), wash (W) and elution (E) fractions by Coomassie staining.

3.2.2 The *ana*LptC periplasmic domain interacts with *Anabaena* sp. LptA homologue

The C-terminal domain of the LptC periplasmic domain was shown to interact with the N-terminal domain of the periplasmic protein LptA in *E. coli* (Freinkman et al., 2012; Martorana et al., 2016). To determine whether *ana*LptC also binds to *ana*LptA *in vitro*, the construct of *ana*LptC$_{\Delta TM}$-His$_{10}$ and the previously generated construct of *ana*LptA-MBP (Hsueh et al., 2015) were used for the interaction study. The purified *ana*LptA-MBP protein via amylose affinity resin was obtained with the expected molecular weight of ca. 60 kDa (Figure 12 A, left). The fact that interaction of *ana*LptC and *ana*LptF was established through Ni-NTA affinity chromatography, therefore, this method was further used to determine interaction between *ana*LptC and *ana*LptA. Moreover, the unspecific binding of *ana*LptA-MBP to magnetic Ni-NTA beads was examined by incubation of *ana*LptA-MBP with the resin without *ana*LptC. The absence of *ana*LptA-MBP in elution fraction showed no binding to magnetic Ni-NTA beads (Figure 12 A, right).

After *ana*LptC$_{\Delta TM}$-His$_{10}$ was incubated with *ana*LptA-MBP for 15 min, the protein complex was immobilized on the magnetic Ni-NTA resin via His-tag, followed by washing steps. The complex

was eluted with buffer containing imidazole, and then *ana*LptC$_{\Delta TM}$-His$_{10}$ and *ana*LptA-MBP proteins in flowthrough, wash and elution fractions were analyzed by Western immunoblotting. The results revealed strong signals of *ana*LptC$_{\Delta TM}$-His$_{10}$ and *ana*LptA-MBP proteins in the elution fraction detected via anti-His and anti-MBP antibodies, respectively, therefore confirmed the interaction between the two proteins. Other fragments, likely degradation products containing MBP-tag present in the *ana*LptA-MBP input sample, were removed and not detected in the elution fraction anymore indicating that these fragments did not bind to *ana*LptC (Figure 12 B).

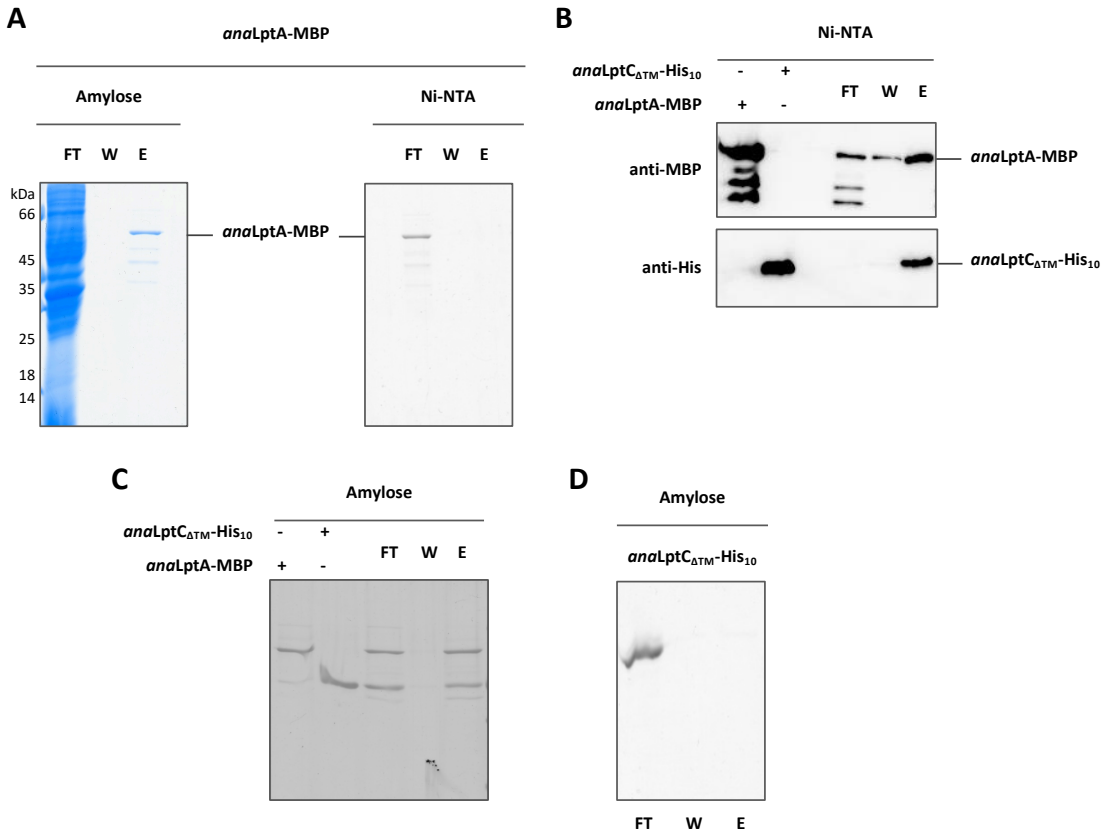

Figure 12: *In vitro* interaction between *ana*LptC and *ana*LptA.
A) The recombinant *ana*LptA-MBP protein was produced in *E. coli* BL21 strain. The purification of *ana*LptA-MBP protein was performed using amylose affinity resin (left), while it did not bind to Ni-NTA affinity beads at all after 15 min of incubation (right). Flowthrough (FT), wash (W) and elution (E) fractions were separated by SDS gel and visualized by Coomassie staining. B) The binding of *ana*LptC$_{\Delta TM}$-His$_{10}$ to *ana*LptA-MBP was assessed by Ni-NTA affinity chromatography. Input proteins *ana*LptC$_{\Delta TM}$-His$_{10}$ and *ana*LptA-MBP were shown. After the two proteins were mixed and incubated for 15 min at 4°C, magnetic Ni-NTA beads were added to the mixture. Proteins in flowthrough (FT), wash (W) and elution (E) fractions were examined and detected by Western Blot with anti-His antibody against *ana*LptC$_{\Delta TM}$-His$_{10}$ and anti-MBP antibody against *ana*LptA-MBP. C) *ana*LptC$_{\Delta TM}$-His$_{10}$ and *ana*LptA-MBP interaction was determined by amylose affinity chromatography. Flowthrough (FT), wash (W) and elution (E) samples were investigated and visualized by Coomassie staining D) Negative control. The *ana*LptC$_{\Delta TM}$-His$_{10}$ protein was incubated with amylose resin without interaction partner *ana*LptA-MBP. The presence of the *ana*LptC$_{\Delta TM}$-His$_{10}$ was investigated in each flowthrough (FT), wash (W) and elution (E) fractions by Coomassie staining.

The binding of *ana*LptC to *ana*LptA was again confirmed by affinity chromatography via amylose resin, whereby *ana*LptC$_{\Delta TM}$-His$_{10}$ and *ana*LptA-MBP proteins in each fractions were examined and visualized by Coomassie staining. The result showed similarly strong signals detected for both proteins *ana*LptC$_{\Delta TM}$-His$_{10}$ and *ana*LptA-MBP in the elution fraction (Figure 12 C, left). This result is consistent with the observation obtained from the interaction analysis of *ana*LptC$_{\Delta TM}$-His$_{10}$ and *ana*LptA-MBP using magnetic Ni-NTA affinity beads (Figure 12 B). Therefore, the interaction between *ana*LptC and *ana*LptA is stochiometric. Furthermore, negative control for *ana*LptC$_{\Delta TM}$-His$_{10}$ with amylose in absence of *ana*LptA-MBP protein was performed and showed that *ana*LptC$_{\Delta TM}$-His$_{10}$ did not bind to amylose resin (Figure 12 D).

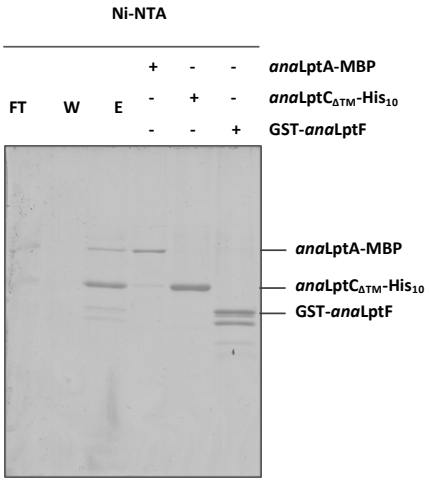

Figure 13: *In vitro* complex formation of *ana*LptC with *ana*LptF and *ana*LptA proteins.
The *ana*LptC$_{\Delta TM}$-His$_{10}$, GST-*ana*LptF and *ana*LptA-MBP proteins were recombinantly overexpressed in *E. coli* BL21 strains. The reaction mixture containing *ana*LptC$_{\Delta TM}$-His$_{10}$, GST-*ana*LptF and *ana*LptA-MBP proteins was incubated for 15 min at 4°C and immobilized on magnetic Ni-NTA affinity beads. The purification of the complex was performed according to procedures described for Ni-NTA affinity chromatography. A sample from each fraction of flowthrough (FT), wash (W) and elution (E) was prepared for SDS-PAGE and stained by Coomassie colloidal.

3.2.3 The *ana*LptC periplasmic domain interacts with LptA and LptF homologues

To further examine, whether *ana*LptC could involve in interaction with both *ana*LptF and *ana*LptA, the three purified recombinant proteins *ana*LptC$_{\Delta TM}$-His$_{10}$, GST-*ana*LptF and *ana*LptA-MBP were incubated in a reaction mixture for 15 min and at 4°C. After the incubation phase completed, the reaction mixture was added to magnetic Ni-NTA and repurified. The result showed that all three proteins were present in the elution fraction, suggesting the complex

formation by the three proteins and that the interaction is *ana*LptC dependent, but not stochiometric (Figure 13).

3.2.4 The *ana*LptC periplasmic domain interacts with LPS from *E. coli*

The previous studies showed that the periplasmic protein LptA and periplasmic domain of LptC protein both bind to LPS *in vitro* in *E. coli* (Tran et al., 2010). The tryptophan fluorescence spectroscopy is the most common method used to investigate interactions between proteins and lipids due to its high sensitivity to the local environment, whereby changes in the intrinsic tryptophan fluorescence often occur upon ligand binding (Zhao & Lappalainen, 2012). Therefore, in order to determine whether *ana*LptC interacts with LPS from *E. coli* (*ec*LPS), the tryptophan fluorescence spectroscopy was used, because the C-terminally His-tagged *ana*LptC periplasmic domain contains five tryptophan residues.

To test how tryptophan fluorescence of *ana*LptC$_{\Delta TM}$-His$_{10}$ changes, 2 µM of the purified *ana*LptC$_{\Delta TM}$-His$_{10}$ sample was prepared in absence and in presence of 8 M urea, 2% (v/v) acrylamide and 1 mg LPS. After the indicated sample was excited at the wavelength of 250 nm, fluorescence spectra were recorded and evaluated with the wavelength from 300 nm to 440 nm. The result of the sample added with acrylamide, a common fluorescence quencher, showed that tryptophan fluorescence of *ana*LptC$_{\Delta TM}$-His$_{10}$ was reduced in comparison to the protein sample without adding acrylamide. A reduction of tryptophan fluorescence was also observed for urea and LPS treated samples. Furthermore, a red shift of the fluorescence maximum was observed for *ana*LptC$_{\Delta TM}$-His$_{10}$ treated with urea indicating that the protein contains tryptophan residues partly buried inside the protein might be then exposed to aqueous environment, as the protein was denatured in the presence of urea (Figure 14 A).

Results of the tryptophan fluorescence spectra could not give any conclusion about the structural organization of the *ana*LptC protein. However, results from fluorescence quenching could be used to determine the dissociation constant value K_D of *ana*LptC for *ec*LPS. Accordingly, 0.2 µM of the purified *ana*LptC$_{\Delta TM}$-His$_{10}$ was incubated with different concentrations of LPS and fluorescence spectra for each concentration were measured. The experiment was performed with two technical and two biological replicates. The dissociation constant was obtained by using

least square fit analysis (f = a*x/(b+x) + y0) via sigma plot resulting in K_D of 55 µM (Figure 14 B), which is in agreement with the estimated affinity of *ec*LptC for *ec*LPS in the range of 28.8-71.4 µM (Sestito et al., 2014), revealing that the periplasmic domain of *ana*LptC interacts with *ec*LPS.

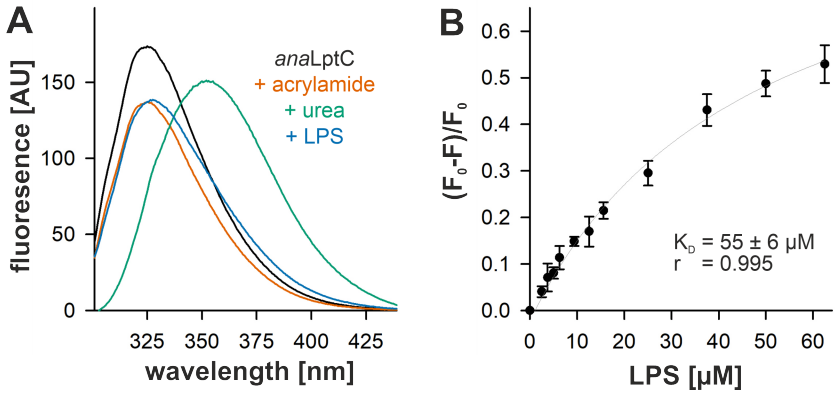

Figure 14: *In vitro* interaction analysis of *ana*LptC$_{\Delta TM}$-His$_{10}$ with LPS from *E. coli* via the tryptophan fluorescence spectroscopy. A) Tryptophan fluorescence quenching of *ana*LptC$_{\Delta TM}$-His$_{10}$ (black) and in the addition of 2% (v/v) acrylamide (orange), 8 M urea (green), or 1 mg LPS (blue) was shown. 2 µM of the purified recombinant protein *ana*LptC$_{\Delta TM}$-His$_{10}$ was added to reaction tubes containing the indicated substances. B) Determination of dissociation constant K_D of *ana*LptC for *ec*LPS according to least square fit analysis with sigma plot. K_D and standard derivations were calculated from fluorescence spectra performed with two technical and two biological replicates.

3.3 Crystallization of the periplasmic domain of *ana*LptC

3.3.1 Generation of the periplasmic domain of *ana*LptC for crystallization

The amino acid sequence of the putative LptC protein from *Anabaena* sp. containing 385 aa is significantly longer than that of LptC from *E. coli* composed of 191 aa (Figure 4 and Figure 5). Both proteins share a transmembrane helix predicted by TMHMM and located near the N-terminus with residues Trp^{7}- Ala^{25} for *ec*LptC and Asn^{7}- Val^{26} for *ana*LptC (Krogh et al., 2001), despite low sequence identity of less than 14% from sequence alignment via ClustalW (Thompson et al., 1994). Based on sequence alignment, *ana*LptC was predicted to contain a larger soluble periplasmic domain than that of *ec*LptC (Ngo et al., 2020). To judge structural and functional aspects between the two proteins, a construct of the C-terminally His-tagged soluble periplasmic domain of *ana*LptC protein encoded by *all0231* gene were generated for crystallization using FX cloning kit with two cloning steps (Addgene, Teddington, UK).

The DNA fragment coding for the periplasmic domain of *Anabaena* sp. LptC in absence of the predicted transmembrane region (*ana*LptC$_{\Delta TM}$) was amplified with gene specific primers and

cloned in pINIT_cat vector at restriction sites for SapI enzyme. The pINIT_cat vector containing *ana*LptC$_{\Delta TM}$ fragment was investigated by digestion reaction test in the presence of the restriction enzyme SapI resulting in an *ana*LptC$_{\Delta TM}$ fragment of ca. 1083 bp (Figure 15 A). The *ana*LptC$_{\Delta TM}$ fragment was then isolated from the derivative pINIT_cat vector and subcloned in the expression vector p7XC3H (Figure 15 B). The derivative p7XC3H encoding *ana*LptC$_{\Delta TM}$-HRV 3C-His$_{10}$ protein (herewith *ana*LptC$_{\Delta TM}$-His$_{10}$) was verified by sequencing.

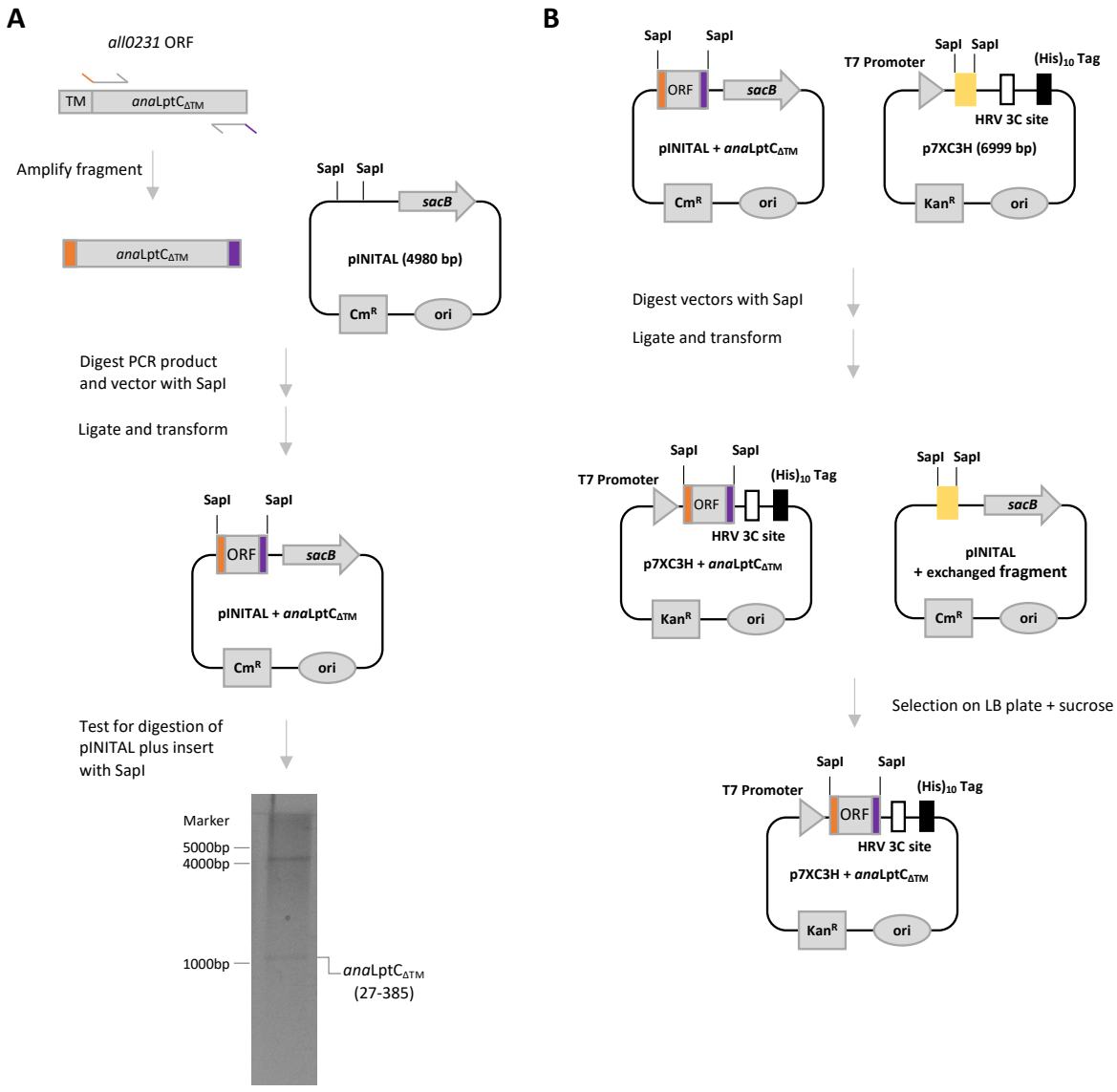

Figure 15: Schematic presentation for the generation of the *ana*LptC soluble domain with FX cloning kit (Addgene, Teddington, UK).

A) 1083 base pairs of *all0231* gene coding for the periplasmic domain without the predicted transmembrane helix *ana*LptC$_{\Delta TM}$ was cloned at SapI restriction sites of pINIT_cat vector. Samples of digestion test with SapI enzyme were examined and visualized in agarose gel. B) The *ana*LptC$_{\Delta TM}$ fragment was subcloned in p7XC3H containing T7 promoter, C-terminal HRV 3C site and His$_{10}$-tag. Cm^R: chloramphenicol resistant. Kan^R: kanamycin resistant.

Expression of *ana*LptC$_{\Delta TM}$-His$_{10}$ protein was performed in *E. coli* strain BL21 under the control of the T7 promoter, which was induced at OD$_{600nm}$ of 0.8 for 3 hours by adding 1 mM isopropyl-β-D-thiogalactopyranoside (IPTG). The purification carried out by using Ni-NTA affinity chromatography via His-tag yielded a high amount of proteins (Figure 16 B, left). Upon His-tag removal, it was repurified by size exclusion chromatography and examined for homogeneity. One single peak was observed from the elution profile of size exclusion chromatography (Figure 16 A). SDS-PAGE analysis of the peak fractions from 1 to 12 showed very high purity for the protein construct (Figure 16 B, right). After the peak fractions were pooled and concentrated to 10 mg/ml, the purity of the sample was confirmed by silver gel which showed a single protein fragment of *ana*LptC$_{\Delta TM}$ (Figure 16 C).

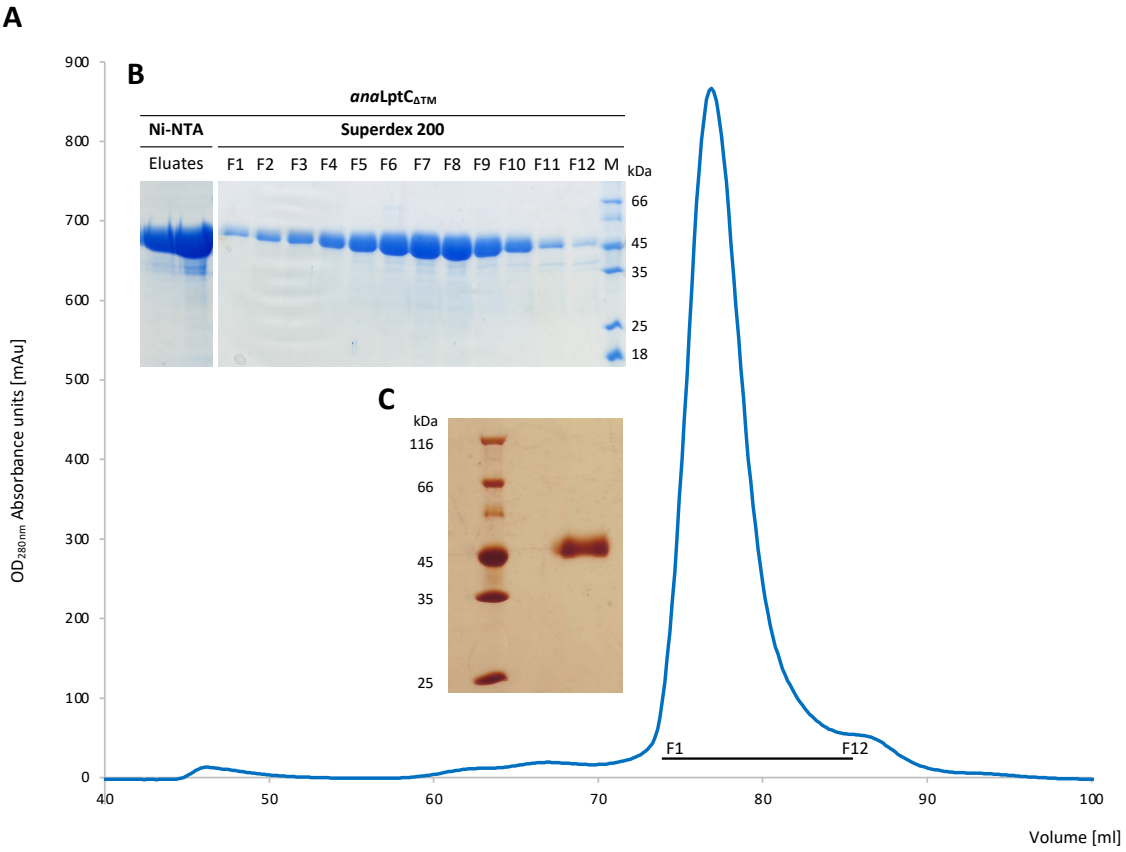

Figure 16: Purification of the soluble domain *ana*LptC$_{\Delta TM}$.
A) The size exclusion chromatography profile of the His-tag removed *ana*LptC$_{\Delta TM}$ with the peak fractions 1 to 12 was shown. B) Elution fractions of the *ana*LptC$_{\Delta TM}$-His$_{10}$ purified by Ni-NTA affinity chromatography were investigated by SDS-PAGE and visualized with Coomassie colloidal staining (left). Peak fractions (F1-F12) of *ana*LptC$_{\Delta TM}$ without His-tag obtained from the size exclusion chromatography were analyzed by SDS-PAGE and stained with Coomassie colloidal (right). C) Peak fractions (F1-F12) from the size exclusion chromatography were pooled and concentrated to 10 mg/ml. The concentrated protein sample was examined by silver gel showing very high purity of *ana*LptC$_{\Delta TM}$. The data shown in this figure and the figure itself were provided by Giang Ngo. The figure was published in Ngo et al., 2020.

3.3.2 Crystallization screening for the periplasmic domain of *ana*LptC

Crystallization trials using commercial screening kits were carried out with two versions of the recombinant *ana*LptC$_{\Delta TM}$, whereby the protein was produced with the presence and absence of His-tag. The *ana*LptC$_{\Delta TM}$-His$_{10}$ version was purified by Ni-NTA affinity resin and subsequently repurified by size exclusion chromatography without His-tag removal. To obtain *ana*LptC$_{\Delta TM}$ version in absence of His-tag, *ana*LptC$_{\Delta TM}$-His$_{10}$ was treated with HRV 3C protease to remove the His-tag before the digested sample was subjected to size exclusion chromatography. Screening for crystallization conditions was then performed in 96-well plates via sitting drop technique.

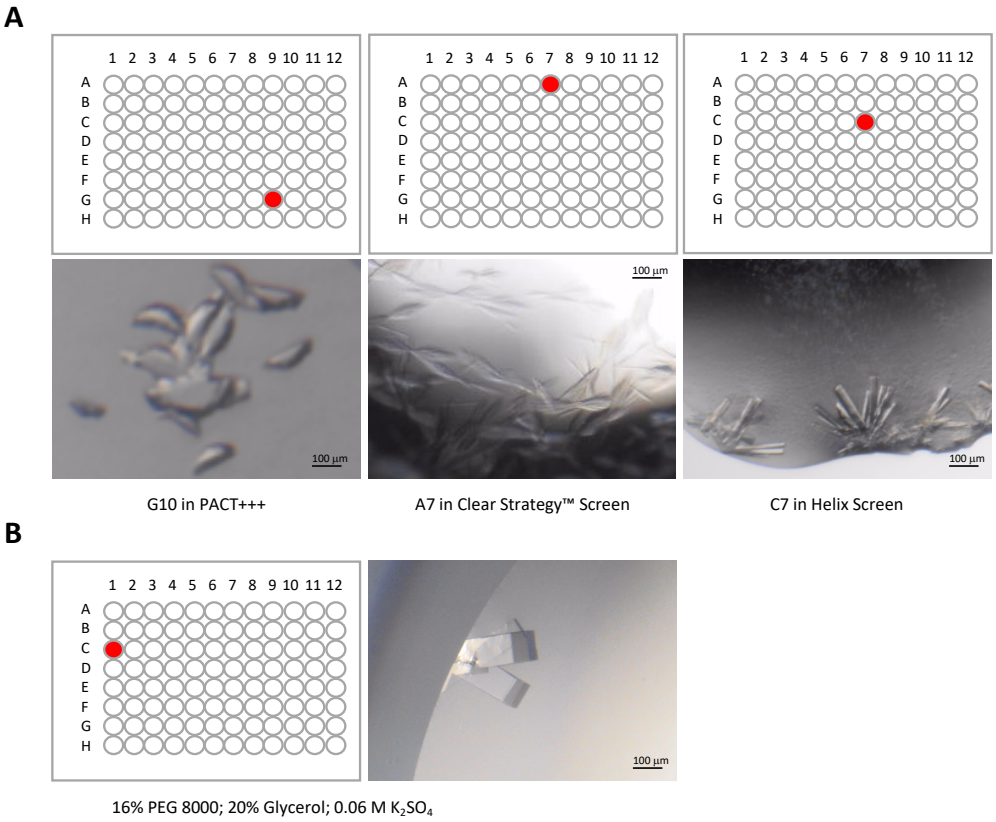

Figure 17: Initial crystallization trials of the soluble domain *ana*LptC$_{\Delta TM}$ in presence and absence of His-tag.
A) The *ana*LptC$_{\Delta TM}$-His$_{10}$ protein crystals were grown in A7 of Clear Strategy™ screen after three days, in G10 of PACT and in C7 of Helix screen mixtures after one week. B) Crystals of the His-tag removed *ana*LptC$_{\Delta TM}$ were observed in condition containing 16% PEG; 20% Glycerol; 0.06 M K_2SO_4 after one week. All crystallization plates were prepared according to sitting drop technique with 10 mg/ml protein concentration and 1:1 protein buffer ratio.

Protein crystals appeared between three days and one week at 18°C, whereby crystals of *ana*LptC$_{\Delta TM}$-His$_{10}$ are very tiny (Figure 17 A). After His$_{10}$-tag was removed, *ana*LptC$_{\Delta TM}$ crystals were improved and grew larger in condition composed of 16% PEG; 20% Glycerol; 0.06 M K_2SO_4

(Figure 17 B). The measurements of crystals revealed that they were all protein crystals. Although the protein crystals without His-tag were diffracted up to 4 Å, they contained multiple lattices and only a few spots were observed. Therefore, the condition of 16% PEG; 20% Glycerol; 0.06 M K_2SO_4 was further optimized to improve the crystal quality.

3.3.3 Crystallization optimization of the periplasmic domain of *ana*LptC

The removal of His-tag improved the crystal quality, therefore, only *ana*LptC$_{\Delta TM}$ without His-tag was further used. Furthermore, varying the concentration of salts, precipitants as well as using the screening additives could also improve the quality of crystals. Optimization of crystallization was carried out in a 24-well plate via sitting-drop vapor diffusion method using 1 µl of protein (10 mg/ml) and 1 µl of crystallization solution.

Table 4. Data collection analysis of optimized *ana*LptC$_{\Delta TM}$ crystals

Properties of measurement	Condition A	Condition B	Condition C
Transmission	10%	20.1%	20.1%
Resolution (corner)	3.00 Å (2.15 Å)	2.69 Å (1.95 Å)	2.50 Å (1.83 Å)
Energy (Wavelength)	11.562 keV (1.0723 Å)	11.562 keV (1.0723 Å)	11.562 keV (1.0723 Å)
Omega range	0.1°	0.1°	0.1°
Exposure time	0.037 s	0.037 s	0.037 s
Flux start / end	5.9 * 10^{10} ph/s	3.43 / 3.71 * 10^{11} ph/s	1.77 / 1.89 * 10^{11} ph/s
Completeness/Resolution (overall)	97.1% / 13.6-3.0 Å	96.5% / 13.5-3.0 Å	**99.7% / 49.5-2.9 Å**
Completeness/Resolution (inner)	93.8% / 100-13.6 Å	93.7% / 100-13.5 Å	**98.7% / 49.5-11.3 Å**
Completeness/Resolution (outer)	78.9% / 3.13-3.05 Å	72.9% / 3.11-3.03 Å	**99.8% / 3.01-2.91 Å**
Properties of crystal	Condition A	Condition B	Condition C
Space group	C 1 2 1	C 1 2 1	C 1 2 1
Unit cell dimension a	95.84 Å	95.63 Å	93.96 Å
Unit cell dimension b	338.75 Å	336.31 Å	336.82 Å
Unit cell dimension c	72.03 Å	73.98 Å	70.95 Å
Unit cell angle	90°	90°	90°
Unit cell angle	129.58°	131.06°	129.11°
Unit cell angle	90°	90°	90°

The results revealed that properties of *ana*LptC$_{\Delta TM}$ crystals obtained from the three optimized crystallization conditions A, B and C have similar unit cell dimensions and angles (Table 4). However, dataset collected from the measurement of the crystal grown in the condition A was not complete due to the presence of two big gaps, while the quality of the crystal grown in the condition B was improved because only one gap was found in the dataset. Nevertheless, the data collection of crystal grown in the condition C was the best result of the three conditions, in fact, it showed that the dataset was complete (Figure 18 C, left and Table 4). Moreover, the spot

quality of crystals grown in condition C was improved a lot compared to condition B (Figure 18 B and C, right).

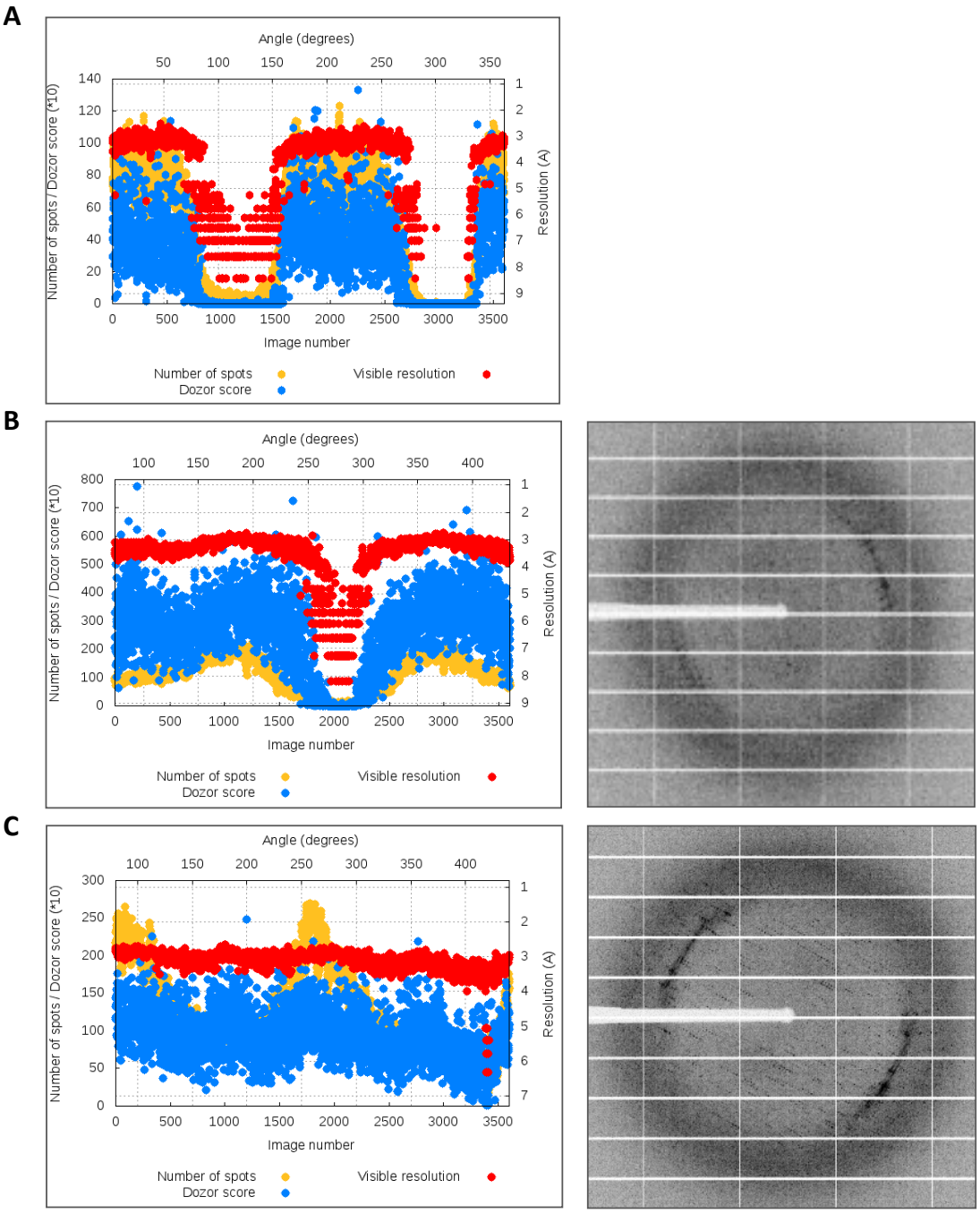

Figure 18: Optimization of crystallization for the soluble domain *ana*LptC$_{\Delta TM}$.
The diffraction quality of *ana*LptC$_{\Delta TM}$ protein crystals was evaluated at the ESRF synchrotron (left). The diffraction pattern of *ana*LptC$_{\Delta TM}$ protein was shown (right). Crystals of *ana*LptC$_{\Delta TM}$ without His$_{10}$-tag was grown in sitting-drop 24-well plate using crystallization condition of (A) 4.1% C1 condition of Morpheus® crystallization screen; 16% PEG 8000; 20% Glycerol and 0.06 M K_2SO_4 (B) 4.1% C1 condition of Morpheus® crystallization screen; 4.1% 0.12 M Monosaccharide mix; 16% PEG 8000; 20% Glycerol and 0.06 M K_2SO_4 (C) 4.1% C1 condition of Morpheus® crystallization screen; 4.1% 0.06 M Divalent mix; 16% PEG 8000; 20% Glycerol and 0.06 M K_2SO_4.

The dataset collection of the crystal grown in the condition C was next used for the first trial to determine the structure of the periplasmic domain of *Anabaena* sp. LptC with molecular replacement method on the basis of the crystal structure of *ec*LptC (PDB 3MY2). However, the trial was not successful and probably due to the low sequence identity between the *Anabaena* sp. and *E. coli* LptC. Therefore, the crystallization condition was further optimized to obtain the best native crystal.

3.4 Determination of the crystal structure of the periplasmic domain of *ana*LptC

3.4.1 The structure of the *ana*LptC periplasmic domain

The soluble domain of *ana*LptC was recombinantly expressed to contain a C-terminal His-tag without the predicted transmembrane helix in *E. coli* BL21 cells. Subsequently, His-tag was removed by proteolysis, the purified *ana*LptC$_{\Delta TM}$ with a concentration of 10 mg/ml was used for crystallization optimization trials. After several rounds, the best diffracting crystal of native *ana*LptC$_{\Delta TM}$ appeared after one week in crystallization condition of 16% PEG 8000; 20% Glycerol; 0.06 M K_2SO_4 and 4.1% of H5 precipitant mixture of the NeXtal Classics II Suite crystallization screen and diffracted up to 2.6 Å (Figure 19 A and Figure 20 A).

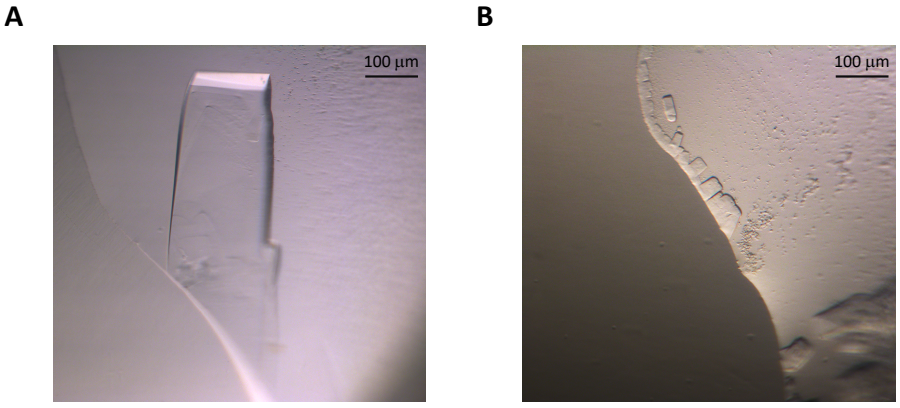

Figure 19: Final optimization of crystallization of *ana*LptC$_{\Delta TM}$.
A) Native protein crystal grew in 4.1% of H5 precipitant mixture of the NeXtal Classics II Suite crystallization screen; 16% PEG 8000; 20% Glycerol and 0.06 M K_2SO_4. B) Selenmethionine-labelled protein crystal crystallized in condition composed of 4.1% C1 condition of Morpheus® crystallization screen; 4.1% 0.12 M Monosaccharide mix; 16% PEG 8000; 20% Glycerol and 0.06 M K_2SO_4. The data shown in this figure and the figure itself were provided by Giang Ngo. The figure was published in Ngo et al., 2020.

The native *ana*LptC$_{\Delta TM}$ crystal has space group C2 containing four molecules in a unit cell. Its dataset was used for an attempt to obtain phase information via molecular replacement method using structurally similar model of LptC from *E. coli* with PDB entry 3MY2. However, the molecular

replacement trial failed to determine the structure of *ana*LptC$_{\Delta TM}$, probably due to low sequence identity of 14% between two proteins performed with ClustalW (Thompson et al., 1994).

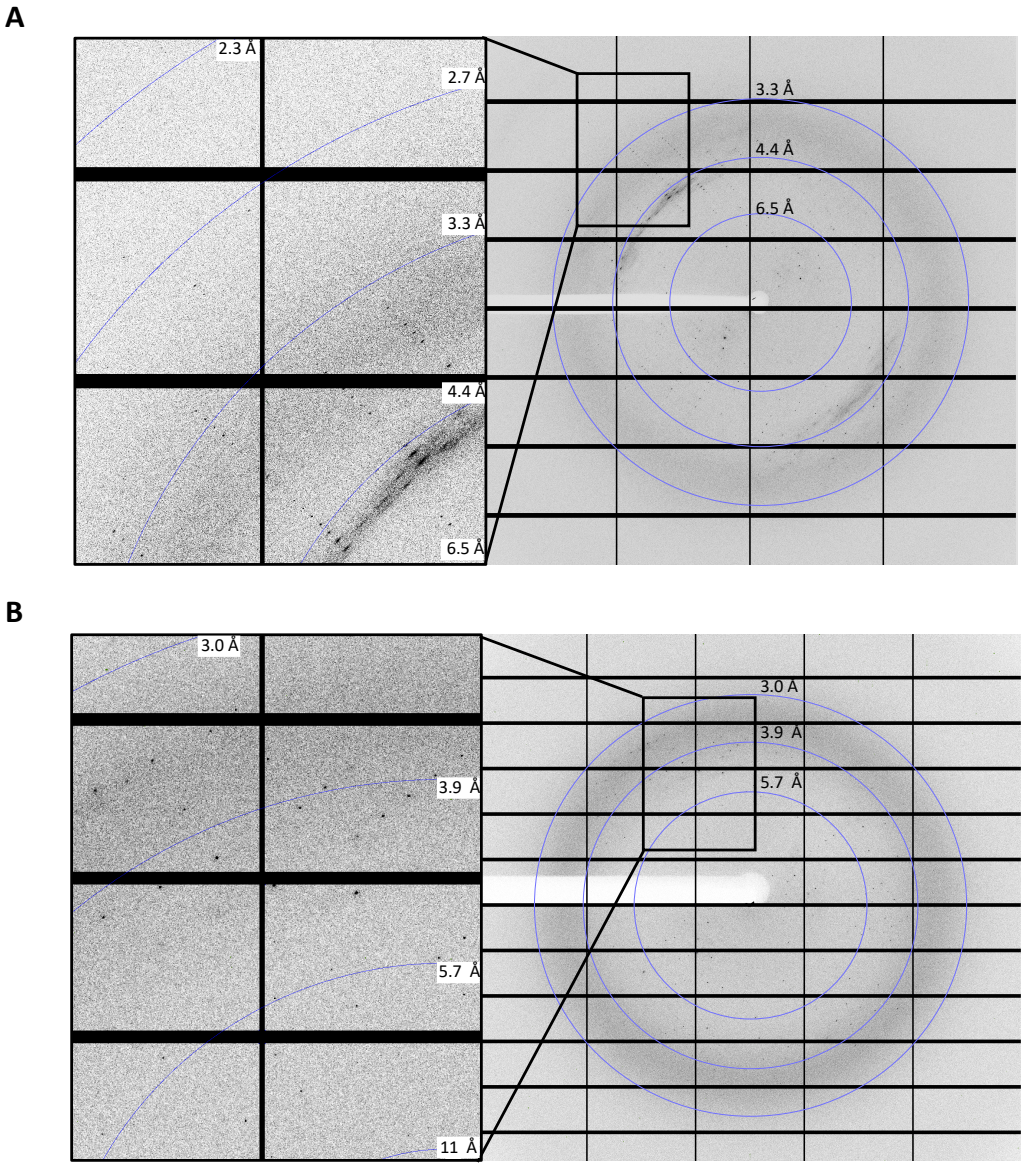

Figure 20: Diffraction pattern of crystals of *ana*LptC$_{\Delta TM}$.
A) Pattern of the best diffracting native protein crystal grew in 4.1% of H5 precipitant mixture of the NeXtal Classics II Suite crystallization screen; 16% PEG 8000; 20% Glycerol and 0.06 M K_2SO_4 is shown. B) Diffraction pattern of selenmethionine-labelled protein crystal crystallized in condition composed of 4.1% C1 condition of Morpheus® crystallization screen; 4.1% 0.12 M Monosaccharide mix; 16% PEG 8000; 20% Glycerol and 0.06 M K_2SO_4.

The next step was to incorporate selenomethionine into *ana*LptC$_{\Delta TM}$ in order to obtain the phase information for the structure determination according to the single-wavelength anomalous diffraction (SAD) method. The selenomethionine-labelled *ana*LptC$_{\Delta TM}$ protein crystallized under a similar condition as that of the native protein, namely in 4.1% C1 condition of Morpheus®

crystallization screen; 4.1% 0.12 M Monosaccharide mix; 16% PEG 8000; 20% Glycerol and 0.06 M K_2SO_4 (Figure 19 B). Although the selenomethionine-labelled *ana*LptC$_{\Delta TM}$ crystals were smaller than the native one, they also diffracted at 2.8 Å (Figure 20 B).

Crystals of selenomethionine labelled *ana*LptC$_{\Delta TM}$ also grew in space group C2 containing four molecules in asymmetric unit with solvent content of about 53.9 %. Unit cell parameters in the crystal of selenomethionine labelled *ana*LptC$_{\Delta TM}$ (a = 94.4 Å, b = 336.1 Å, c = 74.1 Å and β = 131.7°) are similar to those in native crystal (a = 96.5 Å, b = 337.0 Å, c = 71.7 Å and β = 130°) listed in the table 5.

Table 5. Data collection of native and selenomethionine-labelled *ana*LptC$_{\Delta TM}$ crystals

Protein	*ana*LptC$_{\Delta TM}$	selenomethionine-labelled *ana*LptC$_{\Delta TM}$
Crystallization		
Method	Sitting drop	Sitting drop
Temperature	290.15 K	290.15 K
Protein concentration	10 mg/ml	10 mg/ml
Data collection		
X-ray source	Synchrotron radiation (PXII-SLS)	Synchrotron radiation (P13-DESY)
Wavelength (Å)	1.0	0.9793
Space group	C2(5)	C2(5)
Unit-cell dimensions (Å)	a=96.5, b=337.0Å, c=71.7Å	a=94.4, b=336.1Å, c=74.1Å
Unit-cell angle	β=130°	β=131.7
Matthews coefficient (Å^3 Da^{-1})	2.71	2.67
Solvent content (%)	54.7	53.9
No. of molecules per ASU	4	4
Resolution (Å)	50 - 2.8 (2.9 - 2.8)	50 - 2.8 (2.9 - 2.8)
Total observations	300613 (28829)	288698 (28035)
Unique observations	42573 (4126)	83240 (8325)
Completeness (%)	98.4 (95.6)	98.3 (98.7)
R_{meas}	0.06 (2.44)	0.09 (1.94)
$I/\sigma(I)$	12.79 (0.72)	8.36 (0.69)

Based on the phase information obtained by a single set of diffraction data using SAD method for selenomethionine labelled *ana*LptC$_{\Delta TM}$ crystal collected at a wavelength of 0.9793 Å on beamline P13 of the German Electron Synchrotron (DESY), the crystal structure of the soluble domain of *ana*LptC was solved and described at 2.8 Å resolution. Positions of six selenomethionine could be identified in the asymmetric unit after evaluation of phases using SOLVE (Terwilliger & Berendzen, 1999) and the initial model was built using RESOLVE (Terwilliger, 2004). The phases were further improved by the phase information which was obtained for the native data set by molecular replacement, in which the best diffracting data set of native *ana*LptC$_{\Delta TM}$ crystal was phased using phenix.MR against the structure obtained from Se SAD method as a search model.

The structure was then manually inspected, extended and corrected using Coot (Emsley et al., 2010) and refined with phenix.refine (Liebschner et al., 2019). Final crystallographic R factor and R free values for the refined protein are 27.31 % and 32.28 %, respectively. Residues 43-372 were observed in the electron density map, whereas two regions composed of residues 27-42 and 373-385 were disordered and therefore they could not be modeled in the structure. All six methionine (Met 173, 188, 190, 260, 264 and 293) present in the soluble domain of *ana*LptC could be identified in the electron density map (Figure 21).

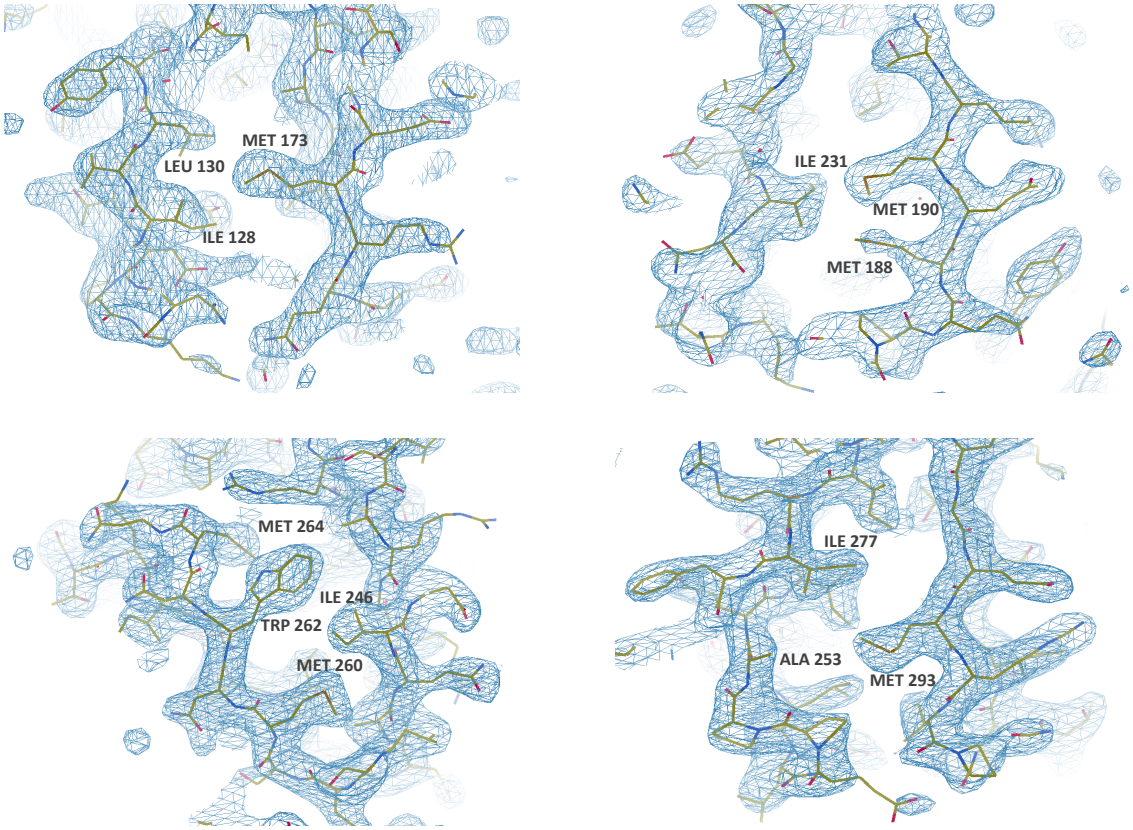

Figure 21: Location of six methionine residues in the soluble domain of *ana*LptC via electron density map.
The electron density map was improved after the phase information was achieved by molecular replacement with phenix.MR using best diffracting data set of native crystal. As a search model structure of selenomethionine labelled *ana*LptC$_{\Delta TM}$ obtained from Se SAD phasing method was used.

The crystal structure of the soluble domain of *ana*LptC is composed of a series of 40 antiparallel β-strands connected with each other via short loops (Figure 22, left). The folding of the amino acid peptide sequence twisted along its own axis of about 180° from N-terminus to the C-terminus of the protein.

Table 6. Measurements of the length for *Anabaena* sp. LptC

N-terminal End	C-terminal End	Distance Å
ASP 43	VAL 372	103
ASP 43	THR 346	95
ASP 43	ALA 344	97
THR 47	VAL 372	96
ASP 50	VAL 372	93
		Average length
		97

Dimensions of the protein were measured by the distance of C_α atoms between two residues via UCSF Chimera, while the length of protein was averaged from by multiple measurements of distances between two positions near the N- and C- terminus (Table 6). As a result, *ana*LptC periplasmic domain is about 97 Å in length, 27 Å in depth and 14 Å in width. Additionally, the top view showed that the whole structure has a diameter of approximately 35 Å (Figure 22, right).

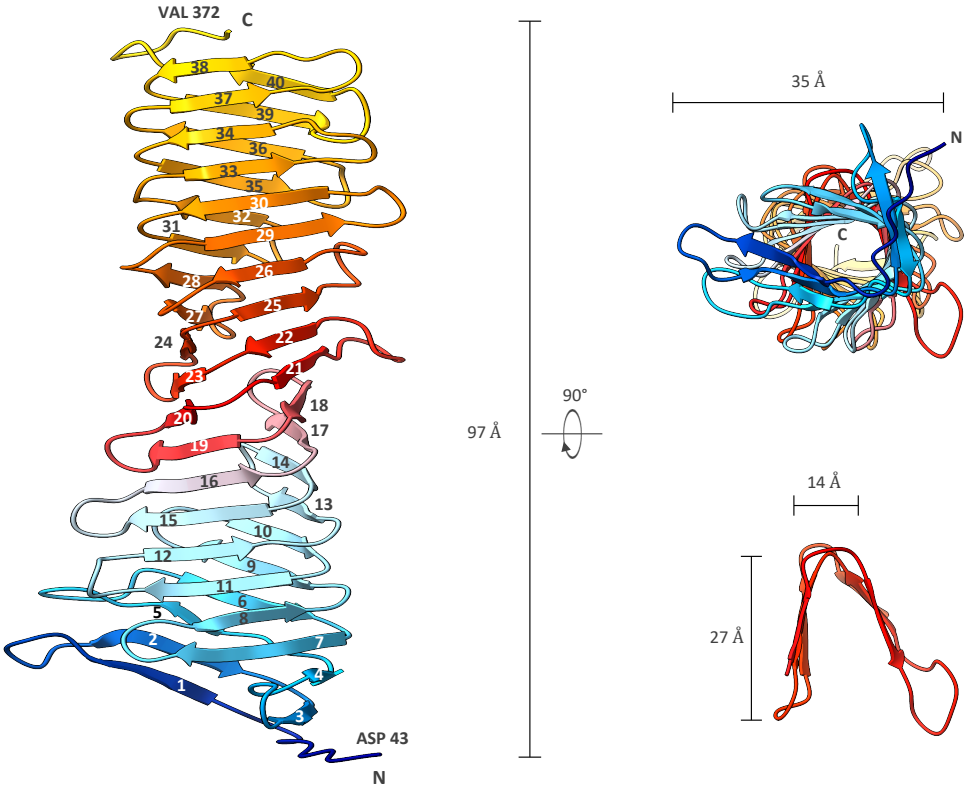

Figure 22: X-ray structure of the periplasmic domain of *ana*LptC.
The overall structure of the soluble domain of *ana*LptC (43-372 aa) composed of 40 antiparallel β-strands is shown (left). The dimensions of the protein are about 97 Å in height, 27 Å in depth and 14 Å in width, while diameter of the whole structure is about 35 Å (right).

LptA from *E. coli* is known to oligomerize itself to form filaments of proteins in head-to-tail fashion, whereby the N-terminal β-strands of one monomer interacts with the C-terminal β-strands of the second monomer to form a continuous groove (Merten et al., 2012). In contrast,

the assembly of *ana*LptC molecules in the crystal revealed that the C-terminus of chain A interacts with C-terminus of chain B in a tail-to-tail manner. This tail-to-tail interaction was also observed between chain C and D indicating that *ana*LptC did not form oligomers in the crystal (Figure 23) and the close contact between them is resulted from the packing of the crystal.

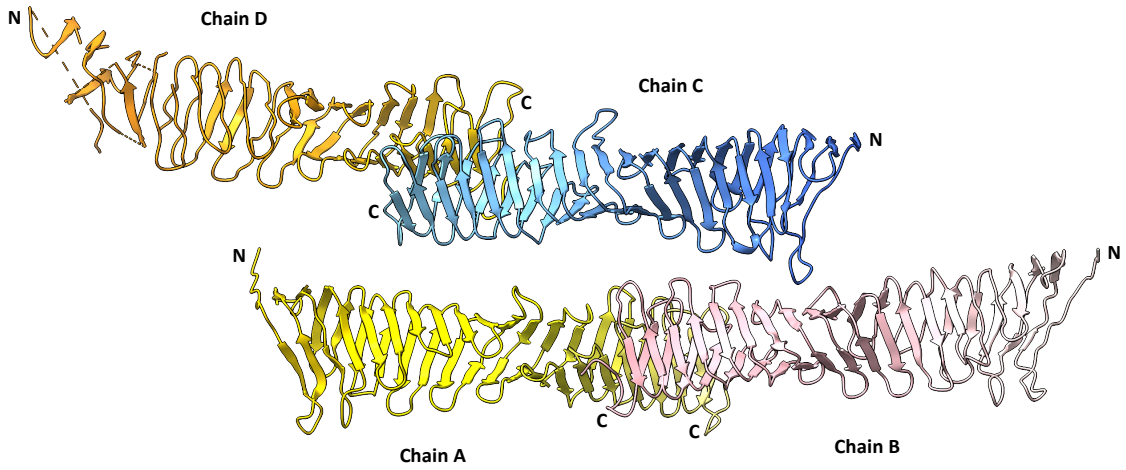

Figure 23: Crystal contacts of the periplasmic domain of *ana*LptC.
Crystal packing of four *ana*LptC$_{\Delta TM}$ molecules. Ribbon diagrams of *ana*LptC$_{\Delta TM}$ proteins presented by chain A in yellow, chain B in pink, chain C in blue and chain D in orange. Polypeptide chains in the crystal interact with each other in a tail-to-tail manner, in which C-terminus of the chain A contacts with C-terminus of the chain B. The same interaction was also observed for chains C and D.

The hydrophobic surface representation revealed that *ana*LptC$_{\Delta TM}$ contains a distinct hydrophilic surface shown in blue (Figure 24 A, left). While a cross-section throughout the protein showed that the protein exposes many hydrophobic residues, which form a highly hydrophobic core shown in orange (Figure 24 A, right). Moreover, the electrostatic potential representation at pH 7.5 showed that its surface is mostly positively charged, except for a small patch at the N-terminal edge possessing negatively charged surface (Figure 24 B).

3.4.2 Structure superposition of *Anabaena* sp. and *E. coli* LptC periplasmic domains

The structurally homologous conserved β-jellyroll fold is a remarkable structure feature spreading in Lpt protein family and shared by five (LptACDFG) out of the seven essential lipopolysaccharide transport proteins (LptABCDEFG) required for LPS transport in Gram-negative bacteria (Villa et al., 2013; Owens et al., 2019). The typical β-jellyroll fold was found in the architecture of the Lpt transenvelope bridge built by LptC, LptA and the N-terminal region of LptD in a head-to-tail oligomeric assembly fashion connecting the inner membrane with the outer

membrane via periplasm (Freinkman et al., 2012). Although the amino acid sequence alignment between *E. coli* LptA and LptC revealed that their sequences are less than 10% identical, their crystal structures are judged to be remarkably similar, whereby both LptA and LptC adopt slightly twisted β-jellyroll structures containing 16 and 15 antiparallel β-strands stretching throughout the length of proteins, respectively (Tran et al., 2010). The N-terminal region of LptD from *Shigella flexneri* also displays similar β-jellyroll fold when superimposed with *E. coli* LptA and LptC (Qiao et al., 2014).

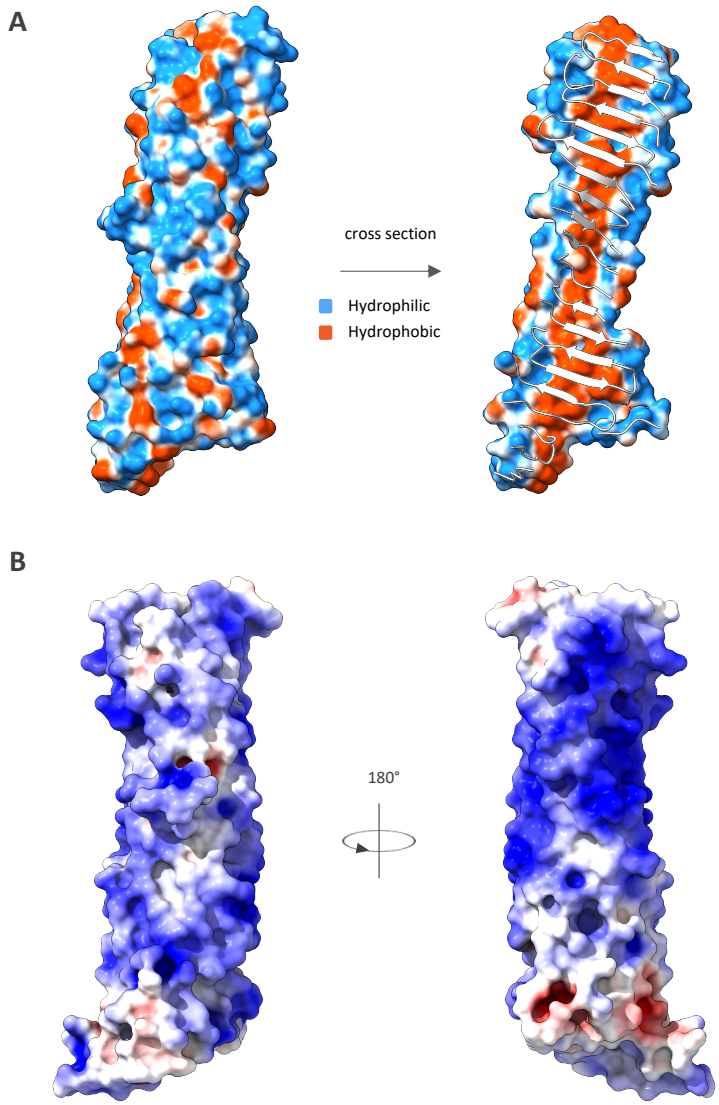

Figure 24: Surface representations of the soluble domain of *ana*LptC.
A) Hydrophobic surface representation of *ana*LptC$_{\Delta TM}$. The blue and orange colors represent hydrophilic and hydrophobic surfaces, respectively. B) Electrostatic surface potential of *ana*LptC$_{\Delta TM}$ at pH 7.5 with the most basic residues in blue and most acidic residues in red.

To investigate whether the obtained crystal structure of *Anabaena* sp. LptC also has this typical β-jellyroll fold, structural comparison was performed between *Anabaena* sp. LptC and the available crystal structure of *E. coli* LptC in the protein database (PDB 3my2). Although amino acid sequence alignment of *Anabaena* sp. and *E. coli* LptC using ClustalW (Thompson et al., 1994) revealed a low sequence identity score of 14% between both proteins, structural alignments performed with UCSF Chimera by shifting the structure of *ec*LptC along the structure of *ana*LptC stepwise every β-hairpin yielded a C_α r.m.s.d value of approximately 1 Å over the whole *ana*LptC molecule (Figure 25 and Table 7) indicating that the two structures of *Anabaena* sp. and *E. coli* LptC share a remarkably similar fold. This is consistent with the secondary structural prediction analysis (Ngo et al., 2020) via HHpred (Söding et al., 2005), which predicted that the periplasmic domain of *Anabaena* sp. LptC is composed of many β-strands with a high structural similarity score of 141 in comparison to *E. coli* LptC.

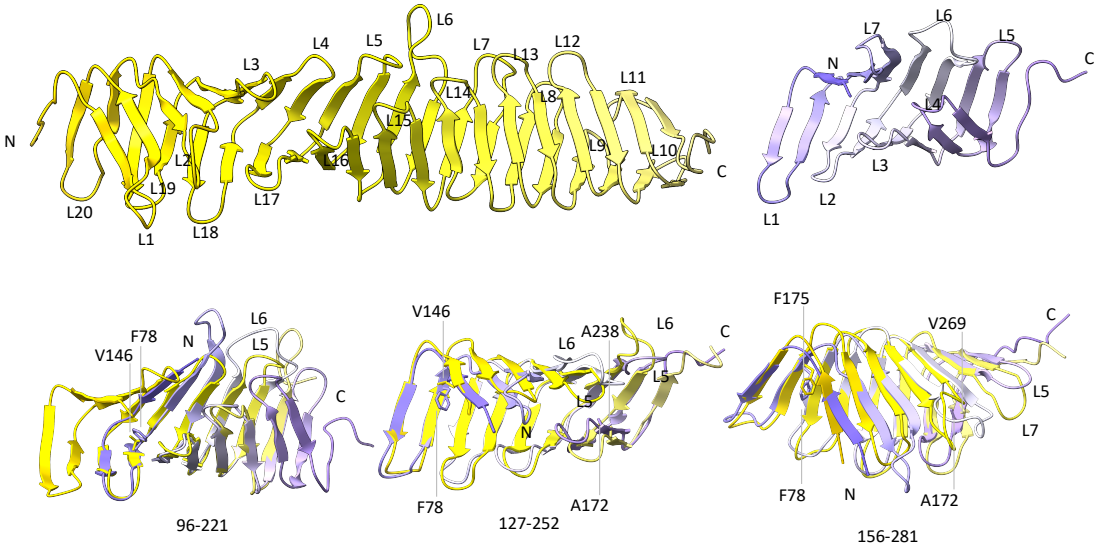

Figure 25: Structure superposition of *Anabaena* sp. LptC with *E. coli* LptC (PDB 3my2).
Anabaena sp. LptC with 20 loops (L1 to L20) and *E. coli* LptC containing 7 loops (L1 to L7) are colored in yellow and violet, respectively. *E. coli* LptC sequence (59 to 184 aa) was superimposed on *ana*LptC$_{\Delta TM}$ with the indicated amino acids sequences shown in the table 7 and the calculated $C_{\alpha\ r.m.s.d}$ values reveal structural similarities. Residues F78 and A172 of *E. coli* LptC bind LPS *in vivo* according to previous studies (Okuda et al., 2012). Corresponding residues of *Anabaena* sp. LptC sharing high similarity or identity are V146 and F175 for F78 in *ec*LptC and A238 and V269 for A172 in *ec*LptC.

Table 7. Residues of *Anabaena* sp. LptC and *E. coli* LptC used for structural comparison

Anabaena sp. LptC		*E.coli* LptC (PDB 3my2)		C_α
N-terminus	C-terminus	N-terminus	C-terminus	RMSD Å
62	187	59	184	1.036
96	221	59	184	0.807
127	252	59	184	0.978
156	281	59	184	1.062
186	311	59	184	1.006
221	346	59	184	1.034
251	372	59	184	1.024

Previous studies showed that *E. coli* LptC residues F78 and A172 bind LPS *in vivo* (Okuda et al., 2012). As shown in table 7, all alignments recognize both *E. coli* and *Anabaena* sp. LptC sequences used for structure superposition. Remarkably, three alignments using *Anabaena* sp. LptC amino acid sequences of 96-221, 127-252 and 156-281 identified residues that share high identity or similarity with the corresponding *E. coli* LptC residues F78 and A172. The structural alignment using residues 96-221 identified the *ana*LptC residue V146 for the *E. coli* residue F78. The structural alignment of residues 127-252 identified *ana*LptC residues V146 and A238, while the comparison of segment from 156 to 281 aa revealed the corresponding residues F175 and V269 from *ana*LptC for *ec*LptC residues F78 and A172, respectively (Figure 25).

3.4.3 Intramolecular interaction of *ana*LptC was observed by *in vitro* crosslinking

The crosslinking experiment using crosslinkers with final concentrations of 50 mM for dihydrazide sulfoxide (DHSO); 0.5 mM for zero length protein crosslinker N,N'-carbonyldiimidazole (CDI); 10 mM for disuccinimidyl dibutyric urea (DSBU) and 10 mM disuccinimidyl sulfoxide (DSSO) was performed as described in the section 2.2.7. The crosslinked peptides were analyzed by LC-MS/MS and evaluated by MaxQuant program (Cox & Mann, 2008).

The result revealed that a crosslink between Lys 77 and Lys 75 residues located N-terminally on loop 2 could be defined by CDI, a zero length crosslinker, in the crystal structure with a distance of approximately 12.6 Å. In contrast, DHSO crosslinks Asp 102 with Asp 107 residues located N-terminally on the outer leaflet of β-strand 7. The distance between them in the structure is about 20.6 Å, while DHSO crosslinker has a space length of 12.4 Å.

Addition of DSSO resulted in most crosslinking events, which are found again N-terminally on β-strands 6, 7, 8 and 9. Crosslinked residues are Lys 75 with Lys 77, Lys 100 with Lys 103, Lys 103

with Lys 118 and Lys 116 with Lys 118. The distance measured between the amide groups is in the range of 12 Å to 17 Å, while the crosslinker itself has a spacer arm of 10.3 Å.

DSBU is the only crosslinker found to crosslink towards the C-terminus of *ana*LptC. The crosslinked residues are Lys 298 with Lys 311. The distance between them measured at the amide groups is about 20 Å, while the spacer arm of the crosslinker is ca. 12.5 Å.

Therefore, the crosslinking observations showed good agreement with the molecular distance of the spacer arm of the crosslinkers used in the experiments. The crosslinked residues mostly lying in the region of the β-hairpin loops showed reasonable distances on the basis of the obtained X-ray structure, indicating the flexibility of the side chains of the *ana*LptC periplasmic domain (Figure 26).

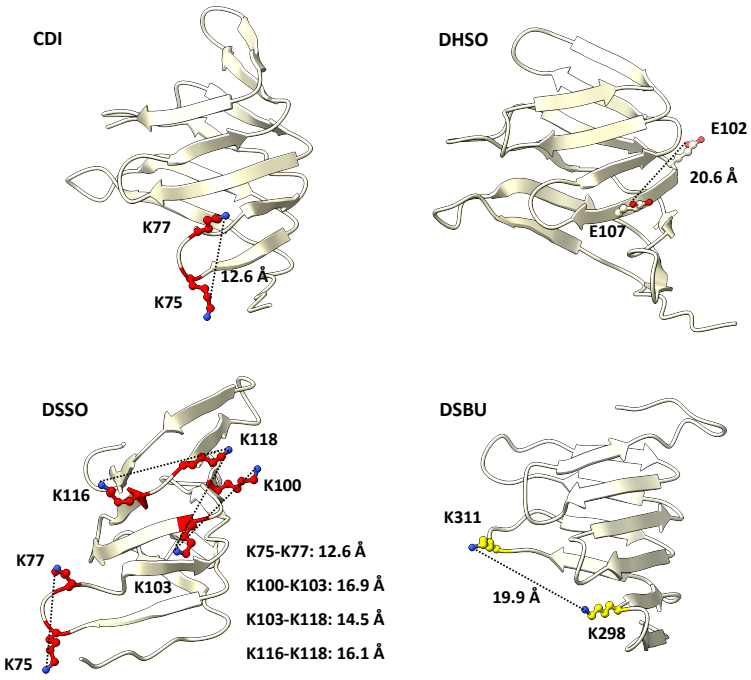

Figure 26: Intramolecular interaction of *ana*LptC via *in vitro* crosslinking.
Crosslinkers used in crosslinking experiments are DHSO; zero length protein crosslinker CDI; DSBU and DSSO. The crosslinked positions were represented on the obtained crystal structure of *ana*LptC using UCSF ChimeraX, while the distance between residues was measured by UCSF Chimera.

4 Discussion

4.1 The putative LptC protein from *Anabaena* sp. is involved in the outer membrane biogenesis

The outer membrane of Gram-negative bacteria possesses several essential functions owing to outer membrane proteins and LPS. It acts as a permeability function barrier by controlling polar solutes through the most abundant outer membrane proteins as such porin (Liu & Ferenci, 1998). It protects cells through LPS and hinders the entry of toxic substances present in their environment, in fact, the high impermeability to bile salts of the outer membrane allows the *E. coli* bacterium to colonize intestines (Nikaido, 2003; Ruiz et al., 2006). Like other membranes, the outer membrane with the hydrophobic nature prevents the passage of large polar molecules through electrostatic repulsion, however, it also inhibits small hydrophobic molecules from intercalation (Okuda et al., 2016).

There are two explanations for the physical properties of LPS that make the outer membrane an effective functional barrier. Firstly, the fatty acid substituents in LPS are all saturated and increased numbers of fatty acyl substituents per LPS molecule result in a decrease in the fluidity of the hydrocarbon chains (Nikaido, 2003). The low fluidity of hydrocarbon domains and the extensively hydrophobic interactions between hydrocarbon domains allow LPS molecules to pack densely in highly ordered membrane (Nikaido, 2003; Bertani & Ruiz, 2018). Secondly, ionic interactions of negative charges from phosphate groups with divalent cations and hydrogen bridges between polysaccharide moieties lead to the strong lateral interactions between LPS molecules that enable the ability of LPS to pack tightly (Nikaido, 2003; Ruiz et al., 2006).

The lateral interactions between LPS molecules were shown via molecular dynamics simulation only possible if divalent cations were present (Kotra et al., 1999; Nikaido, 2003). Divalent cations are very important for the structure of the outer membrane, as they intercalate between LPS molecules so that they prevent repulsion between the negatively charged phosphate groups of adjacent LPS molecules (Ruiz et al., 2006). Therefore, the assembled LPS molecules can form a highly ordered structure with a high density of charges and sugar chains on the cell surface that makes the permeability of hydrophobic molecules into the densely packed membrane unfavorable (Okuda et al., 2016).

The insertion mutant of *ana*LptC exhibited sensitivity to substances such as ethanol, salt, SDS and proteinase K. Similarly, the sensitivity of insertion mutants of *ana*LptD and *ana*LptA was demonstrated by the decreased viability in conditions containing these substances (Figure 7), suggesting that the outer membrane permeability of mutant strains AFS-I-*analptC*, AFS-I-*analptA*, AFS-I-*analptD* was affected. This conclusion is supported by early studies showing increased permeability of the outer membrane to chemicals upon inactivation of *anaomp85*, *analptD* in *Anabaena* sp. (Nicolaisen et al., 2009b; Hsueh et al., 2015) and *lptD* in *E. coli* (Freinkman et al., 2011). The alteration of the outer membrane due to the change in level of either proteins or LPS could be the reason for the sensitivity of the mutants towards harmful substances. Indeed, previous studies have shown that deletion of YaeT, a component of the complex composed of YaeT, YfiO, YfgL and NlpB required for the assembly of the outer membrane proteins, leads to a dramatical reduction of proteins in the outer membrane resulting in a decrease in the outer membrane density (Wu et al., 2005; Wu et al., 2006). However, the protein profile of AFS-I-*analptC* in the LPS isolation experiment was comparable with that of AFS-I-*anaomp85* and *Anabaena* sp. wild-type (Figure 8, right). In fact, the amount of the LPS with O-antigen decreased in the AFS-I-*analptC* strain, although the content of the core region and the lipid A was similar in the three strains (Figure 8, left). Thus, this result strongly suggests that *ana*LptC protein plays an important role in the LPS transport for outer membrane biogenesis.

The growth of both insertion mutants of *analptC* and *analptD* in the liquid media $BG11_0$ was completely inhibited, whereas the growth of the *ana*LptA mutant was severely impaired (Figure 6 C), suggesting an alteration of the outer membrane, which might result in the compromised ultra-structure of the cell envelope under condition without nitrogen. Under nitrogen deprivation, vegetative cells are enforced to develop into mature heterocysts for fixation of nitrogen. The cell envelope of these differentiated cells contain additional heterocyst-specific glycolipid layers, which function as a diffusion layer by creating a microoxic environment to protect the highly oxygen-sensitive nitrogenase from inactivation (Hahn & Schleiff, 2014). Therefore, the improperly assembled cell envelope resulted from the alteration of the outer membrane might be harmful for the cell in diazotrophic condition.

The study via transmission electron microscope showed that all mutants of *ana*LptC, *ana*LptA and *ana*LptD appear to be smaller in cell size than *Anabaena* sp. wild-type (Figure 9). The decrease in cell size seems to be a common phenotype of the compromised Lpt transport in *Anabaena* sp. and provides indirect evidence indicating that the cell coordinates growth of the entire cell envelope in highly cooperative manner to prevent mistargeting of LPS by defective machines. The small size phenotype likely results from a decrease in the rate of cell envelope growth, thereby restoring a balance between the rates of LPS assembly at the cell surface and envelope biogenesis, as reported by the analysis of a suppressor mutation that allows the survival of a *E. coli* LptF/G mutant strain with limited Lpt function (Yao et al., 2012). The molecular mechanism by which LPS biogenesis regulates the LPS quality control is not clear so far. However, the σ^E stress response factor shown in *E. coli* to be activated by either misfolded OMPs or defective LPS triggers a damage-repair pathway leading to the transcription of the genes in its regulon encoding chaperons required for the delivery and assembly of either porins or LPS (Tam & Missiakas, 2005; Johansen et al., 2006; Ruiz et al., 2006; Thompson et al., 2007; Ades, 2008). Despite the fact that in *Anabaena* sp. the σ^E stress response system is not identified, the gene *alr3280* coding for σ^E factor is found (Kaneko et al., 2001), indicating a similar quality control mechanism also exists in this organism and needs further to be investigated.

Furthermore, none of the three *Anabaena* sp. mutants of *ana*LptC, *ana*LptA and *ana*LptD were observed to have the previously described abnormal membrane structure of the *E. coli lptD* or *lptE* depletion mutants, in which the membranous material present in the periplasm (Wu et al., 2006). Even the mutant of *ana*LptD used in this study did not show any abnormal membrane structure, which has been demonstrated in the previous publication for the *ana*LptD mutant analyzed by transmission electron microscopy (Hsueh et al., 2015). There is no obvious explanation for this observation, but one can speculate that the effect might depend on segregation status of the mutant. It might be that the mutant of *ana*LptD in the previous study had different segregation level than the *ana*LptD mutant generated in this study.

4.2 The interaction of *ana*LptC with both, *ana*LptF and *ana*LptA, contributes to the formation of a trans-periplasmic bridge for the LPS transport

The crystal structures of seven components of the Lpt machinery, LptC from *E. coli*, LptA from *E. coli* and *Pseudomonas aeruginosa*, the LptDE outer membrane complex from *Shigella flexneri* and *Salmonella enterica serovar Typhimurium*, LptF and LptG in the $LptB_2FGC$ complex from *Vibrio cholerae* and *Enterobacter cloacae* have been solved (Suits et al., 2008; Tran et al., 2010; Dong et al., 2014; Qiao et al., 2014; Sherman et al., 2014; Wang et al., 2014; Bollati et al., 2015; Owens et al., 2019). Remarkably, the periplasmic loop of LptF and LptG, the LptC periplasmic domain, LptA and the periplasmic N-terminal domain of LptD share a similar β-jellyroll fold made of a variable number of antiparallel β-strands, and through this structurally homologous domain, LptC interacts with LptF, LptG and LptA, which finally interacts with the N-terminus of LptD (Martorana et al., 2016; Owens et al., 2019).

The secondary structural predictions via HHpred server revealed that *ana*LptA, *ana*LptF and *ana*LptC share structural similarities with *ec*LptA, *ec*LptF and *ec*LptC, respectively, indicating that the β-jellyroll fold might also be present in *ana*LptA protein, the periplasmic loop of *ana*LptF and the periplasmic domain of *ana*LptC (Hsueh et al., 2015; Ngo et al., 2020; Figure 5 and Figure 27). The pulldown experiments demonstrated that the *ana*LptC periplasmic domain interacts with the periplasmic loop of *ana*LptF and *ana*LptA (Figure 11 and Figure 12), suggesting that the interaction might occur via the β-jellyroll fold as well. However, these experiments did not determine exact positions of the binding. Nevertheless, these results showed that transmembrane helix region of *ana*LptC appears to be dispensable and not required for interaction with either *ana*LptF or *ana*LptA, since the *ana*LptC periplasmic domain alone is functional. Indeed, *ana*LptC forms a stable complex with *ana*LptA, while *ana*LptC binds to *ana*LptF less efficiently, indicating that the transmembrane helix may facilitate the interaction of *ana*LptC with *ana*LptF. Alternatively, the weak interaction between *ana*LptC with *ana*LptF could be due to the lack of *ana*LptB as an interaction partner and whether *ana*LptB may help enhancing the interaction has to be studied in future.

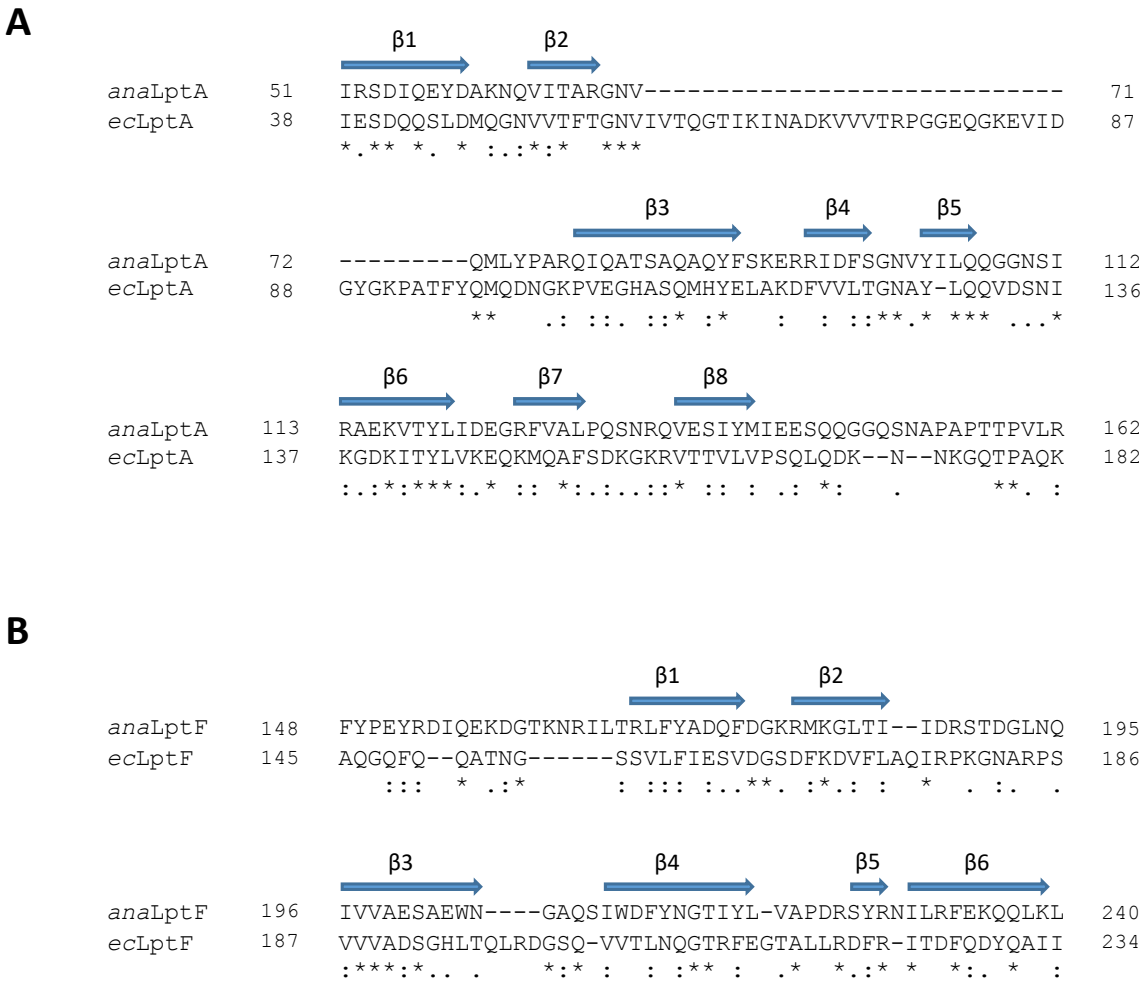

Figure 27: The secondary structural prediction for *ana*LptA and *ana*LptF.
The secondary structural alignment shows the structural similarities between *ana*LptA and *ec*LptA (A) as well as the periplasmic loop of *ana*LptF and *ec*LptF (B) via HHpred server (Söding et al., 2005). Proteins *ana*LptA and *ana*LptF were predicted to contain the secondary structural element of β-strands found in *ec*LptA and *ec*LptF, respectively. The results of the protein sequence alignment performed with T-coffee show conserved residues with high sequence identity or similarity (https://www.ebi.ac.uk/Tools/msa/tcoffee/).

The interaction of the *ana*LptC periplasmic domain with the predicted periplasmic loop of *ana*LptF and *ana*LptA suggests that *ana*LptC might form a trans-periplasmic bridge with *ana*LptF and *ana*LptA. This suggestion is further supported by the data of the previous interaction analysis between *ana*LptA and N-terminal region of *ana*LptD (Hsueh et al., 2015), indicating *ana*LptA might be anchored to the inner membrane and the outer membrane via docking sites of *ana*LptC and *ana*LptD, respectively. This proposal is in line with the architecture of *E. coli* LptCAD bridge, which suggested the C-terminal region of LptC in interaction with N-terminal region of LptA and C-terminal region of LptA in association with N-terminal region of LptD (Freinkman et al., 2012).

Furthermore, the model of the LptBFGC bridge proposed N-terminal region of LptC in association with C-terminal periplasmic loop of LptF (Owens et al., 2019). Consistently, the LptA monomers were found to be packed in linear filaments in crystals obtained in the presence of LPS suggesting that the oligomerization of LptA molecules might connect the inner membrane with the outer membrane (Suits et al., 2008; Sperandeo et al., 2011). The finding about Alr4069 sharing the same similarity to the protein sequence of both *E. coli* LptF and LptG (Haarmann et al., 2010) suggests that the composition of the inner membrane localized ABC transporter complex in *Anabaena* sp. may be somehow different from that of *E. coli*, in which transmembrane components probably exist as homodimer instead of heterodimer as in *E. coli*.

Little is known about how specific Lpt proteins interact with each other. Previous studies showed that the interaction of *ana*LptA with *ana*LptD *in vitro* is species-specific, as *ana*LptA did not recognize LptD or Lipid A from *E. coli* (Hsueh et al., 2015), however, the possibility about an interaction between *ana*LptA and with *ana*LptF or *ana*LptD and *ana*LptC was not excluded, despite the fact that they are all predicted to contain the β-jellyroll fold. The assembly of the Lpt transenvelope bridge has been shown to be finely regulated to prevent LPS mistargeting, in fact, the proper interaction of LptC with LptBFG is crucial for the recruitment of LptA (Villa et al., 2013; Martorana et al., 2016). Accordingly, the G56V amino acid substituted LptC mutant protein but not the G153R substituted LptC mutant protein from *E. coli* was previously shown unable to interact with LptBFG subcomplex suggesting that LptC interaction with the LptBFG seems to be mediated through the N-terminal region of the LptC periplasmic domain (Villa et al., 2013). LptC mutant protein G56V does not copurify LptA indicating that the impaired interaction with LptBFG destabilizes the whole Lpt complex which cannot be copurified as a single complex (Villa et al., 2013). Furthermore, the *in vivo* interaction in *E. coli* between LptA and the N-terminal region of LptD was showed that it only occurs if the outer membrane complex LptDE is correctly assembled, which in turn requires the formation of at least one non-consecutive disulfide bond in LptD (Freinkman et al., 2012; Martorana et al., 2016).

This study showed that *ana*LptC is capable of forming a complex with *ana*LptF and *ana*LptA in absence of LPS, indicating an LPS-independent interaction. However, the affinity of binding between either *ana*LptC and *ana*LptF or *ana*LptC and *ana*LptA is still not determined due to

inappropriate approaches. Previously in *E. coli* LptA was shown to interact with LptC through its N-terminus to form a LptC-LptA complex with an affinity of 4 µM, while it can interact with itself to form a LptA-LptA multimer an affinity of 29 µM (Schultz et al., 2013), suggesting that the interaction of LptA with LptC is stronger than that of LptA with itself. One can speculate that stronger affinity may help to ensure the binding of LptA to LptC in the periplasm and the multimerization property of LptA is not always strongly assembled, which is in agreement with the observation that monomeric LptA is able to support the mutant cell growth *in vivo* (Laguri et al., 2017).

The binding analysis of *E. coli* LPS to the *ana*LptC periplasmic domain lacking a transmembrane helix via fluorescence spectroscopy to decipher the role of *ana*LptC in the transfer of LPS through periplasm revealed that the interaction between them occurs in an ATP independent manner with a dissociation constant Kd of 55 µM, which is consistent with the estimated affinity of *ec*LptC for LPS in the range 28.8-71.4 µM (Sestito et al., 2014). This result supports the role of *ana*LptC involved in LPS transport. LptC has been shown that it does not affect the ATPase activity while associated with the $LptB_2FG$ complex, despite the fact that it is a part of the inner membrane ABC transporter complex (Narita & Tokuda, 2009). The energy in form of ATP does not seem to be required for the assembly of the Lpt complex (Okuda et al., 2012), in contrast, ATP hydrolysis by the LptB ATPase of $LptB_2FG$ transporter is required for LPS extraction from the inner membrane and LPS transfer to LptC (Martorana et al., 2016).

4.3 *Anabaena* sp. LptC structural and functional relationship

The X-ray structure of the periplasmic domain of *Anabaena* sp. LptC, which contains 40 consecutive antiparallel β-strands and lacks the 26 residues long N-terminal transmembrane helix region, appears to be correctly folded. This conclusion is supported by the results of pulldown experiments showing that *ana*LptC binds to both *ana*LptF and *ana*LptA (Figure 11 and Figure 12). Furthermore, *ana*LptC also interacts with LPS of *E. coli* to form a complex with an affinity of 55 µM (Figure 14 B). The protein sequence of the periplasmic domain of *Anabaena* sp. LptC consists of 359 amino acids (residues 27 to 385). While one region with residues 43-372 was observed in the electron density map, two other regions residues 27-42 at N-terminus and 373-

385 at C-terminus were not mapped, implicating that these regions are disordered. Disordered regions were reported in outer membrane receptors in previous studies demonstrating that colicin binding to disordered regions of its receptors causes partially folded proteins to fold into an ordered structure (Tozawa et al., 2005; Hecht et al., 2009). Consistently, *E. coli* LptC lacking the disordered region in the C-terminal end fails to interact with LptA, suggesting that disordered regions might be reorganized and folded upon binding to a partner molecule or protein (Sperandeo et al., 2011).

The obtained crystal structure of the *ana*LptC periplasmic domain solved at 2.8 Å reveals an overall structure sharing several striking similarities with *ec*LptC. Both structures of *ana*LptC and *ec*LptC are composed of consecutive antiparallel β-strands spreading throughout proteins and twisting 180° around their axis (Figure 22, left and Figure 25). Furthermore, the structural alignment between *ana*LptC and *ec*LptC confirms the similarity in folding with C_α r.m.s.d value of approximately 1 Å (Table 7), indicating that *ana*LptC also adopts the conserved β-jellyroll fold, as observed in Lpt proteins (Martorana et al., 2016; Owens et al., 2019). Remarkably, the β-jellyroll fold of *ec*LptC is found throughout the whole structure of *ana*LptC, when *ec*LptC structure is superimposed along the structure of *ana*LptC stepwise every β-hairpin (Figure 25), supporting the proposal that the β-jellyroll fold might be the key element in the assembly of the Lpt complex (Martorana et al., 2016). Conserved residues V146 and F175 as well as A238 and V269 in *ana*LptC show high similarity or identity via the structural alignment to F78 and A172 in *ec*LptC, respectively (Figure 25). The fact that residues F78 and A172 from *ec*LptC were previously shown to bind LPS *in vivo* (Okuda et al., 2012), suggests that the residues V146, F175, A238 and V269 in *ana*LptC could also be the binding site for LPS.

Moreover, *ana*LptC showed the same orientation of hydrophobic residues toward the interior cavity, as observed in *ec*LptC. On one hand, the hydrophobicity surface represented that the cross section through longitudinal axis of *ana*LptC exhibits a highly hydrophobic core with most of the hydrophobic amino acids buried inside the molecule, which could potentially serve as binding sites for LPS (Figure 24 A). On the other hand, the hydrophobicity surface representation demonstrated that the solvent exposed surface of *ana*LptC did not show any distinct patches of hydrophobicity but a high level of hydrophilicity, as expected for the soluble domain. In fact, the

electrostatic potential representation at pH of 7.5 showed that the surface of *ana*LptC consists of mostly positively charged residues, apart from a small patch at the N-terminal edge containing negatively charged residues, suggesting that these residues may mediate electrostatic interactions with LPS (Figure 24 B).

There are some differences between the two structures of *ana*LptC and *ec*LptC, beside the above mentioned similarities. For example, loop 6 and loop 7 in *ana*LptC sind longer than loop 5 in *ec*LptC. In contrast, loop 5 of *ana*LptC is shorter than loop 6 of *ec*LptC (Figure 25). Another remarkable difference is that the length of *ana*LptC is more than two times longer than that of *ec*LptC. The length of *ana*LptC composed of 40 β-strands is roughly 100 Å long, in contrast, *ec*LptC is only 40 Å long and consists of 15 β-strands (Figure 25). This result is in agreement with the observation showing that the *Anabaena* sp. peptidoglycan diameter of 14 nm thickness is more than two times thicker than that of approximately 6.4 nm in *E. coli* (Matias et al., 2003; Wilk et al., 2011). Consistently, the distance of the periplasmic space between the outer membrane and the inner membrane in *Anabaena* sp. is 46 ± 3 nm significantly larger compared to that of 18-21 nm in *E. coli*. (Silhavy et al., 2010; Wilk et al., 2011). Here, one can make an assumption that due to evolutionary pressure, *Anabaena* sp. evolved a longer structure of *ana*LptC in order to overcome the long periplasmic space for LPS transport, supporting the proprosal that the trans-periplasmic bridge could dynamically assemble, potentially depending on the local periplasm width and the presence of LPS (Laguri et al., 2017).

4.4 The proposed model of LptC function in *Anabaena* sp.

The electrostatic repulsion between LPS molecules resulted from the negative charges of LPS might separate them at the outer leaflet of the inner membrane (Dong et al., 2014). In close proximity, *ana*LptC links to *ana*LptF and *ana*LptA, forming a proteinaceous trans-envelope complex together with other Lpt proteins from the inner membrane to the outer membrane. Since no cavity is found in the *ana*LptC crystal structure, *ana*LptC would have to undergo comformation changes in order to accommodate the lipid A subunits of LPS, as suggested for *ec*LptC (Tran et al., 2010). This model suggests that via ATP hydrolysis by the ATPase *ana*LptB, the LPS is extracted from the inner membrane and tranfered to *ana*LptC through *ana*LptF (Figure 28

①). At this stage, *ana*LptC might be in a closed state. LPS binding to *ana*LptC might trigger changes in the comformation of *ana*LptC, resulting in a open state of *ana*LptC (Figure 28 ②). The hydrophobic conversed residues identified in *ana*LptC via structural superposition with *ec*LptC might serve as binding sites for LPS. In an affinity-driven manner, LPS moves through the hydrophobic interior of *ana*LptC, which then delivers it to *ana*LptA for further transport to the outer membrane (Figure 28 ③). After LPS is handed over to *ana*LptA, *ana*LptC might change back to the closed comformation.

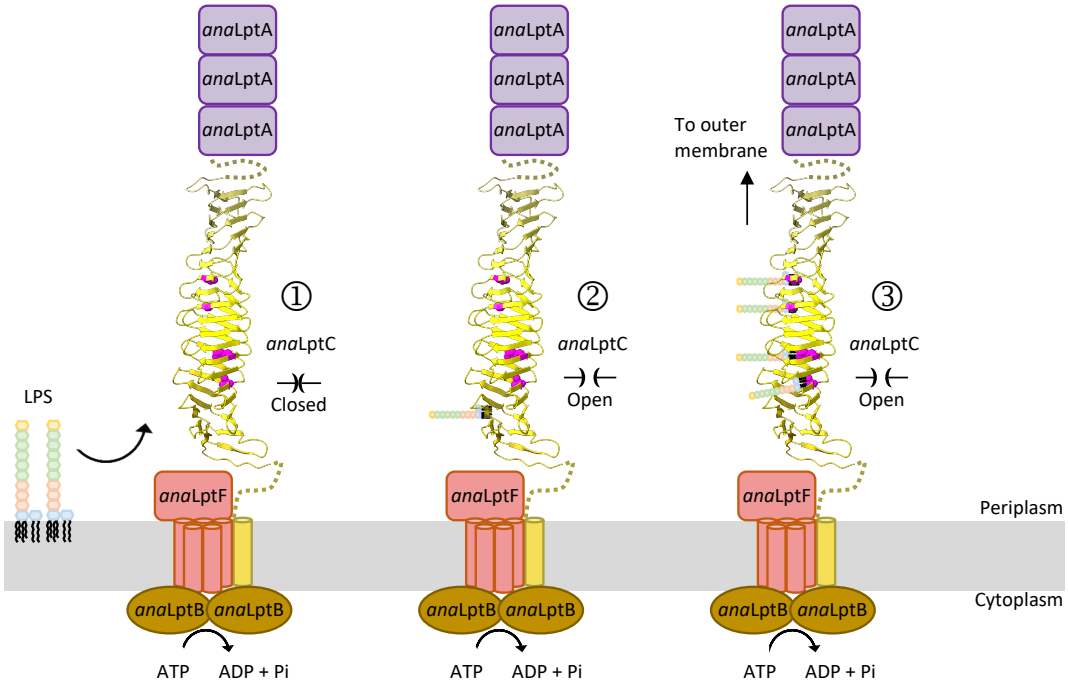

Figure 28: Model of LptC function in *Anabaena* sp. PCC 7120.

At the periplasmic side of the inner membrane, *ana*LptC interacts with *ana*LptF and *ana*LptA,forming the trans-envelope complex. By using the *ana*LptB hydrolyzed ATP, LPS is extracted from the inner membrane and delivered to *ana*LptC in a closed state through *ana*LptF ①. Upon binding to LPS, *ana*LptC changes its comformation to a open state ②. LPS molecules bind to the hydrophobic conserved resides (magenta) residing inside *ana*LptC, which passes LPS to *ana*LptA ③.

4.5 Future prospects

The crystal structure of the periplasmic domain of *ana*LptC displays some distinctions from *ec*LptC. However, *ana*LptC periplasmic domain shares the same β-jellyroll structure as well as several conserved residues found in *ec*LptC. Conserved residues of *ec*LptC were previously shown to bind to LPS *in vivo*. Therefore, it will be exciting to elucidate whether the conserved residues

identified from the crystal structure of *ana*LptC are potential binding sites of LPS. Conserved residues of *ana*LptC can be substituted with *p*BPA and the interaction with LPS can be confirmed via photo-crosslinking experiments.

The soluble domain of *ana*LptC interacts with both *ana*LptF and *ana*LptA, as observed in *ec*LptC (Freinkman et al., 2012; Owens et al., 2019). In the model of *E. coli* LptCAD bridge the C-terminal region of LptC was proposed to interact with the N-terminal region of LptA (Freinkman et al., 2012), while N-terminal region of LptC was suggested in association with C-terminal periplasmic loop of LptF in the model of the LptBFGC bridge (Owens et al., 2019). Thus, it is of special interest to define which of functional regions of *ana*LptC are in interaction with *ana*LptF and *ana*LptA. C- and N-terminal segments of *ana*LptC containing His-tag can be recombinantly generated. *In vitro* interaction studies of C- and N-terminal fragments of *ana*LptC with either *ana*LptF or *ana*LptA can then be performed using Ni-NTA affinity chromatography method.

One open question is that whether in *Anabaena* sp. the homolog of *ec*LptE exists, which functions as a plug protein located inside the *ec*LptD outer membrane protein. To answer this question, the complex of Lpt proteins containing the missing component needs to be isolated via a combined approach between crosslinking and immunoprecipitation. Since the purification using the construct of the soluble domain of *ana*LptC showed high purity and a high amount of the protein in this study, an antibody against *ana*LptC can be generated and used in an immunoprecipitation experiment to isolate the complex.

5 References

Ades, S. E. (2008). Regulation by destruction: design of the σE envelope stress response. *Current Opinion in Microbiology*, *11*(6), 535–540. https://doi.org/10.1016/j.mib.2008.10.004

Anderson, M. S., & Raetz, C. R. (1987). Biosynthesis of lipid A precursors in Escherichia coli. A cytoplasmic acyltransferase that converts UDP-N-acetylglucosamine to UDP-3-O-(R-3-hydroxymyristoyl)-N-acetylglucosamine. *Journal of Biological Chemistry*, *262*(11), 5159–5169. https://doi.org/10.1016/s0021-9258(18)61169-x

Aono, R., Negishi, T., Aibe, K., Inoue, A., & Horikoshi, K. (1994). Mapping of Organic Solvent Tolerance Gene ostA in Escherichia coli K-12 . *Bioscience, Biotechnology, and Biochemistry*, *58*(7), 1231–1235. https://doi.org/10.1271/bbb.58.1231

Apicella, M. A., Griffiss, J., & Schneider, H. (1994). Isolation and characterization of lipopolysaccharides, lipooligosaccharides, and lipid A. *Methods in Enzymology*, *235*(C), 242–252. https://doi.org/10.1016/0076-6879(94)35145-7

Bertani, B., & Ruiz, N. (2018). Function and Biogenesis of Lipopolysaccharides. *EcoSal Plus*, *8*(1), 1–33. https://doi.org/10.1128/ecosalplus.esp-0001-2018

Bollati, M., Villa, R., Gourlay, L. J., Benedet, M., Dehò, G., Polissi, A., Barbiroli, A., Martorana, A. M., Sperandeo, P., Bolognesi, M., & Nardini, M. (2015). Crystal structure of LptH, the periplasmic component of the lipopolysaccharide transport machinery from Pseudomonas aeruginosa. *FEBS Journal*, *282*(10), 1980–1997. https://doi.org/10.1111/febs.13254

Bos, M. P., Robert, V., & Tommassen, J. (2007). Biogenesis of the gram-negative bacterial outer membrane. *Annual Review of Microbiology*, *61*, 191–214. https://doi.org/10.1146/annurev.micro.61.080706.093245

Brouwer, E.-M., Ngo, G., Yadav, S., Ladig, R., & Schleiff, E. (2019). Tic22 from Anabaena sp. PCC 7120 with holdase function involved in outer membrane protein biogenesis shuttles between plasma membrane and Omp85. *Molecular Microbiology*, *111*(5). https://doi.org/10.1111/mmi.14222

Chimalakonda, G., Ruiz, N., Chng, S. S., Garner, R. A., Kahne, D., & Silhavy, T. J. (2011). Lipoprotein LptE is required for the assembly of LptD by the β-barrel assembly machine in the outer membrane of Escherichia coli. *Proceedings of the National Academy of Sciences of the*

United States of America, *108*(6), 2492–2497. https://doi.org/10.1073/pnas.1019089108

Chittora, D., Meena, M., Barupal, T., & Swapnil, P. (2020). Cyanobacteria as a source of biofertilizers for sustainable agriculture. *Biochemistry and Biophysics Reports*, *22*(January), 100737. https://doi.org/10.1016/j.bbrep.2020.100737

Chng, S., Gronenberg, L., & Kahne, D. (2010). Proteins required for lipopolysaccharide assembly in Escherichia coli form a trans-envelope complex. *Biochemistry*, *49*(22), 4565–4567. https://doi.org/10.1021/bi100493e.Proteins

Chng, S. S., Ruiz, N., Chimalakonda, G., Silhavy, T. J., & Kahne, D. (2010). Characterization of the two-protein complex in Escherichia coli responsible for lipopolysaccharide assembly at the outer membrane. *Proceedings of the National Academy of Sciences of the United States of America*, *107*(12), 5363–5368. https://doi.org/10.1073/pnas.0912872107

Comte, K., Šabacká, M., Carré-Mlouka, A., Elster, J., & Komárek, J. (2007). Relationships between the Arctic and the Antarctic cyanobacteria; three Phormidium-like strains evaluated by a polyphasic approach. *FEMS Microbiology Ecology*, *59*(2), 366–376. https://doi.org/10.1111/j.1574-6941.2006.00257.x

Cowan, S., Schirmer, T., Rummel, G., Steiert, M., Ghosh, R., Pauptit, R., Jansonius, J., & Rosenbusch, J. (1992). Crystal structures explain functional properties of two E. coli porins. *Nature*, *358*, 727–733.

Cox, J., & Mann, M. (2008). MaxQuant enables high peptide identification rates, individualized p.p.b.-range mass accuracies and proteome-wide protein quantification. *Nature Biotechnology*, *26*(12), 1367–1372. https://doi.org/10.1038/nbt.1511

Delcour, A. H. (2009). Outer membrane permeability and antibiotic resistance. *Biochimica et Biophysica Acta - Proteins and Proteomics*, *1794*(5), 808–816. https://doi.org/10.1016/j.bbapap.2008.11.005

Demoulin, C. F., Lara, Y. J., Cornet, L., François, C., Baurain, D., Wilmotte, A., & Javaux, E. J. (2019). Cyanobacteria evolution: Insight from the fossil record. *Free Radical Biology and Medicine*, *140*(May), 206–223. https://doi.org/10.1016/j.freeradbiomed.2019.05.007

Doerrler, W. T., Gibbons, H. S., Christian, R., & Raetz, H. (2004). MsbA-dependent translocation of lipids across the inner membrane of Escherichia coli. *Journal of Biological Chemistry*, *279*(43), 45102–45109. https://doi.org/10.1074/jbc.M408106200

Dong, H., Xiang, Q., Gu, Y., Wang, Z., Paterson, N. G., Stansfeld, P. J., He, C., Zhang, Y., Wang, W., & Dong, C. (2014). Structural basis for outer membrane lipopolysaccharide insertion. *Nature*, *511*(7507), 52–56. https://doi.org/10.1038/nature13464

Dor, I., & Danin, A. (1996). Cyanobacterial desert crusts in the Dead Sea Valley, Israel. *Algological Studies*, *83*, 197–206. https://doi.org/10.1127/algol_stud/83/1996/197

Ducruix, A., & Giege´, R. (1999). Crystallization of Nucleic Acids and Proteins: A Practical Approach. 2nd ed. Oxford University Press

Duong, F., Eichler, J., Price, A., Leonard, M. R., & Wickner, W. (1997). Biogenesis of the gram-negative bacterial envelope. *Cell*, *91*(5), 567–573. https://doi.org/10.1016/S0092-8674(00)80444-4

Durai, P., Batool, M., & Choi, S. (2015). Structure and effects of cyanobacterial lipopolysaccharides. *Marine Drugs*, *13*(7), 4217–4230. https://doi.org/10.3390/md13074217

Ebbensgaard, A., Mordhorst, H., Aarestrup, F. M., & Hansen, E. B. (2018). The role of outer membrane proteins and lipopolysaccharides for the sensitivity of escherichia coli to antimicrobial peptides. *Frontiers in Microbiology*, *9*, 1–13. https://doi.org/10.3389/fmicb.2018.02153

El-Gebali, S., Mistry, J., Bateman, A., Eddy, S. R., Luciani, A., Potter, S. C., Qureshi, M., Richardson, L. J., Salazar, G. A., Smart, A., Sonnhammer, E. L. L., Hirsh, L., Paladin, L., Piovesan, D., Tosatto, S. C. E., & Finn, R. D. (2019). The Pfam protein families database in 2019. *Nucleic Acids Research*, *47*(D1), D427–D432. https://doi.org/10.1093/nar/gky995

Elhai, J., Vepritskiy, A., Muro-Pastor, A. M., Flores, E., & Wolk, C. P. (1997). Reduction of conjugal transfer efficiency by three restriction activities of Anabaena sp. strain PCC 7120. *Journal of Bacteriology*, *179*(6), 1998–2005. https://doi.org/10.1128/jb.179.6.1998-2005.1997

Elhai, J., & Wolk, C. P. (1988). Conjugal Transfer of DNA to Cyanobacteria. *Methods in Enzymology*, *167*(C), 747–754. https://doi.org/10.1016/0076-6879(88)67086-8

Emsley, P., Lohkamp, B., Scott, W. G., & Cowtan, K. (2010). Features and development of Coot. *Acta Crystallographica Section D: Biological Crystallography*, *66*(4), 486–501. https://doi.org/10.1107/S0907444910007493

Finn, R. D., Tate, J., Mistry, J., Coggill, P. C., Sammut, S. J., Hotz, H. R., Ceric, G., Forslund, K., Eddy,

S. R., Sonnhammer, E. L. L., & Bateman, A. (2008). The Pfam protein families database. *Nucleic Acids Research*, *36*(SUPPL. 1), 281–288. https://doi.org/10.1093/nar/gkm960

Flores, E., & Herrero, A. (2010). Compartmentalized function through cell differentiation in filamentous cyanobacteria. *Nature Reviews Microbiology*, *8*(1), 39–50. https://doi.org/10.1038/nrmicro2242

Flores, E., Herrero, A., Wolk, C. P., & Maldener, I. (2006). Is the periplasm continuous in filamentous multicellular cyanobacteria? *Trends in Microbiology*, *14*(10), 439–443. https://doi.org/10.1016/j.tim.2006.08.007

Freinkman, E., Chng, S. S., & Kahne, D. (2011). The complex that inserts lipopolysaccharide into the bacterial outer membrane forms a two-protein plug-and-barrel. *Proceedings of the National Academy of Sciences of the United States of America*, *108*(6), 2486–2491. https://doi.org/10.1073/pnas.1015617108

Freinkman, E., Okuda, S., Ruiz, N., & Kahne, D. (2012). Regulated Assembly of the Transenvelope Protein Complex Required for Lipopolysaccharide Export. *Biochemistry*, *51*(24), 4800–4806. https://doi.org/10.1021/bi300592c

Gademann, K., & Portmann, C. (2008). Secondary Metabolites from Cyanobacteria: Complex Structures and Powerful Bioactivities. *Current Organic Chemistry*, *12*(4), 326–341. https://doi.org/10.2174/138527208783743750

Gan, L., Chen, S., & Jensen, G. J. (2008). *Molecular organization of Gram-negative peptidoglycan*. *105*(48), 1–8. papers3://publication/uuid/6822BC4E-DBEF-4D37-9A8A-CEA665CC0E1B

Geertsma, E. R., & Dutzler, R. (2011). A versatile and efficient high-throughput cloning tool for structural biology. *Biochemistry*, *50*(15), 3272–3278. https://doi.org/10.1021/bi200178z

Glauner, B., Holtje, J. V., & Schwarz, U. (1988). The composition of the murein of Escherichia coli. *Journal of Biological Chemistry*, *263*(21), 10088–10095. https://doi.org/10.1016/s0021-9258(19)81481-3

Golden, J. W., & Yoon, H. S. (1998). Heterocyst formation in Anabaena. *Current Opinion in Microbiology*, *1*(6), 623–629. https://doi.org/10.1016/S1369-5274(98)80106-9

Golecki, J. R. (1977). Studies on ultrastructure and composition of cell walls of the cyanobacterium Anacystis nidulans. *Archives of Microbiology*, *114*(1), 35–41. https://doi.org/10.1007/BF00429627

Haarmann, R., Ibrahim, M., Stevanovic, M., Bredemeier, R., & Schleiff, E. (2010). The properties of the outer membrane localized Lipid A transporter LptD. *Journal of Physics Condensed Matter*, *22*(45). https://doi.org/10.1088/0953-8984/22/45/454124

Hahn, A., & Schleiff, E. (2014). The Cell Envelope. In E. Flores & A. Herrero (Eds.), *The Cell Biology of Cyanobacteria* (pp. 29–87). Caister Academic Press.

Hecht, O., Ridley, H., Lakey, J. H., & Moore, G. R. (2009). A Common Interaction for the Entry of Colicin N and Filamentous Phage into Escherichia coli. *Journal of Molecular Biology*, *388*(4), 880–893. https://doi.org/10.1016/j.jmb.2009.03.035

Heinrichs, D. E., Yethon, J. A., & Whitfield, C. (1998). Molecular basis for structural diversity in the core regions of the lipopolysaccharides of Escherichia coli and Salmonella enterica. *Molecular Microbiology*, *30*(2), 221–232. https://doi.org/10.1046/j.1365-2958.1998.01063.x

Herrero, A., Stavans, J., & Flores, E. (2016). The multicellular nature of filamentous heterocyst-forming cyanobacteria. *FEMS Microbiology Reviews*, *40*(6), 831–854. https://doi.org/10.1093/femsre/fuw029

Hoiczyk, E., & Baumeister, W. (1995). Envelope structure of four gliding filamentous cyanobacteria. *Journal of Bacteriology*, *177*(9), 2387–2395. https://doi.org/10.1128/jb.177.9.2387-2395.1995

Hoiczyk, Egbert, & Hansel, A. (2000). Cyanobacterial cell walls: News from an unusual prokaryotic envelope. *Journal of Bacteriology*, *182*(5), 1191–1199. https://doi.org/10.1128/JB.182.5.1191-1199.2000

Horath, T., & Bachofen, R. (2009). Molecular characterization of an endolithic microbial community in dolomite rock in the central Alps (switzerland). *Microbial Ecology*, *58*(2), 290–306. https://doi.org/10.1007/s00248-008-9483-7

Hsueh, Y. C., Brouwer, E. M., Marzi, J., Mirus, O., & Schleiff, E. (2015). Functional properties of LptA and LptD in Anabaena sp. PCC 7120. *Biological Chemistry*, *396*(9–10), 1151–1162. https://doi.org/10.1515/hsz-2014-0322

Hu, B., Yang, G., Zhao, W., Zhang, Y., & Zhao, J. (2007). MreB is important for cell shape but not for chromosome segregation of the filamentous cyanobacterium Anabaena sp. PCC 7120. *Molecular Microbiology*, *63*(6), 1640–1652. https://doi.org/10.1111/j.1365-

2958.2007.05618.x

Hug, I., Couturier, M. R., Rooker, M. M., Taylor, D. E., Stein, M., & Feldman, M. F. (2010). Helicobacter pylori lipopolysaccharide is synthesized via a novel pathway with an evolutionary connection to protein N-glycosylation. *PLoS Pathogens*, *6*(3). https://doi.org/10.1371/journal.ppat.1000819

Iacobucci, C., Götze, M., Ihling, C.H., Piotrowski, C., Arlt, C., Schäfer, M., Hage, C., Schmidt, R., & Sinz, A. (2018). A cross-linking/mass spectrometry workflow based on MS-cleavable cross-linkers and the MeroX software for studying protein structures and protein–protein interactions. *Nature protocols*, *13*, 2864–2889. https://doi.org/10.1038/s41596-018-0068-8

Johansen, J., Rasmussen, A. A., Overgaard, M., & Valentin-Hansen, P. (2006). Conserved Small Non-coding RNAs that belong to the σE Regulon: Role in Down-regulation of Outer Membrane Proteins. *Journal of Molecular Biology*, *364*(1), 1–8. https://doi.org/10.1016/j.jmb.2006.09.004

Joseleau-Petit, D., Liébart, J. C., Ayala, J. A., & D'Ari, R. (2007). Unstable Escherichia coli L forms revisited: Growth requires peptidoglycan synthesis. *Journal of Bacteriology*, *189*(18), 6512–6520. https://doi.org/10.1128/JB.00273-07

Jürgens, U. J., Drews, G., & Weckesser, J. (1983). Primary structure of the peptidoglycan from the unicellular cyanobacterium Synechocystis sp. strain PCC 6714. *Journal of Bacteriology*, *154*(1), 471–478. https://doi.org/10.1128/jb.154.1.471-478.1983

Kabsch, W. (1993). Automatic processing of rotation diffraction data from crystals of initially unknown symmetry land cell constants. *Journal of Applied Crystallography*, *26*(pt 6), 795–800. https://doi.org/10.1107/S0021889893005588

Kabsch, W. (2010). XDS. *Acta Crystallographica Section D: Biological Crystallography*, *66*, 125–132. https://doi.org/10.1107/S0907444909047337

Kaneko, T., Nakamura, Y., Wolk, C. P., Kuritz, T., Sasamoto, S., Watanabe, A., Iriguchi, M., Ishikawa, A., Kawashima, K., Kimura, T., Kishida, Y., Kohara, M., Matsumoto, M., Matsuno, A., Muraki, A., Nakazaki, N., Shimpo, S., Sugimoto, M., Takazawa, M., … Tabata, S. (2001). Complete genomic sequence of the filamentous nitrogen-fixing cyanobacterium Anabaena sp. Strain PCC 7120. *DNA Research*, *8*(5), 205–213. https://doi.org/10.1093/dnares/8.5.205

Karow, M., & Georgopoulos, C. (1993). The essential Escherichia coli msbA gene, a multicopy

suppressor of null mutations in the htrB gene, is related to the universally conserved family of ATP-dependent translocators. *Molecular Microbiology*, *7*(1), 69–79. https://doi.org/10.1111/j.1365-2958.1993.tb01098.x

Keeling, P. J. (2010). The endosymbiotic origin, diversification and fate of plastids. *Philosophical Transactions of the Royal Society B: Biological Sciences*, *365*(1541), 729–748. https://doi.org/10.1098/rstb.2009.0103

Keleti, G., & Sykora, J. L. (1982). Production and properties of cyanobacterial endotoxins. *Applied and Environmental Microbiology*, *43*(1), 104–109. https://doi.org/10.1128/aem.43.1.104-109.1982

Kodani, S., Ishida, K., & Murakami, M. (1999). Occurrence and identification of UDP-N-acetylmuramyl-pentapeptide from the cyanobacterium Anabaena cylindrica. *FEMS Microbiology Letters*, *176*(2), 321–325. https://doi.org/10.1016/S0378-1097(99)00251-7

Koebnik, R., Locher, K. P., & Van Gelder, P. (2000). Structure and function of bacterial outer membrane proteins: barrels in a nutshell. *Molecular Microbiology*, *37*(2), 239–253. https://doi.org/10.1046/j.1365-2958.2000.01983.x

Konovalova, A., Kahne, D. E., & Silhavy, T. J. (2017). Outer Membrane Biogenesis. *Annual Review of Microbiology*, *71*, 539–556. https://doi.org/10.1146/annurev-micro-090816-093754

Kotra, L. P., Golemi, D., Amro, N. A., Liu, G. Y., & Mobashery, S. (1999). Dynamics of the lipopolysaccharide assembly on the surface of Escherichia coli. *Journal of the American Chemical Society*, *121*(38), 8707–8711. https://doi.org/10.1021/ja991374z

Köster, S., Kühlbrandt, W., & Yildiz, Ö. (2009). Purification, crystallization and preliminary X-ray diffraction analysis of the FeoB G domain from Methanococcus jannaschii. *Acta Crystallographica Section F: Structural Biology*, *65*, 684-687. https://doi.org/10.1107/S1744309109019216

Krogh, A., Larsson, B., Von Heijne, G., & Sonnhammer, E. L. L. (2001). Predicting transmembrane protein topology with a hidden Markov model: Application to complete genomes. *Journal of Molecular Biology*, *305*(3), 567–580. https://doi.org/10.1006/jmbi.2000.4315

Kumar, K., Mella-Herrera, R. A., & Golden, J. W. (2010). Cyanobacterial heterocysts. *Cold Spring Harbor Perspectives in Biology*, *2*(4), 1–20. https://doi.org/10.1101/cshperspect.a000315

Laguri, C., Sperandeo, P., Pounot, K., Ayala, I., Silipo, A., Bougault, C. M., Molinaro, A., Polissi, A.,

& Simorre, J. P. (2017). Interaction of lipopolysaccharides at intermolecular sites of the periplasmic Lpt transport assembly. *Scientific Reports*, *7*(1), 1–13. https://doi.org/10.1038/s41598-017-10136-0

Lerouge, I., & Vanderleyden, J. (2002). O-antigen structural variation: mechanisms and possible roles in animal/plant-microbe interactions. *FEMS Microbiology Reviews*, *26*(1), 17–47. https://doi.org/10.1016/S0168-6445(01)00070-5

Liebschner, D., Afonine, P. V., Baker, M. L., Bunkoczi, G., Chen, V. B., Croll, T. I., Hintze, B., Hung, L. W., Jain, S., McCoy, A. J., Moriarty, N. W., Oeffner, R. D., Poon, B. K., Prisant, M. G., Read, R. J., Richardson, J. S., Richardson, D. C., Sammito, M. D., Sobolev, O. V., … Adams, P. D. (2019). Macromolecular structure determination using X-rays, neutrons and electrons: Recent developments in Phenix. *Acta Crystallographica Section D: Structural Biology*, *75*, 861–877. https://doi.org/10.1107/S2059798319011471

Liu, X., & Ferenci, T. (1998). Regulation of porin-mediated outer membrane permeability by nutrient limitation in Escherichia coli. *Journal of Bacteriology*, *180*(15), 3917–3922. https://doi.org/10.1128/jb.180.15.3917-3922.1998

Martorana, A. M., Benedet, M., Maccagni, E. A., Sperandeo, P., Villa, R., Dehò, G., & Polissia, A. (2016). Functional interaction between the cytoplasmic ABC protein LptB and the inner membrane LptC protein, components of the lipopolysaccharide transport machinery in Escherichia coli. *Journal of Bacteriology*, *198*(16), 2192–2203. https://doi.org/10.1128/JB.00329-16

Matias, V. R. F., Al-Amoudi, A., Dubochet, J., & Beveridge, T. J. (2003). Cryo-transmission electron microscopy of frozen-hydrated sections of Escherichia coli and Pseudomonas aeruginosa. *Journal of Bacteriology*, *185*(20), 6112–6118. https://doi.org/10.1128/JB.185.20.6112-6118.2003

McFadden, G. I. (2014). Origin and evolution of plastids and photosynthesis in eukaryotes. *Cold Spring Harbor Perspectives in Biology*, *6*(4). https://doi.org/10.1101/cshperspect.a016105

Merten, J. A., Schultz, K. M., & Klug, C. S. (2012). Concentration-dependent oligomerization and oligomeric arrangement of LptA. *Protein Science*, *21*(2), 211–218. https://doi.org/10.1002/pro.2004

Moslavac, S., Bredemeier, R., Mirus, O., Granvogl, B., Eichacker, L. A., & Schleiff, E. (2005).

Proteomic analysis of the outer membrane of Anabaena sp. strain PCC 7120. *Journal of Proteome Research*, *4*(4), 1330–1338. https://doi.org/10.1021/pr050044c

Moslavac, S., Reisinger, V., Berg, M., Mirus, O., Vosyka, O., Plöscher, M., Flores, E., Eichacker, L. A., & Schleiff, E. (2007). The proteome of the heterocyst cell wall in Anabaena sp. PCC 7120. *Biological Chemistry*, *388*(8), 823–829. https://doi.org/10.1515/BC.2007.079

Narita, S. ichiro, & Tokuda, H. (2009). Biochemical characterization of an ABC transporter LptBFGC complex required for the outer membrane sorting of lipopolysaccharides. *FEBS Letters*, *583*(13), 2160–2164. https://doi.org/10.1016/j.febslet.2009.05.051

Ngo, G., Centola, M., Krasnoselska, G., Pogoryelov, D., Yildiz, Ö., & Schleiff, E. (2020). LptC from Anabaena sp. PCC 7120: Expression, purification and crystallization. *Protein Expression and Purification*, *175*(June), 105689. https://doi.org/10.1016/j.pep.2020.105689

Nickelsen, J., Rengstl, B., Stengel, A., Schottkowski, M., Soll, J., & Ankele, E. (2011). Biogenesis of the cyanobacterial thylakoid membrane system - an update. *FEMS Microbiology Letters*, *315*(1), 1–5. https://doi.org/10.1111/j.1574-6968.2010.02096.x

Nicolaisen, K., Hahn, A., & Schleiff, E. (2009). The cell wall in heterocyst formation by Anabaena sp. PCC 7120. *Journal of Basic Microbiology*, *49*(1), 5–24. https://doi.org/10.1002/jobm.200800300

Nicolaisen, K., Mariscal, V., Bredemeier, R., Pernil, R., Moslavac, S., López-Igual, R., Maldener, I., Herrero, A., Schleiff, E., & Flores, E. (2009). The outer membrane of a heterocyst-forming cyanobacterium is a permeability barrier for uptake of metabolites that are exchanged between cells. *Molecular Microbiology*, *74*(1), 58–70. https://doi.org/10.1111/j.1365-2958.2009.06850.x

Nikaido, H. (2003). Molecular basis of bacterial outer membrane permeability revisited. *Microbiology and Molecular Biology Reviews*, *67*(4), 593–656. https://doi.org/10.1128/mmbr.49.1.1-32.1985

Okuda, S., Freinkman, E., & Kahne, D. (2012). Cytoplasmic ATP Hydrolysis Powers Transport of Lipopolysaccharide Across the Periplasm in E. coli. *Science*, *November*, 1214–1217.

Okuda, S., Sherman, D. J., Silhavy, T. J., Ruiz, N., & Kahne, D. (2016). Lipopolysaccharide transport and assembly at the outer membrane: The PEZ model. *Nature Reviews Microbiology*, *14*(6), 337–345. https://doi.org/10.1038/nrmicro.2016.25

Owens, T. W., Taylor, R. J., Pahil, K. S., Bertani, B. R., Ruiz, N., Kruse, A. C., & Kahne, D. (2019). Structural basis of unidirectional export of lipopolysaccharide to the cell surface. *Nature*, *567*(7749), 550–553. https://doi.org/10.1038/s41586-019-1039-0

Polissi, A., & Sperandeo, P. (2014). The lipopolysaccharide export pathway in Escherichia coli: Structure, organization and regulated assembly of the Lpt machinery. *Marine Drugs*, *12*(2), 1023–1042. https://doi.org/10.3390/md12021023

Qiao, S., Luo, Q., Zhao, Y., Zhang, X. C., & Huang, Y. (2014). Structural basis for lipopolysaccharide insertion in the bacterial outer membrane. *Nature*, *511*(7507), 108–111. https://doi.org/10.1038/nature13484

Raetz, C. R. H., Guan, Z., Ingram, B. O., Six, D. A., Song, F., Wang, X., & Zhao, J. (2009). Discovery of new biosynthetic pathways: The lipid A story. *Journal of Lipid Research*, *50*(SUPPL.), 103–108. https://doi.org/10.1194/jlr.R800060-JLR200

Raetz, C. R. H., & Whitfield, C. (2002). Lipopolysaccharide endotoxins. *Annual Review of Biochemistry*, *71*, 635–700. https://doi.org/10.1146/annurev.biochem.71.110601.135414

Raetz, C. R., Reynolds, C. M., & Trent, M. S. (2007). LIPID A MODIFICATION SYSTEMS IN GRAM-NEGATIVE BACTERIA. *Annu Rev Biochem. 2007*, *76*, 295–329. https://doi.org/10.1146/annurev.biochem.76.010307.145803.LIPID

Reed, R. H., Chudek, J. A., Foster, R., & Stewart, W. D. P. (1984). Osmotic adjustment in cyanobacteria from hypersaline environments. *Archives of Microbiology*, *138*(4), 333–337. https://doi.org/10.1007/BF00410900

Ricci, D. P., & Silhavy, T. J. (2012). The Bam machine: A molecular cooper. *Biochimica et Biophysica Acta - Biomembranes*, *1818*(4), 1067–1084. https://doi.org/10.1016/j.bbamem.2011.08.020

Rippka, R., Deruelles, J., & Waterbury, J. B. (1979). Generic assignments, strain histories and properties of pure cultures of cyanobacteria. *Journal of General Microbiology*, *111*(1), 1–61. https://doi.org/10.1099/00221287-111-1-1

Ruiz, N., Chng, S. S., Hinikera, A., Kahne, D., & Silhavy, T. J. (2010). Nonconsecutive disulfide bond formation in an essential integral outer membrane protein. *Proceedings of the National Academy of Sciences of the United States of America*, *107*(27), 12245–12250. https://doi.org/10.1073/pnas.1007319107

Ruiz, N., Gronenberg, L. S., Kahne, D., & Silhavy, T. J. (2008). Identification of two inner-membrane proteins required for the transport of lipopolysaccharide to the outer membrane of Escherichia coli. *Proceedings of the National Academy of Sciences of the United States of America*, *105*(14), 5537–5542. https://doi.org/10.1073/pnas.0801196105

Ruiz, N., Kahne, D., & Silhavy, T. J. (2006). Advances in understanding bacterial outer-membrane biogenesis. *Nature Reviews Microbiology*, *4*(1), 57–66. https://doi.org/10.1038/nrmicro1322

Sambrook, J., Fritsch, E.F., & Maniatis, T. (1989). *Molecular Cloning: A Laboratory Manual*. (Cold Spring Harbor, New York: Cold Spring Harbor Laboratory Press)

Sampson, B. A., Misra, R., & Benson, S. A. (1989). Identification and characterization of a new gene of Escherichia coli K-12 involved in outer membrane permeability. *Genetics*, *122*(3), 491–501. https://doi.org/10.1093/genetics/122.3.491

Schmidt, W., Drews, G., Weckesser, J., & Mayer, H. (1980). Lipopolysaccharides in four strains of the unicellular cyanobacterium Synechocystis. *Archives of Microbiology*, *127*(3), 217–222. https://doi.org/10.1007/BF00427196

Schopf, W. J. (2000). Fossil record cyanobacteria. *The Ecology of Cyanobacteria*, 13–35.

Schultz, K. M., Feix, J. B., & Klug, C. S. (2013). Disruption of LptA oligomerization and affinity of the LptA-LptC interaction. *Protein Science*, *22*(11), 1639–1645. https://doi.org/10.1002/pro.2369

Schulz, G. E. (2002). The structure of bacterial outer membrane proteins. *Biochimica et Biophysica Acta - Biomembranes*, *1565*(2), 308–317. https://doi.org/10.1016/S0005-2736(02)00577-1

Sestito, S. E., Sperandeo, P., Santambrogio, C., Ciaramelli, C., Calabrese, V., Rovati, G. E., Zambelloni, L., Grandori, R., Polissi, A., & Peri, F. (2014). Functional characterization of E. coli LptC: Interaction with LPS and a synthetic ligand. *ChemBioChem*, *15*(5), 734–742. https://doi.org/10.1002/cbic.201300805

Shah, H. N., Gharbia, S. E., & Collins, M. D. (1997). The gram stain: a declining synapomorphy in an emerging evolutionary tree. *Reviews in Medical Microbiology*, *8*(2), 103–110.

Sherman, D. J., Lazarus, M. B., Murphy, L., Liu, C., Walker, S., Ruiz, N., & Kahne, D. (2014). Decoupling catalytic activity from biological function of the ATPase that powers lipopolysaccharide transport. *Proceedings of the National Academy of Sciences of the United*

States of America, *111*(13), 4982–4987. https://doi.org/10.1073/pnas.1323516111

Silhavy, T. J., Kahne, D., & Walker, S. (2010). The Bacterial Cell Envelope. *Cold Spring Harb Perspect Biol*, *2*, 1–16. https://www.ncbi.nlm.nih.gov/pmc/articles/PMC2857177/pdf/cshperspect-PRK-a000414.pdf

Singh, R., Parihar, P., Singh, M., Bajguz, A., Kumar, J., Singh, S., Singh, V. P., & Prasad, S. M. (2017). Uncovering potential applications of cyanobacteria and algal metabolites in biology, agriculture and medicine: Current status and future prospects. *Frontiers in Microbiology*, *8*(APR), 1–37. https://doi.org/10.3389/fmicb.2017.00515

Snyder, D. S., Brahamsha, B., Azadi, P., & Palenik, B. (2009). Structure of compositionally simple lipopolysaccharide from marine Synechococcus. *Journal of Bacteriology*, *191*(17), 5499–5509. https://doi.org/10.1128/JB.00121-09

Söding, J., Biegert, A., & Lupas, A. N. (2005). The HHpred interactive server for protein homology detection and structure prediction. *Nucleic Acids Research*, *33*(SUPPL. 2), 244–248. https://doi.org/10.1093/nar/gki408

Sperandeo, P., Lau, F. K., Carpentieri, A., De Castro, C., Molinaro, A., Dehò, G., Silhavy, T. J., & Polissi, A. (2008). Functional analysis of the protein machinery required for transport of lipopolysaccharide to the outer membrane of Escherichia coli. *Journal of Bacteriology*, *190*(13), 4460–4469. https://doi.org/10.1128/JB.00270-08

Sperandeo, P., Villa, R., Martorana, A. M., Šamalikova, M., Grandori, R., Dehò, G., & Polissi, A. (2011). New insights into the Lpt machinery for lipopolysaccharide transport to the cell surface: LptA-LptC interaction and LptA stability as sensors of a properly assembled transenvelope complex. *Journal of Bacteriology*, *193*(5), 1042–1053. https://doi.org/10.1128/JB.01037-10

Suits, M. D. L., Sperandeo, P., Dehò, G., Polissi, A., & Jia, Z. (2008). Novel Structure of the Conserved Gram-Negative Lipopolysaccharide Transport Protein A and Mutagenesis Analysis. *Journal of Molecular Biology*, *380*(3), 476–488. https://doi.org/10.1016/j.jmb.2008.04.045

Tam, C., & Missiakas, D. (2005). Changes in lipopolysaccharide structure induce the σE-dependent response of Escherichia coli. *Molecular Microbiology*, *55*(5), 1403–1412.

https://doi.org/10.1111/j.1365-2958.2005.04497.x

Terwilliger, T. (2004). SOLVE and RESOLVE: Automated structure solution, density modification, and model building. *Journal of Synchrotron Radiation*, *11*(1), 49–52. https://doi.org/10.1107/S0909049503023938

Terwilliger, T. C., & Berendzen, J. (1999). Automated MAD and MIR structure solution. *Acta Crystallographica Section D: Biological Crystallography*, *55*(4), 849–861. https://doi.org/10.1107/S0907444999000839

Thompson, J. D., Higgins, D. G., & Gibson, T. J. (1994). CLUSTAL W (improving the sensitivity of progressive multiple sequence alignment through sequence weighting, position-specific gap penalties and weight matrix choice). *Nucleic Acids Research*, *22*(22), 4673–4680. https://doi.org/10.1007/978-1-4020-6754-9_3188

Thompson, K. M., Rhodius, V. A., & Gottesman, S. (2007). σE regulates and is regulated by a small RNA in Escherichia coli. *Journal of Bacteriology*, *189*(11), 4243–4256. https://doi.org/10.1128/JB.00020-07

Tozawa, K., Macdonald, C. J., Penfold, C. N., James, R., Kleanthous, C., Clayden, N. J., & Moore, G. R. (2005). Clusters in an intrinsically disordered protein create a protein-binding site: The TolB-binding region of colicin E9. *Biochemistry*, *44*(34), 11496–11507. https://doi.org/10.1021/bi0503596

Tran, A. X., Dong, C., & Whitfield, C. (2010). Structure and functional analysis of LptC, a conserved membrane protein involved in the lipopolysaccharide export pathway in Escherichia coli. *Journal of Biological Chemistry*, *285*(43), 33529–33539. https://doi.org/10.1074/jbc.M110.144709

Tripp, J., Hahn, A., Koenig, P., Flinner, N., Bublak, D., Brouwer, E. M., Ertel, F., Mirus, O., Sinning, I., Tews, I., & Schleiff, E. (2012). Structure and conservation of the periplasmic targeting factor Tic22 protein from plants and cyanobacteria. *Journal of Biological Chemistry*, *287*(29), 24164–24173. https://doi.org/10.1074/jbc.M112.341644

Van De Meene, A. M. L., Hohmann-Marriott, M. F., Vermaas, W. F. J., & Roberson, R. W. (2006). The three-dimensional structure of the cyanobacterium Synechocystis sp. PCC 6803. *Archives of Microbiology*, *184*(5), 259–270. https://doi.org/10.1007/s00203-005-0027-y

Vanthoor-Koopmans, M., Cordoba-Matson, M., Arredondo-Vega, B., Lozano-Ramirez, C., Garcia-

Trejo, J., & Rodriguez-Palacio, M. (2014). Microalgae and Cyanobacteria Production for Feed and Food Supplements. In R. Guevara-Gonzalez & I. Torres-Pacheco (Eds.), *Biosystems Engineering: Biofactories for Food Production in the Century XXI* (pp. 253–275). https://doi.org/10.1007/978-3-319-03880-3

Villa, R., Martorana, A. M., Okuda, S., Gourlay, L. J., Nardini, M., Sperandeo, P., Dehò, G., Bolognesi, M., Kahne, D., & Polissia, A. (2013). The Escherichia coli lpt transenvelope protein complex for lipopolysaccharide export is assembled via conserved structurally homologous domains. *Journal of Bacteriology*, *195*(5), 1100–1108. https://doi.org/10.1128/JB.02057-12

Vollmer, W., Blanot, D., & De Pedro, M. A. (2008). Peptidoglycan structure and architecture. *FEMS Microbiology Reviews*, *32*(2), 149–167. https://doi.org/10.1111/j.1574-6976.2007.00094.x

Wang, Zhongshan, Xiang, Q., Zhu, X., Dong, H., He, C., Wang, H., Zhang, Y., Wang, W., & Dong, C. (2014). Structural and functional studies of conserved nucleotide-binding protein LptB in lipopolysaccharide transport. *Biochemical and Biophysical Research Communications*, *452*(3), 443–449. https://doi.org/10.1016/j.bbrc.2014.08.094

Wang, Zhou, Wang, J., Ren, G., Li, Y., & Wang, X. (2015). Influence of core oligosaccharide of lipopolysaccharide to outer membrane behavior of Escherichia coli. *Marine Drugs*, *13*(6), 3325–3339. https://doi.org/10.3390/md13063325

Ward, D. M., Ferris, M. J., Nold, S. C., & Bateson, M. M. (1998). A Natural View of Microbial Biodiversity within Hot Spring Cyanobacterial Mat Communities. *Microbiology and Molecular Biology Reviews*, *62*(4), 1353–1370. https://doi.org/10.1128/mmbr.62.4.1353-1370.1998

Whitfield, C., & Stephen Trent, M. (2014). Biosynthesis and export of bacterial lipopolysaccharides. *Annual Review of Biochemistry*, *83*(February), 99–128. https://doi.org/10.1146/annurev-biochem-060713-035600

Whitton, B. A., & Potts, M. (2000). Introduction to the Cyanobacteria. In *The Ecology of Cyanobacteria* (pp. 1–11). https://doi.org/10.1007/0-306-46855-7_1

Wilk, L., Strauss, M., Rudolf, M., Nicolaisen, K., Flores, E., Kühlbrandt, W., & Schleiff, E. (2011). Outer membrane continuity and septosome formation between vegetative cells in the filaments of Anabaena sp. PCC 7120. *Cellular Microbiology*, *13*(11), 1744–1754. https://doi.org/10.1111/j.1462-5822.2011.01655.x

Wolk, C. P. (1968). Movement of carbon from vegetative cells to heterocysts in Anabaena cylindrica. *Journal of Bacteriology*, *96*(6), 2138–2143. https://doi.org/10.1128/jb.96.6.2138-2143.1968

Wolk, C. P., Thomas, J., Shaffer, P. W., Austin, S. M., & Galonsky, A. (1976). Pathway of nitrogen metabolism after fixation of 13N labeled nitrogen gas by the cyanobacterium, Anabaena cylindrica. *Journal of Biological Chemistry*, *251*(16), 5027–5034. https://doi.org/10.1016/s0021-9258(17)33216-7

Wolk, C. P., Vonshak, A., Kehoe, P., & Elhai, J. (1984). Construction of shuttle vectors capable of conjugative transfer from Escherichia coli to nitrogen-fixing filamentous cyanobacteria. *Isotopenpraxis*, *20*(1), 1561–1565. https://doi.org/10.1073/pnas.81.5.1561

Wu, T., Malinverni, J., Ruiz, N., Kim, S., Silhavy, T. J., & Kahne, D. (2005). Identification of a multicomponent complex required for outer membrane biogenesis in Escherichia coli. *Cell*, *121*(2), 235–245. https://doi.org/10.1016/j.cell.2005.02.015

Wu, T., McCandlish, A. C., Gronenberg, L. S., Chng, S. S., Silhavy, T. J., & Kahne, D. (2006). Identification of a protein complex that assembles lipopolysaccharide in the outer membrane of Escherichia coli. *Proceedings of the National Academy of Sciences of the United States of America*, *103*(31), 11754–11759. https://doi.org/10.1073/pnas.0604744103

Wyckoff, T. J. O., Lin, S., Cotter, R. J., Dotson, G. D., & Raetz, C. R. H. (1998). Hydrocarbon rulers in UDP-N-acetylglucosamine acyltransferases. *Journal of Biological Chemistry*, *273*(49), 32369–32372. https://doi.org/10.1074/jbc.273.49.32369

Yao, Z., Davis, R. M., Kishony, R., Kahne, D., & Ruiz, N. (2012). Regulation of cell size in response to nutrient availability by fatty acid biosynthesis in Escherichia coli. *Proceedings of the National Academy of Sciences of the United States of America*, *109*(38). https://doi.org/10.1073/pnas.1209742109

Zhao, H., & Lappalainen, P. (2012). A simple guide to biochemical approaches for analyzing protein-lipid interactions. *Molecular Biology of the Cell*, *23*(15), 2823–2830. https://doi.org/10.1091/mbc.E11-07-0645

Zhou, Z., White, K. A., Polissi, A., Georgopoulos, C., & Raetz, C. R. H. (1998). Function of Escherichia coli MsbA, an essential ABC family transporter, in lipid A and phospholipid

biosynthesis. *Journal of Biological Chemistry*, *273*(20), 12466–12475. https://doi.org/10.1074/jbc.273.20.12466

6 Table of Figures

Publications

Ngo, G., Girbas, M., Schätzle, H., Hammer, H., Safarian, S., Hübinger, M., & Schleiff, E. (2021). The two TpsB-like proteins in Anabaena sp. PCC 7120 are involved in secretion of secreted substrates. *Journal of Bacteriology*, *203*(4). https://doi.org/10.1128/JB.00568-20

Ngo, G., Centola, M., Krasnoselska, G., Pogoryelov, D., Yildiz, Ö., & Schleiff, E. (2020). LptC from Anabaena sp. PCC 7120: Expression, purification and crystallization. *Protein Expression and Purification*, *175*(June), 105689. https://doi.org/10.1016/j.pep.2020.105689

Brouwer, E.-M., Ngo, G., Yadav, S., Ladig, R., & Schleiff, E. (2019). Tic22 from Anabaena sp. PCC 7120 with holdase function involved in outer membrane protein biogenesis shuttles between plasma membrane and Omp85. *Molecular Microbiology*, *111*(5). https://doi.org/10.1111/mmi.14222

Rudolf, M., Tetik, N., Ramos-León, F., Flinner, N., Ngo, G., Stevanovic, M., Burnat, M., Pernil, R., Flores, E., & Schleiff, E. (2015). The peptidoglycan-binding protein SjcF1 influences septal junction function and channel formation in the filamentous cyanobacterium Anabaena. MBio, *6*(4). https://doi.org/10.1128/mBio.00376-15

Erklärung

Ich erkläre hiermit, dass ich mich bisher keiner Doktorprüfung unterzogen habe.

Frankfurt am Main, den .....

Versicherung

Ich erkläre hiermit, dass ich die vorgelegte Dissertation über

“Characterization of a putative LptC homologue involved in the transport of lipopolysaccharide in *Anabaena* sp. PCC 7120”

selbständig angefertigt und mich anderer Hilfsmittel als der in ihr angegebenen nicht bedient habe, insbesondere, dass alle Entlehnungen aus anderen Schriften mit Angabe der betreffenden Schrift gekennzeichnet sind.

Ich versichere, die Grundsätze der guten wissenschaftlichen Praxis beachtet, und nicht die Hilfe einer kommerziellen Promotionsvermittlung in Anspruch genommen zu haben.

Frankfurt am Main, den.....